

2 wk
mkt

(NASA-CR-121280) HIGH VOLTAGE SOLAR
ARRAY EXPERIMENTS Final Report (Boeing
Aerospace Co., Seattle, Wash.) 138 p HC
\$10.00 CSCL 101

N74-17788

Unclas
G3/03 31349

CR-121280



HIGH VOLTAGE SOLAR ARRAY EXPERIMENTS

by

K. L. Kennerud

THE **BOEING** COMPANY

Reproduced by
NATIONAL TECHNICAL
INFORMATION SERVICE
US Department of Commerce
Springfield, VA. 22151



Prepared for

NATIONAL AERONAUTICS AND SPACE ADMINISTRATION

NASA Lewis Research Center
Contract NAS3-14364
S. Domitz, Project Manager

NOTICE

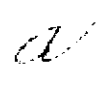
This report was prepared as an account of Government-sponsored work. Neither the United States, nor the National Aeronautics and Space Administration (NASA), nor any person acting on behalf of NASA:

- A.) Makes any warranty or representation, expressed or implied, with respect to the accuracy, completeness, or usefulness of the information contained in this report, or that the use of any information, apparatus, method, or process disclosed in this report may not infringe privately-owned rights; or
- B.) Assumes any liabilities with respect to the use of, or for damages resulting from the use of any information, apparatus, method or process disclosed in this report.

As used above, "person acting on behalf of NASA" includes and employee or contractor of NASA, or employee of such contractor, to the extent that such employee or contractor of NASA or employee of such contractor prepares, disseminates, or provides access to any information pursuant to his employment or contract with NASA, or his employment with such contractor.

Requests for copies of this report should be referred to

National Aeronautics and Space Administration
Scientific and Technical Information Facility
P.O. Box 33
College Park, MD. 20740



FINAL REPORT
HIGH VOLTAGE SOLAR ARRAY EXPERIMENTS
Contract NAS3-14364

by

K. L. Kennerud

The Boeing Aerospace Company
A Division of the Boeing Company
Kent Space Center
P.O. Box 3999
Seattle, Washington 98124

MARCH, 1974

Prepared for

NATIONAL AERONAUTICS AND SPACE ADMINISTRATION

NASA-Lewis Research Center
Cleveland, Ohio 44135
S. Domitz, Project Manager



FOREWORD

The following persons made significant technical contributions to the work described in this report: Dr. M. J. Kofoed, W. F. Springgate, H. V. Cleva, D. F. Watkins and C. A. Walker of the Boeing Company.

ABSTRACT

A detailed experimental investigation of the interaction between the components of a high voltage solar array and a simulated space plasma was performed. The purpose of the investigation was to obtain data for the design of a high voltage solar array capable of 15kW at 2 to 16kV. Testing was conducted in a vacuum chamber 1.5-m long by 1.5-m diameter having a plasma source which simulated the plasma conditions existing in Earth orbit between 400 nautical miles and synchronous altitude. Test samples included solar array segments (uninsulated, insulated, and screen-shielded), pinholes in insulation covering high voltage electrodes, and plain dielectric samples. Quantitative data is presented in the areas of plasma power losses, plasma and high voltage induced damage, and dielectric properties. Limitations of the investigation are described.

TABLE OF CONTENTS

	Page
FOREWORD	ii
ABSTRACT	iii
LIST OF ILLUSTRATIONS.	vi
LIST OF TABLES.	xi
1.0 SUMMARY	1
2.0 INTRODUCTION.	2
3.0 TEST FACILITIES AND PROCEDURES.	6
3.1 Large Plasma Chamber	6
3.2 Small Plasma Chamber	14
3.3 Charge Deposition Apparatus.	18
4.0 RESULTS	21
4.1 Space Plasma Simulation.	22
4.2 Pinhole Current Collection	26
4.2.1 Effect of Voltage, Pinhole Size, and Plasma Density	26
4.2.2 Large Hole Versus Pinhole	33
4.2.3 Pinhole Current Versus Type of Insulation	33
4.2.4 Insulator/Electrode Area Effects.	38
4.2.5 Slit vs. Pinhole Current Collection	46
4.2.6 Effect of Adhesive.	46
4.2.7 Short Life Tests.	46
4.2.8 Plasma Sheath Equipotential Lines	52
4.3 Solar Panel Current Collection	58
4.3.1 Conventional Panels (Bare Interconnectors).	58
4.3.2 Completely Insulated Panels	70
4.3.3 Screen - Shielded Solar Panel	74
4.4 Dielectric Tests	83
4.4.1 Dielectric Breakdown.	83
4.4.2 Bulk Resistivity.	83
4.4.3 Surface Resistance.	90
5.0 DISCUSSION OF RESULTS	94
6.0 CONCLUSIONS	102
7.0 LIMITATIONS	105

TABLE OF CONTENTS (Continued)

	Page
REFERENCES	106
APPENDIX A - PLASMA DIAGNOSTICS.	107
APPENDIX B - CURRENT COLLECTION BY A SPHERICAL PROBE	116
APPENDIX C - PARTIALLY INSULATED SPHERICAL PROBE MODEL	120

LIST OF ILLUSTRATIONS

	Page
Figure 1 Large Plasma Chamber	7
Figure 2 Plasma Source Operating Principles	8
Figure 3 Schematic of Three-Grid Disc Probe Used for Measuring Ion Energy Spectrum	10
Figure 4 Test Specimen Holder	12
Figure 5 Kapton in Specimen Holder	13
Figure 6 High Voltage Leakage Current Measurement System	15
Figure 7 Small Plasma Chamber	17
Figure 8 Charge Deposition Apparatus	19
Figure 9 Test Specimen Holder with Potential Measurement Ring	20
Figure 10 Effect of Applied Voltage on the Leakage Current Collected by a Spherical Probe Immersed in the Large Plasma Chamber	23
Figure 11 Effect of Plasma Conditions on the Leakage Current Collected by a Spherical Probe Immersed in the Large Plasma Chamber	24
Figure 12 Current-Voltage Curve of a 2.54-cm Diameter Sphere in a Plasma	25
Figure 13 Effect of Voltage and Defect Size on Leakage Current - 0.005 Inch Thick Kapton - Positive Electrode Voltages	27
Figure 14 Comparison of Equal Area Pinhole and Sphere Plasma Leakage	28
Figure 15 Effect of Plasma Conditions on the Leakage Current Collected by a 0.38-cm Diameter Hole in a 0.005-Inch Thick Kapton	29
Figure 16 Effect of Voltage and Defect Size on Leakage Current - 0.005 Inch Thick Kapton - Negative Electrode Voltages	32

LIST OF ILLUSTRATIONS (Continued)

	Page
Figure 17 Comparison of I-V Curves of a Large and Small Hole in Large Plasma Chamber - Plasma Density: 1.0×10^4 Electrons/cm ³	34
Figure 18 Effect of Voltage and Defect Size on Leakage Current - 0.005-Inch Thick FEP Teflon	35
Figure 19 Effect of Voltage and Defect Size on Leakage Current - 0.006-Inch Thick Microsheet Glass	36
Figure 20 Leakage Current Collected by a 10-Inch by 15-Inch Copper Plate Encapsulated in 0.005-Inch Thick Kapton - With and Without a Defect	39
Figure 21 Effect of Electrode Size on the Plasma Leakage Current Collected by a 0.015-Inch Diameter Pinhole in 0.005-Inch Thick Kapton	40
Figure 22 Surface Tracking Around a Pinhole in Kapton After 10 Minute Exposure to Plasma at a +10,000 Volt Electrode Voltage	41
Figure 23 Leakage Current Collected by a 10-Inch Diameter Aluminum Disc Encapsulated in 0.005-Inch Thick Kapton - With and Without a Defect	43
Figure 24 Plasma Leakage Current Collected by 0.038 cm Pinholes in Large and Small Area Kapton Covered Electrodes	44
Figure 25 Photograph of Large Area Disc Electrode	45
Figure 26 Leakage Current Collected by a Slit in 0.005-Inch Thick Kapton in the Large Plasma Chamber	47
Figure 27 Comparison of Plasma Leakage Current to Pinholes in Kapton Bonded to Electrodes with Different Adhesives	48
Figure 28 Plasma Leakage Current vs Time Collected by 0.015 Inch Diameter Pinhole in 0.005-Inch Thick Kapton - Positive Electrode Voltage	50
Figure 29 Erosion and Surface Darkening Around a Pinhole in Kapton After More Than 4 Days Exposure to Plasma With a +3,000 Volt Electrode Voltage	51
Figure 30 Pinhole Test Specimen	53

LIST OF ILLUSTRATIONS (Continued)

	Page
Figure 31 Comparison of Plasma Sheath Voltage Distribution for Pinhole, Sphere, and Disc	54
Figure 32 Potential Distribution Around a 0.38-cm Diameter Pinhole at 10,000 Volts in Large Plasma Chamber	56
Figure 33 Potential Distribution Around a 3.56-cm-Diameter Disc Electrode at +10,000 Volts in Large Plasma Chamber	57
Figure 34 High Voltage Solar Array Design Concepts	59
Figure 35 Solar Array - Uninsulated	60
Figure 36 Photograph of Solar Array in Large Plasma Chamber	61
Figure 37 Plasma Leakage Current Collected by a Solar Panel with Uninsulated Interconnectors	62
Figure 38 Electron Sheath Equipotential Line Around a 1 ft ² Solar Panel with Bare Interconnectors	64
Figure 39 Effect of Plasma Conditions on the Plasma Leakage Current Collected by a Positively Biased Solar Panel with Bare Interconnectors	65
Figure 40 Effect of Plasma Conditions on the Plasma Leakage Current Collected by a Negatively Biased Solar Panel with Bare Interconnectors	67
Figure 41 Effect of 114-Hour Exposure to Plasma on Solar Panel with Bare Interconnectors at +4kV	69
Figure 42 Plasma Leakage Current Collected by a positively Biased, Completely Insulated, Aluminum Dummy Solar Panel	75
Figure 43 Post-Test Photograph of Totally Insulated Aluminum Dummy Solar Cell Panel	76
Figure 44 Electrostatic Screen Shield Tests in Large Plasma Chamber	78

LIST OF ILLUSTRATIONS (Continued)

	Page
Figure 45 Effect of Electrostatic Screen in the Plasma Leakage Current Collected by a Positively Biased Solar Panel with Uninsulated Interconnectors	79
Figure 46 Effect of Electrostatic Screen on the Plasma Current Collected by a Positively Biased Solar Panel with Uninsulated Interconnectors	80
Figure 47 Effect of Electrostatic Screen on the Plasma Leakage Current Collected by a Negatively Biased Solar Panel with Uninsulated Interconnectors	82
Figure 48 Kapton - Bulk Resistivity vs Electric Field	87
Figure 49 Comparison of Bulk Resistance Leakage Currents for FEP-Teflon and Kapton	88
Figure 50 Effect of Proton and Ultraviolet Radiation on Kapton High Voltage Leakage Current	89
Figure 51 Effect of Plasma Current Collection on Kapton Surface Resistivity	91
Figure 52 Effect of Background Pressure on Kapton Surface Resistivity	92
Figure 53 Effect of Free Charge on Surface Resistance of Kapton	93
Figure A-1 Determination of Plasma Number Density by "Saturation Current" Method	108
Figure A-2 Determination of Plasma Number Density by "Positive Slope" Method at Low Voltages	110
Figure A-3 Determination of Plasma Number Density by "Positive Slope" Method at Medium Voltages	111
Figure A-4 Determination of Plasma Number Density by "Positive Slope" Method at High Voltages	112
Figure A-5 Ion Current Density vs Ion Retarding Voltage	113
Figure A-6 Differential Ion Current Density vs Ion Energy	114

LIST OF ILLUSTRATIONS (Continued)

	Page
Figure B-1 Comparison of Impact Parameter and Space Charge Sheath Radius for a 1.27-cm Diameter Sphere in Large Plasma Chamber	119
Figure C-1 Effect of Solar Panel Area on Plasma Power Loss per Square Foot - Synchronous Altitude	123
Figure C-2 Effect of Solar Panel Area on Plasma Power Loss per Square Foot - Low Altitude	124
Figure C-3 Calculated Plasma Power Losses for a 15kW High Voltage Solar Array at Different Altitudes	125

LIST OF TABLES

	Page
I Comparison of Plasma Parameters in Laboratory and Space	11
II Leakage Current "Healing" in FEP Teflon	37
III Damage Due to Pinhole Currents	49
IV Plasma Leakage Power Losses ₃ in a Shielded ₃ and Unshielded Solar Panel - $n_e = 2.5 \times 10^3$ electrons/cm ³	81
V Plasma Leakage Power Losses in a Shielded and Unshielded Solar Panel - $n_e = 26$ electrons/cm ³	81
VI Dielectric Breakdown Voltage of Selected Materials with a Plasma Acting as One Electrode	84
VII Dielectric Breakdown Voltage of Selected Materials with Deposited Charge Acting as One Electrode	85
VIII Bulk Resistivity of Selected Materials with Charge Deposition Apparatus	86

1.0 SUMMARY

A detailed experimental investigation of the interaction between the components of a high voltage solar array and a simulated space plasma was performed. The purpose of the investigation was to obtain data for the design of a high voltage solar array (HVSA) capable of 15kW at 2 to 16 kV. Most testing was conducted in a vacuum chamber 1.5-m long by 1.5-m diameter which simulated the plasma conditions existing in earth orbit between 400 nautical miles and synchronous altitude. Test samples included: (1) biased solar array segments with either bare interconnectors, insulated interconnectors, or electrostatic shielding, (2) biased flat electrodes covered by array insulation having pinholes, and (3) plain samples of various array dielectric materials. Data was obtained in the areas of: (1) plasma current collection, (2) plasma- and high voltage-induced damage, and (3) dielectric properties.

Several potential problems have been identified which must be better understood before a reliable HVSA can be designed. Most significant is that pinhole plasma currents: (1) are several orders of magnitude higher than calculated, (2) become even larger as the area of surrounding insulation surface is increased, and (3) can damage insulation at relatively low power levels (e.g. 0.5 to 5 watts per pinhole). Because of the "area effect" just mentioned, pinhole currents might be particularly dangerous for an isolated pinhole (e.g. micrometeoroid puncture) in the substrate of a large-area HVSA. Also, when a solar panel attains a negative potential relative to the plasma, arcing occurs at unexpectedly low voltage and current levels (e.g. 400 volts at 10^{-4} amperes/ft²). Solar panels attaining a positive bias with respect to the plasma are relatively immune to arcing but are susceptible to damage producing hot spots when the interconnectors are coated with insulation. Generally, it appears best to leave interconnectors bare and restrict the altitude of operation, or voltage, to levels where the plasma power losses are acceptable. One analytical model, which is consistent with test data obtained in this program on a one-square-foot solar panel, predicts that plasma power losses for a 2 to 16kV HVSA with bare interconnectors will not be important at altitudes above about 500 nautical miles. Bulk dielectric properties of candidate array materials appear to be unaffected by the presence of a plasma but surface dielectric properties appear to degrade with extended plasma exposure in the presence of high voltage.

Generally the results of this investigation indicate that a HVSA can probably be built much like a low voltage solar array with bare interconnectors and a .005-inch thick Kapton substrate. However, several unresolved problems still remain. For example, although the tests described above have established that the area of the array is an important factor influencing plasma current collection, tests have not been conducted on large enough samples to extrapolate these results to a large area HVSA in a quantitative manner. Similarly, although the short term (several day) tests conducted in this program have provided some insight to the nature of plasma and high voltage induced damage, longer (several month) tests are needed.

2.0 INTRODUCTION

High voltage solar cell arrays, capable of 15 kW at 2 to 16 kV, are being considered for power generation on future Earth-orbiting spacecraft. Such arrays could be used to directly power high voltage devices such as ion thrusters and microwave power tubes without the need for heavy power conditioning equipment. Past studies (refs. 1 and 2) have indicated that the primary concern in designing such arrays is their interaction with the space plasma existing between 100 nautical miles (ionosphere) and synchronous altitude. The basis of this concern is that power losses and physical damage can result from space plasma particles being collected by exposed high voltage conductors such as the bare interconnectors between solar cells. Such exposed conductors can attain large voltages of either polarity relative to the surrounding space plasma. Calculations made in the above-referenced studies indicate that for missions at the higher altitudes, conventional array designs with bare interconnectors would collect insignificant plasma currents even when used in a high voltage configuration. However in lower regions of the ionosphere the calculated plasma currents collected by bare interconnectors at high voltage would result in power losses comparable to the array output. One of the objectives of the experimental investigation described in this report was to provide experimental data which could be used to make a judgment of the validity of these calculations.

The following paragraphs first review past work (subsection 2.1) and then discuss the basis of the present work, divided into four distinct categories:

2.2 Space Plasma Simulation

2.3 Pinhole Current Collection

2.4 Solar Panel Current Collection

2.5 Dielectrics

2.1 BACKGROUND

The pioneering experiments of Cole, Ogawa and Sellen (Reference 3) indicated that solar array segments and pinholes biased at high voltage in a plasma collected far more current than one would expect on the basis of simple analytical models. These currents were often high enough to damage test samples even in very short tests. This early work, although limited in scope (only a few test samples and restricted to high plasma density, 10^6 electrons/cm³), did much to generate interest in subsequent plasma testing of high voltage solar array materials and components as well as suggest fruitful areas of investigation. In later experiments Grier and McKenzie studied dielectric breakdown (Reference 4) and pinhole current collection (Reference 5) in a wider variety of solar array materials, however their work was also limited to high plasma densities ($\sim 10^6$ electrons/cm³). Recently, Bayless, et al (Reference 6) have conducted laboratory plasma experiments, at lower plasma densities, which provide further insight regarding plasma current collection; in particular these investigators must be credited with discovery of the pinhole "area effect"

whereby pinhole currents are found to be enhanced by the presence of large areas of surrounding insulation. Results of plasma experiments performed at NASA-LeRC (private communication with S. Domitz and N. T. Grier) were also very helpful in planning and understanding the tests described in this report.

The present work broadens the scope of inquiry by including more realistic plasma densities (~ 10 to 10^4 electrons/cm³), more realistic samples, wider variety of materials, and geometries more applicable to HVSA's. Testing was conducted in a vacuum chamber 1.5-m long by 1.5-m in diameter having a plasma source which simulated the plasma conditions existing in Earth orbit between 400 nautical miles and synchronous altitude. Test samples included solar array segments (uninsulated, insulated, and screen-shielded), pinholes in insulation, and plain dielectric samples.

2.2 SPACE PLASMA SIMULATION

Validation tests were performed to insure that the plasma source used to simulate the space plasma neither inhibited or exaggerated the amount of current collected by high voltage test samples. This validation process involved two steps. The first step was to measure the value of the pertinent plasma parameters (plasma density, electron temperature) at a given setting of the plasma source and then calculate how much current should be collected by a small (0.5-inch diameter) sphere biased at high voltage in that plasma, under ideal conditions. The second step was to actually measure the current collected by such a sphere in the plasma at voltages ranging from 0 to +16kV and compare the resulting values with the calculated values. Good agreement would mean that our test technique was a valid method of relating the current collected by small high voltage test samples (e.g. pinholes) to plasma parameters. This same validation procedure was repeated for all the different plasma source settings used during the investigations.

2.3 PINHOLE CURRENT COLLECTION

A great deal of effort was spent in the present investigation towards characterizing and understanding pinhole currents. This effort consisted primarily of measuring pinhole currents collected by a wide variety of high voltage test specimens in the plasma chamber. Parameters which were varied in these tests include: pinhole size, insulation type, area of electrode and surrounding insulation, plasma density, voltage level and polarity, type of insulation adhesive, background pressure, and length of plasma exposure. Furthermore, equipotential lines in the plasma sheath surrounding a current-collecting pinhole were mapped with a hot wire probe to provide a better understanding of the physics of pinhole current collection.

A heavy emphasis was put on pinholes because it is a near certainty that even completely insulated solar arrays will eventually develop pinholes due to micrometeoroids, dielectric breakdown, insulation voids and other phenomenon which will allow plasma current collection. As mentioned earlier, laboratory experiments by Cole, et al (Reference 3) indicate that tiny pinholes can attract huge currents and therefore cannot be neglected.

Large pinhole currents are potentially dangerous in two ways: (1) they may negate the benefits of total insulation by creating intolerable power losses; and (2) concentration of large currents at small holes can result in localized high temperature that may damage array materials.

2.4 SOLAR PANEL CURRENT COLLECTION

Tests of full-size HVSA's are desirable but were not feasible in this program because of limitations in vacuum chamber size. Therefore, tests were conducted on smaller solar panel segments ($\leq 1 \text{ ft}^2$). The samples were made as realistic as possible by using real solar cells and flight hardware technology for most testing. Three categories of solar panels were tested: (1) conventional solar panels having exposed interconnects; (2) completely insulated solar panels and (3) a screen-shielded solar panel.

In the category of conventional solar panels was a one-square foot solar panel, completely insulated on the backside, but having bare interconnects and glass covers on the front side. It was biased at voltages up to $+16\text{kV}$ in the plasma chamber under conditions corresponding to high and low altitudes. The plasma currents collected by the panel were measured and then compared with calculations based on an analytical model. Tests of several days duration were performed on smaller ($\sim .1 \text{ ft}^2$) panels of the same general configuration to see if any adverse effects result from low level plasma currents which would not be of concern from a power loss standpoint. Illuminated solar panel output measurements were made before and after plasma exposure to assist in this evaluation.

Included in the category of completely insulated solar panels were: (1) a 0.1 square foot segment having conventional 2 cm by 2 cm solar cells with .012-inch fused silica covers and silicone adhesive covering the interconnects; (2) a segment identical to the above except the solar cells have wrap-around contacts; and (3) a small segment of four 2 cm by 2 cm solar cells completely encapsulated between layers of FEP-Teflon sheet. These completely-insulated solar panels were tested for several days at voltages up to $+16\text{kV}$ to see how well they reduced plasma current collection in comparison to conventional solar panels.

The screen-shielded category consisted of a one-square foot conventional solar panel which was tested with and without a biased screen suspended about one inch above the front of the panel. The tests were performed under plasma conditions corresponding to high and low altitudes at panel voltages ranging up to $+10\text{kV}$ and screen bias voltages up to 150 volts. The idea of the screen shield, suggested in earlier studies (References 1 and 2), is to allow plasma currents to be collected by the low voltage screen, therefore drastically reducing the solar panel power loss.

2.5 DIELECTRICS

In this program two different facilities were used to determine dielectric strength and bulk resistivity for candidate array materials. In one facility a high voltage disc electrode was covered with selected test insulations and exposed to a dilute plasma while monitoring electrode current. In the other facility a beam of charge was directed on the outer surface of the test insulations until it charged up to the desired voltage; the current flowing

through the test insulation to a grounded electrometer was then monitored. Both these methods of test have in common the feature that one of the two electrodes consisted of free charged particles instead of a metal plate. Test insulation samples included selected thicknesses of the following materials:

Kapton Sheet	(substrate)
FEP Teflon Sheet	(cover material)
Fused Silica	(cover material)
Microsheet Glass	(cover material)
Dow Corning R63-489 Silicone	(interconnector insulation)
Dow Corning 93-500 Silicone	(interconnector insulation)

A few samples (Kapton and Teflon) were tested before and after exposure to ultraviolet and proton radiation as well as at high temperatures (90°C).

Dielectric properties are important because insulating materials such as solar cell covers, solar array substrate, and interconnector insulation must have a good dielectric strength to minimize the probability of pinholes. Also, the resistance of these materials must be sufficiently high that current flow through them does not cause damage or significant power loss.

3.0 TEST FACILITIES AND PROCEDURES

Three different test facilities were used: (1) Large Plasma Chamber (LPC), (2) Small Plasma Chamber (SPC), and (3) Charge Deposition Apparatus (CDA). Both the LPC and SPC consisted of a vacuum chamber in which nitrogen gas was ionized to produce a plasma similar to that in earth orbit between 400 nautical miles and synchronous altitude. The LPC was used primarily to determine how much plasma current was collected by high voltage test specimens under known plasma conditions. The SPC was used primarily for short life tests (e.g., to determine how much damage was caused by fixed plasma currents being collected by a test specimen at a fixed voltage over short periods of time). The CDA produced a beam of electrons or argon ions which were deposited on dielectric test samples at voltages up to 20kV. It was used primarily to investigate the bulk and surface dielectric properties of insulating materials using the deposited charge as one electrode and a grounded conductor as the other electrode.

3.1 LARGE PLASMA CHAMBER (LPC)

3.1.1 Test Chamber and Plasma Source

The LPC, shown schematically in Figure 1, consisted of a vacuum chamber, a plasma source, plasma diagnostic probes, and a sample test volume. The vacuum chamber was 1.5 meters in diameter and 1.5 meters long. An ion sputter pump, separated from the main chamber by a chevron baffle, was used to maintain an ambient pressure of less than 1×10^{-5} Torr during all tests. Normal procedure was to pump to less than 1×10^{-5} Torr and then backfill with dry nitrogen gas until the chamber pressure stabilized between 1×10^{-5} and 1×10^{-6} Torr. A window in the chamber made it possible to view the front surface of test specimens. A plasma source similar to that built and tested by Burrowbridge (Reference 7) was used to simulate the space plasma environment. This source, shown schematically in Figure 2, uses a 100eV electron beam to ionize the background nitrogen gas, and a series of screens to direct the created ions into a beam 60-cm in diameter which fills the test volume. Electrons from the primary electron beam and ionization volume reach the test volume as the result of diffusion and scatter to mingle with the ion beam and form a neutral plasma. High energy electrons coming directly from the 100eV electron beam are prevented from entering the test volume by means of a suppressor screen biased at -150 volts. The resulting test volume plasma was characterized by ions with an average directed energy of about 25eV and omnidirectional electrons with an average energy of about 5eV. The density of this plasma could be varied from about 25 electrons/cm³ to 10⁴ electrons/cm³ by adjusting the intensity of the 100eV electron beam (the background pressure was kept constant).

3.1.2 Plasma Diagnostics

Measurement of plasma parameters was accomplished by the use of two movable probes located in the test volume. A Langmuir probe consisting of a 1.27-cm diameter sphere was used to determine the electron parameters: j_{eo} , electron thermal current density; \bar{E}_e , average electron energy; and n_e , electron number density. A three-grid disc probe having a 2.54-cm diameter aperture was used to determine the ion parameters, j_{io} , ion beam current density; \bar{E}_i , average ion energy; and n_i , ion number density. The Langmuir

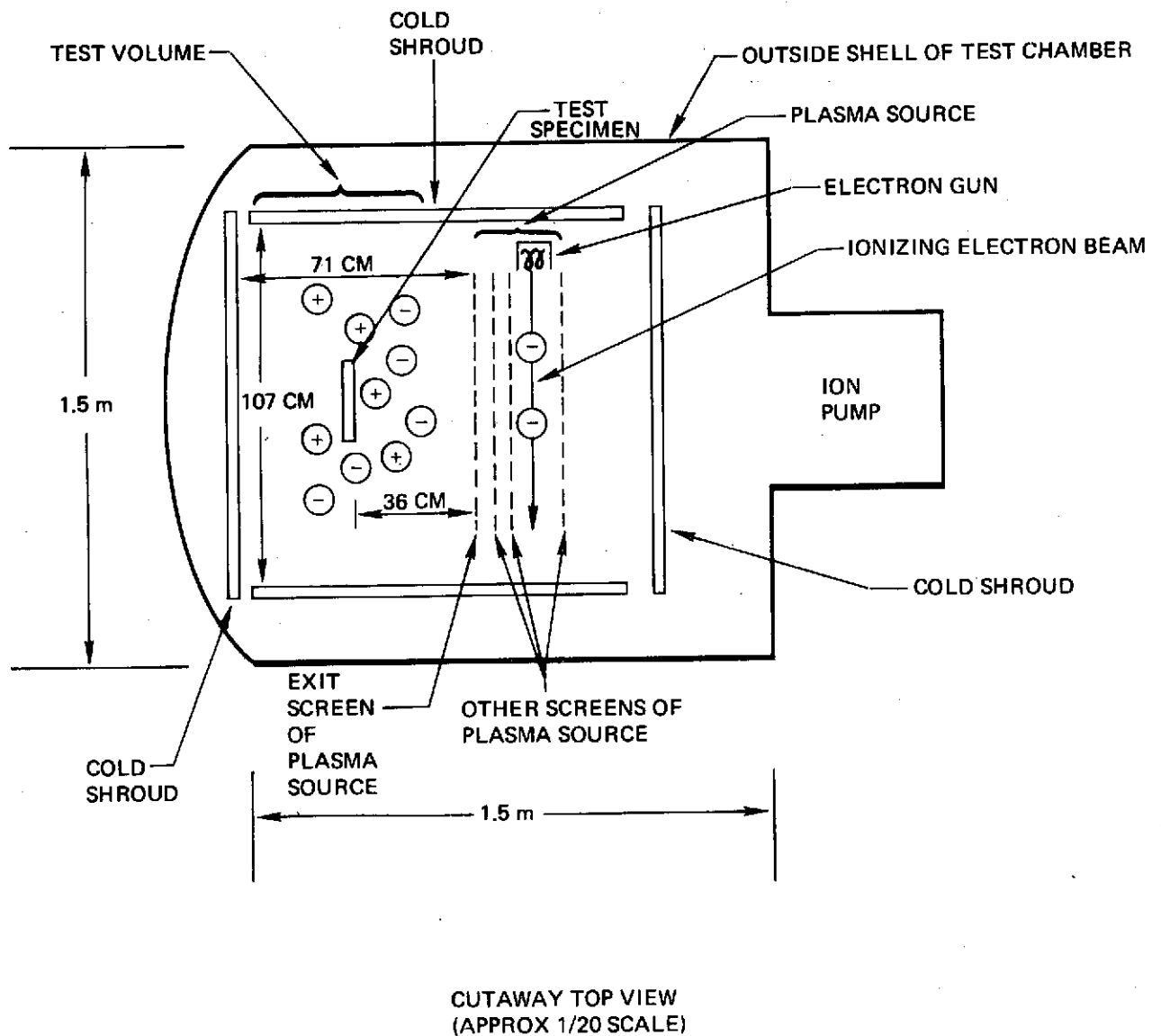


Figure 1: LARGE PLASMA CHAMBER

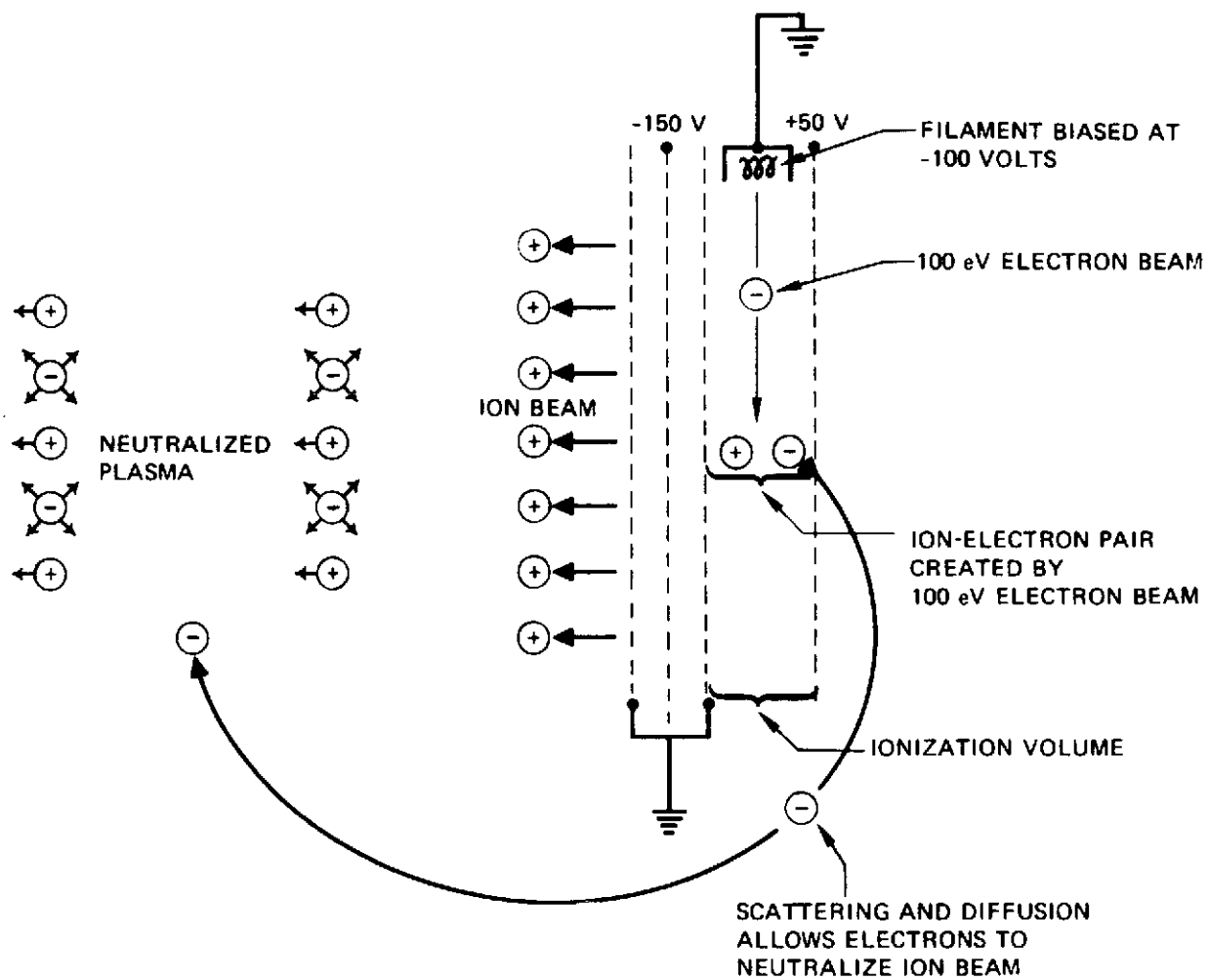


Figure 2: PLASMA SOURCE OPERATING PRINCIPLES

probe was used in the classical manner, j_{eo} being determined from the "saturation" current of the probe, \bar{E}_e being determined from the retarding portion of the current voltage (I-V) curve, and n_e being calculated from j_{eo} and \bar{E}_e . That the electron energy distribution was near-Maxwellian was evident from the linearity of plots of $\ln I$ versus V in the retarding portion of the Langmuir probe I-V curve. Uniformity scans made with the Langmuir probe indicate that j_{eo} was uniform within +25% over the test volume. The three-grid disc probe, shown schematically in Figure 3, utilizes a fine mesh grid to span its outer aperture to prevent penetration of plasma into the probe. Electrons are prevented from reaching the collector by biasing the electron suppressor grid at -100 volts. A variable retarding voltage was applied to the ion retarding grid to determine the energy spectrum. (All three grids were made from 88% transparent gold mesh.) It was found necessary to give a small negative bias (-10 volts) to the collector in order to prevent the collection of electrons. Values of j_{io} were determined from the collector current measured when no ion retarding voltage was used. Uniformity scans made with the probe indicate that j_{io} was uniform within +20% over the test volume. \bar{E}_i was determined from an analysis of the collector current versus ion retarding voltage, usually averaging about 25eV with the energy spectrum having a half-width at half-maximum of about 7eV. The ion number density n_i was calculated from the measured values of j_{io} and \bar{E}_i . That the created plasma was roughly neutral is supported by the fact that the measured electron and ion number densities (n_e , n_i) usually agreed within a factor of two, although the difference was sometimes as much as four. For mathematical details and sample calculations of plasma parameters determined from probe data, see Appendix A). Table I compares the measured plasma parameters with those anticipated in earth orbit at high and low altitudes.

3.1.3 Test Specimens and Procedures

Test specimens were normally located as shown in Figure 1, about 36-cm from the exit screen of the plasma source, with the test surface facing the ion beam. A special test specimen holder, shown in Figures 4 and 5 was used for most of the dielectric breakdown and pinhole tests conducted in the LPC. Test specimens used in this holder consisted simply of discs of stainless steel onto which the desired test insulations were bonded. When fastened in the test holder, the test specimen edges and backside were sealed from the plasma by means of two O-rings and contact to a high voltage lead was made automatically. (This arrangement made replacement of test specimens an easy matter, requiring no potting operations.) As a result the only portion of the test specimen exposed to the plasma was a 3.5-cm diameter disc of test insulation recessed 0.635-cm in the test holder. Pinholes, when desired, were put in the center of this exposed disc. Other test specimens such as solar panels and large area electrodes were individually designed and are described separately in section 4.0, "RESULTS."

The high voltage lead from the test specimen was normally potted with an epoxy (Scotchcast 280) or silicone adhesive (R63-489) at all electrical connections (e.g., at test specimen and vacuum chamber feedthrough) to ensure a good seal from the plasma.

Measurement of plasma currents collected by the test specimens were made with a battery-operated electrometer (e.g., Keithly 600A) located electrically between the high voltage power supply and the test specimen (see

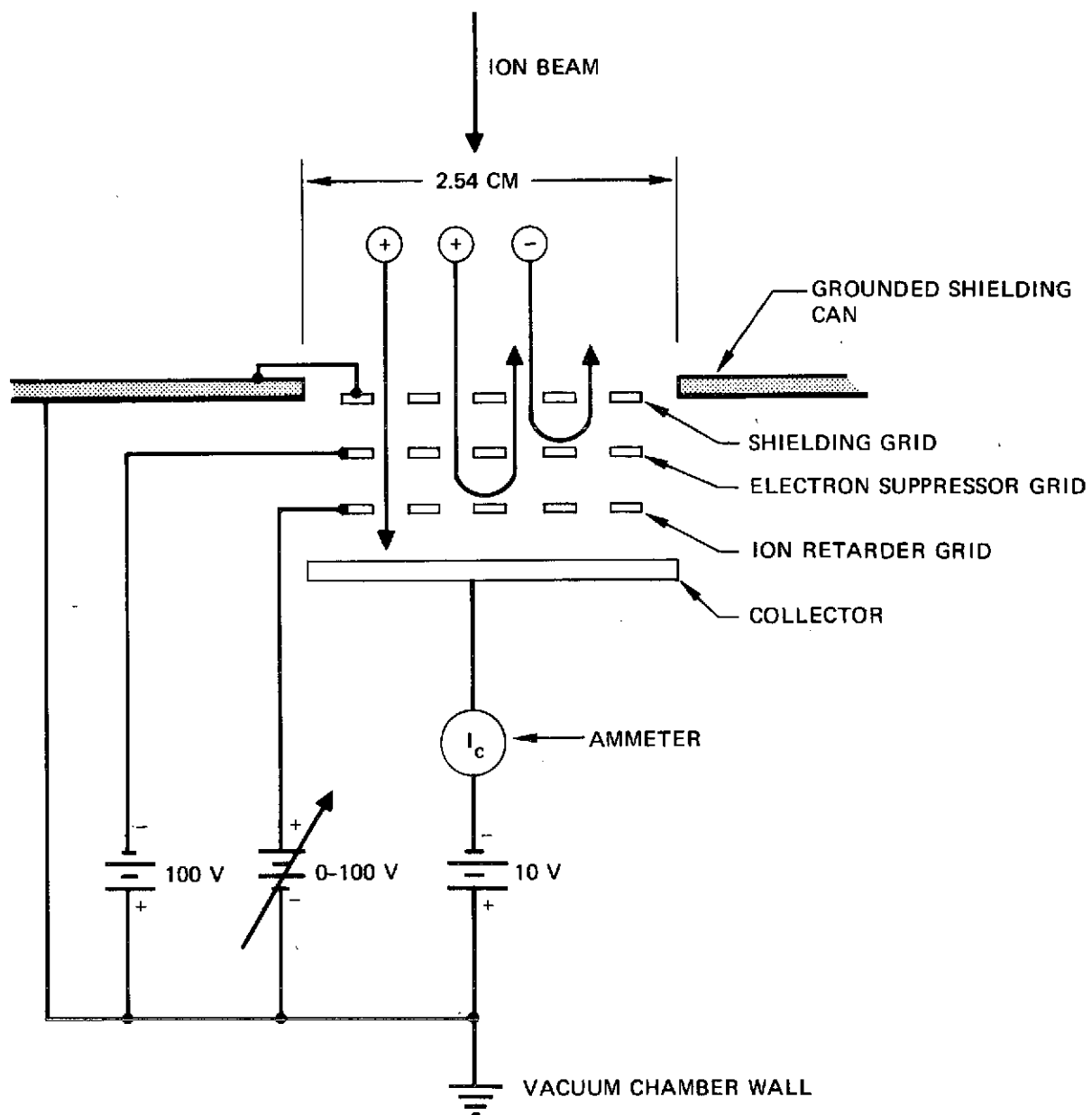





Figure 3 : SCHEMATIC OF THREE-GRID DISC PROBE USED FOR MEASURING ION ENERGY SPECTRUM

**TABLE I: COMPARISON OF PLASMA PARAMETERS
IN LABORATORY AND SPACE**

ALTITUDE	LOCATION	ELECTRON PARAMETERS			ION PARAMETERS				PRESSURE
		THERMAL CURRENT DENSITY	AVERAGE ENERGY	NUMBER DENSITY	CURRENT DENSITY	AVERAGE ENERGY	NUMBER DENSITY	MAJOR IONS	
		j_{eo}	E_e	N_e	j_o	E_i	N_i		
		(AMPS/CM ²)	(eV)	(CM ⁻³)	(AMPS/CM ²)	(eV)	(CM ⁻³)		
LOW (~400 NAUTICAL MILES)	LARGE  PLASMA CHAMBER	2×10^{-7}	6	2.5×10^4	4×10^{-9}	24	2×10^4	N ⁺	1×10^{-6}
	SPACE PLASMA	2×10^{-7}	0.3	1.4×10^5	2×10^{-8}	6	1.4×10^5	O ⁺ , He ⁺	$< 10^{-8}$
HIGH (SYNCHRONOUS ALTITUDE)	LARGE  PLASMA CHAMBER	2×10^{-10}	8	26	2×10^{-11}	24	98	N ⁺	1×10^{-6}
	SPACE PLASMA	2×10^{-10}	2	65	6×10^{-12}	2	65	H ⁺	$< 10^{-8}$

 VALUES REPRESENT ELECTRON AND ION PARAMETERS OBTAINED AT A SINGLE SETTING OF PLASMA SOURCE. COMPARISON WITH SPACE PLASMA PARAMETERS WAS DONE ON THE BASIS OF EQUAL j_{eo} .

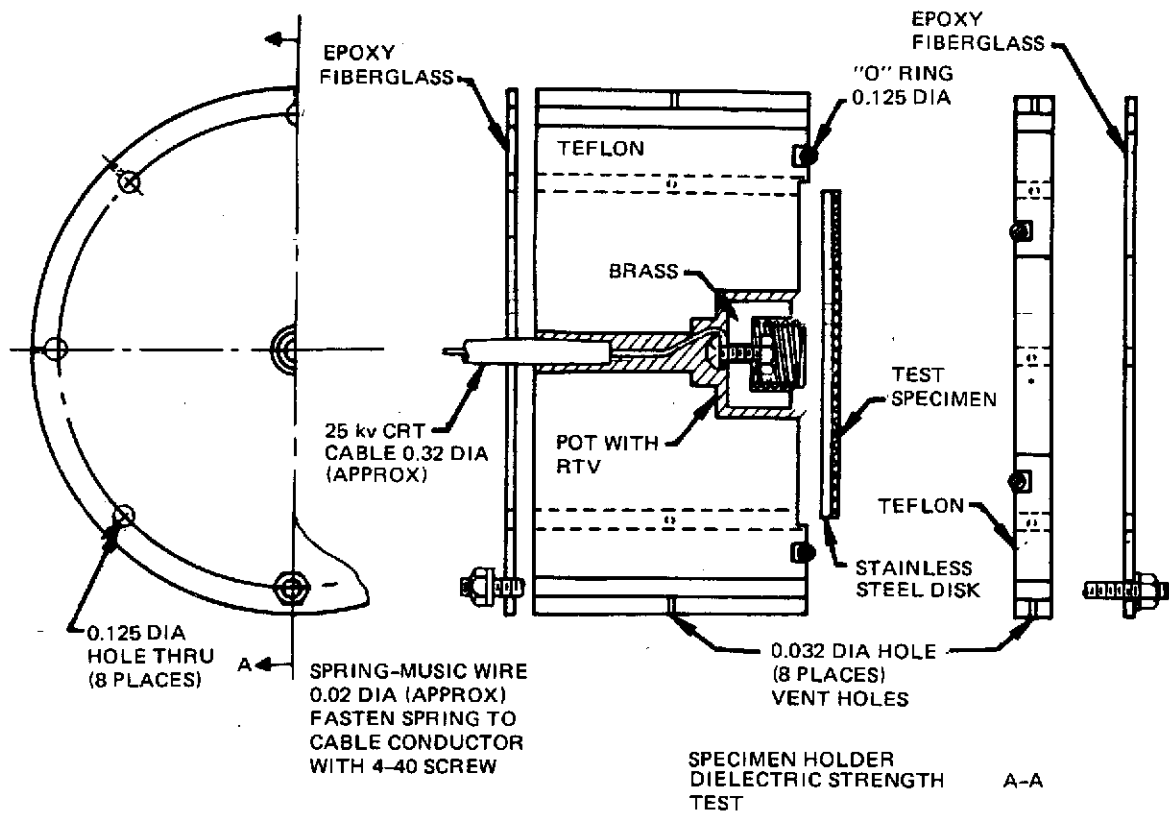


Figure 4 : TEST SPECIMEN HOLDER

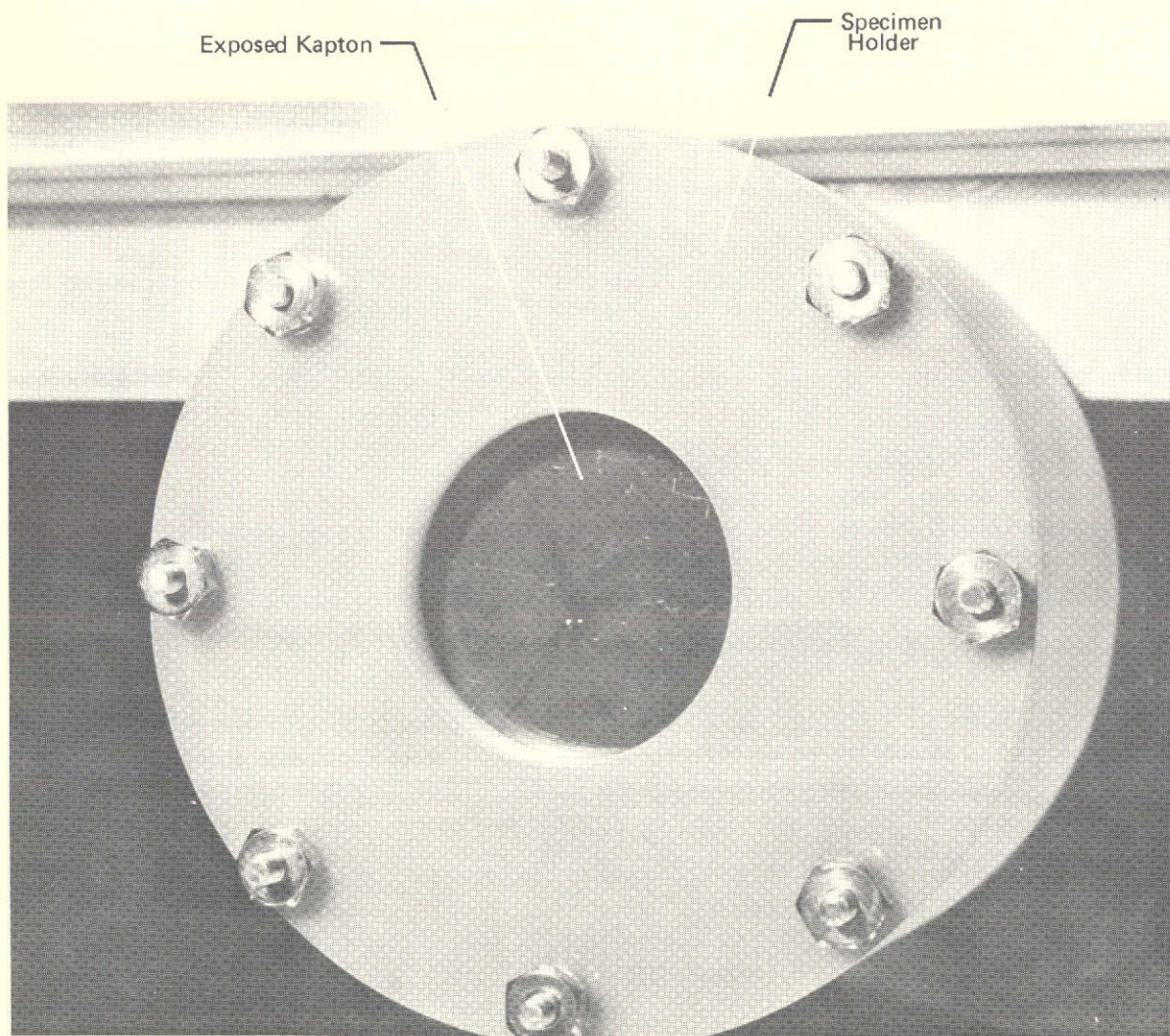


Figure 5: KAPTON IN SPECIMEN HOLDER

This page is reproduced at the back of the report by a different reproduction method to provide better detail.

Figure 6). The circuit was completed by connecting the other terminal of the high voltage power supply to laboratory ground thereby allowing current to flow to the plasma source which, in turn, made charged particles (plasma) available for collection by the test specimen.

Normal procedure involved first measuring the current at various voltages with the plasma off and then repeating the test with the plasma on. Also pinhole experiments were normally run first without a pinhole. Both these practices were followed in order to establish a "background" current level for each test.

3.1.4 Sheath Measurements

It was possible to map the equipotential lines in the plasma sheath surrounding test specimens through use of a movable, hot wire probe. The probe was nothing more than a hairpin shaped filament of .0127-cm diameter tungsten wire 1.27-cm long capable of being biased. In the absence of high voltage it was necessary to bias the probe slightly negative (ΔV) relative to the undisturbed plasma potential (V_p) in order to obtain temperature-limited emission from the filament.

With the filament biased V_f volts positive relative to V_p it was necessary for the potential at the location of the filament to be at least $V_1 = V_f + \Delta V$ above V_p in order for temperature limited emission to occur. When the positively-biased probe was moved toward a high voltage test specimen, a position would eventually be reached at which temperature-limited emission would occur; this position represents one point of a V_1 equipotential line in the plasma sheath surrounding the test specimen. By repeating this procedure at different locations a series of points could be determined and the shape of the equipotential line obtained.

By this means sheath equipotential lines surrounding a sphere, a disc (section 4.2.8) and a pinhole (section 4.2.8) at high voltage were mapped. Figure 6a shows the measured and calculated potential distribution around a 1.27-cm diameter sphere at +10,000 volts in vacuum.

3.2 SMALL PLASMA CHAMBER (SPC)

The SPC, shown schematically in Figure 7, was essentially the same as the LPC except for the size of the chamber and the type and location of the vacuum pump. As in the LPC, test specimens were located with the test surface facing the plasma source ion beam. The smaller size of this chamber restricted the plasma sheath growth of some specimens biased above about 1,000 volts and was therefore not suitable for determining maximum levels of current collected by test specimens under fixed plasma conditions. However, it was suitable for running plasma life tests at fixed current and voltage levels. Also, because it could easily be pumped down to 1×10^{-8} Torr in a relatively short time, it was valuable for determining the effect of pressure on pinhole "hot spots" and the surface resistivity of insulation.

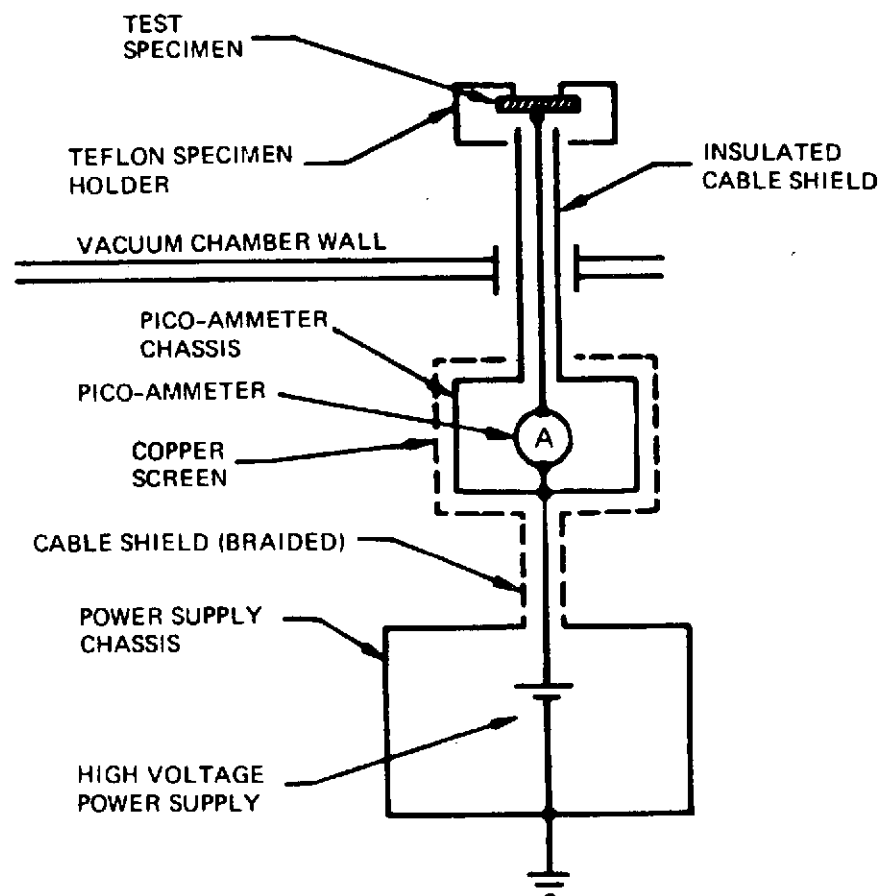


Figure 6: HIGH VOLTAGE LEAKAGE CURRENT MEASUREMENT SYSTEM

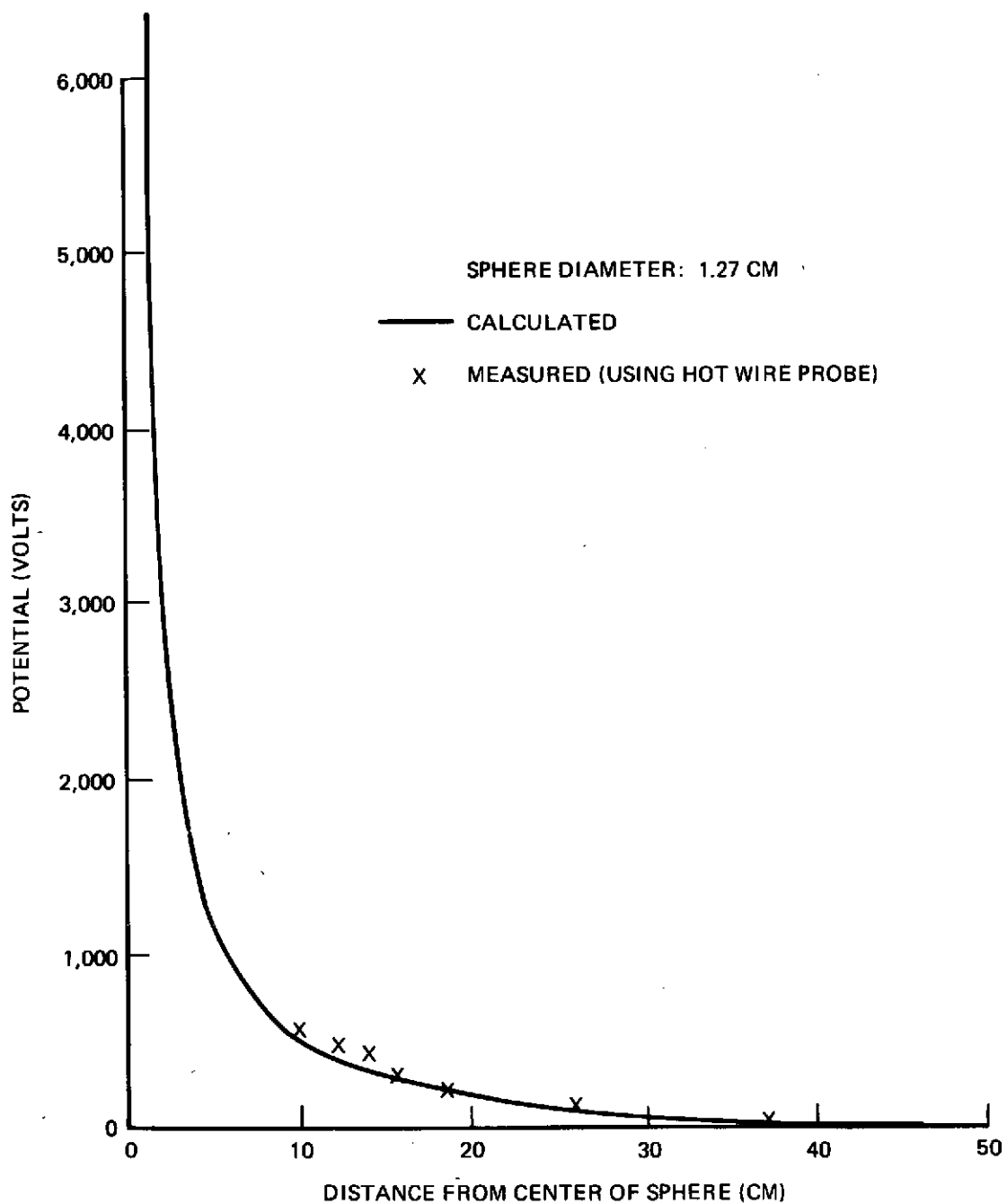


Figure 6A : HOT WIRE PROBE MEASUREMENTS OF THE POTENTIAL DISTRIBUTION AROUND A 10,000 VOLT SPHERE IN VACUUM

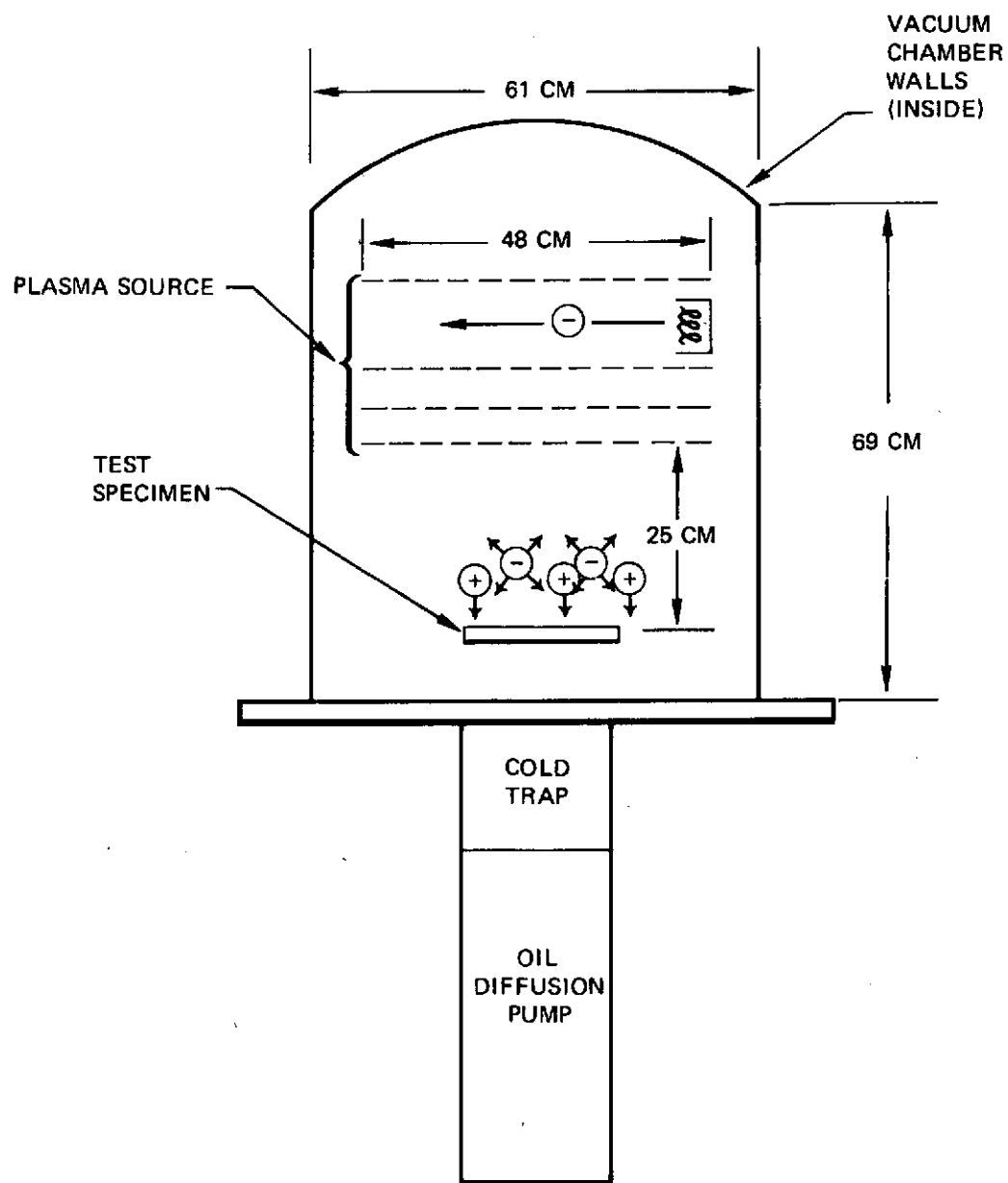


Figure 7: SMALL PLASMA CHAMBER

3.3 CHARGE DEPOSITION APPARATUS (CDA)

The CDA, shown schematically in Figure 8, is comprised basically of a duoplasmatron ion or electron source, a unipotential accelerating lens, an electron or ion beam, and a test volume maintained less than 1×10^{-6} Torr.

The test specimen normally consisted of a disc of test insulation bonded to a stainless steel disc which, in turn, was mounted in the test holder described in section 3.1.3 (see Figure 4). By choosing the proper polarity of beam voltage a 1-cm diameter beam of electrons or argon ions could be extracted from the duoplasmatron discharge and directed onto the surface of the test insulation. An electrometer, placed electrically between the test specimen electrode and ground, was used to measure the amount of current conducted through the test insulation. Theoretically, the voltage imposed across the test insulation should be equal to the beam voltage, which was known precisely. However, in practice, the top surface of the insulation charged up to a voltage slightly less than the beam voltage. To determine what the actual surface voltage was, a metal ring placed on the top surface (Figure 9) was monitored with an electrostatic voltmeter. So that this metal ring would not have to be used during all tests (and possibly invalidate data), an empirical relationship between ring voltages and voltages of a nearby screen, was made so that only the screen voltages needed to be monitored later and the ring could be removed.

The measured voltages and currents were used primarily to determine breakdown strength and measure bulk resistivity. However, some surface resistivity measurements (see section 4.4.3.2) were made by depositing the beam on a small metal cylinder disc on the top surface of the test insulation and measuring the resultant current flow to a metal ring placed on the insulation surface concentric to, but of larger diameter than the disc.

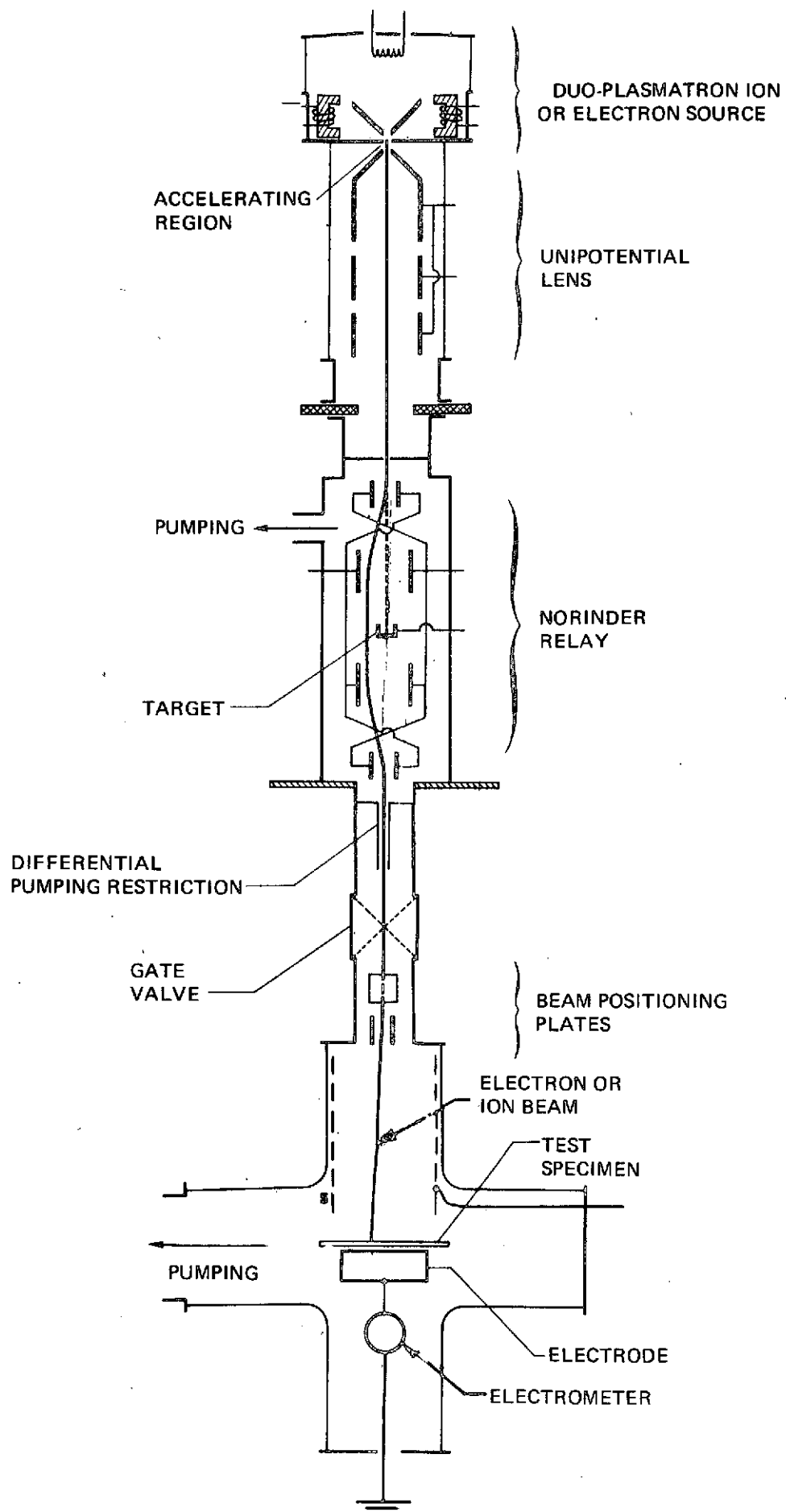


Figure 8: CHARGE DEPOSITION APPARATUS

This page is reproduced at the back of the report by a different reproduction method to provide better detail.

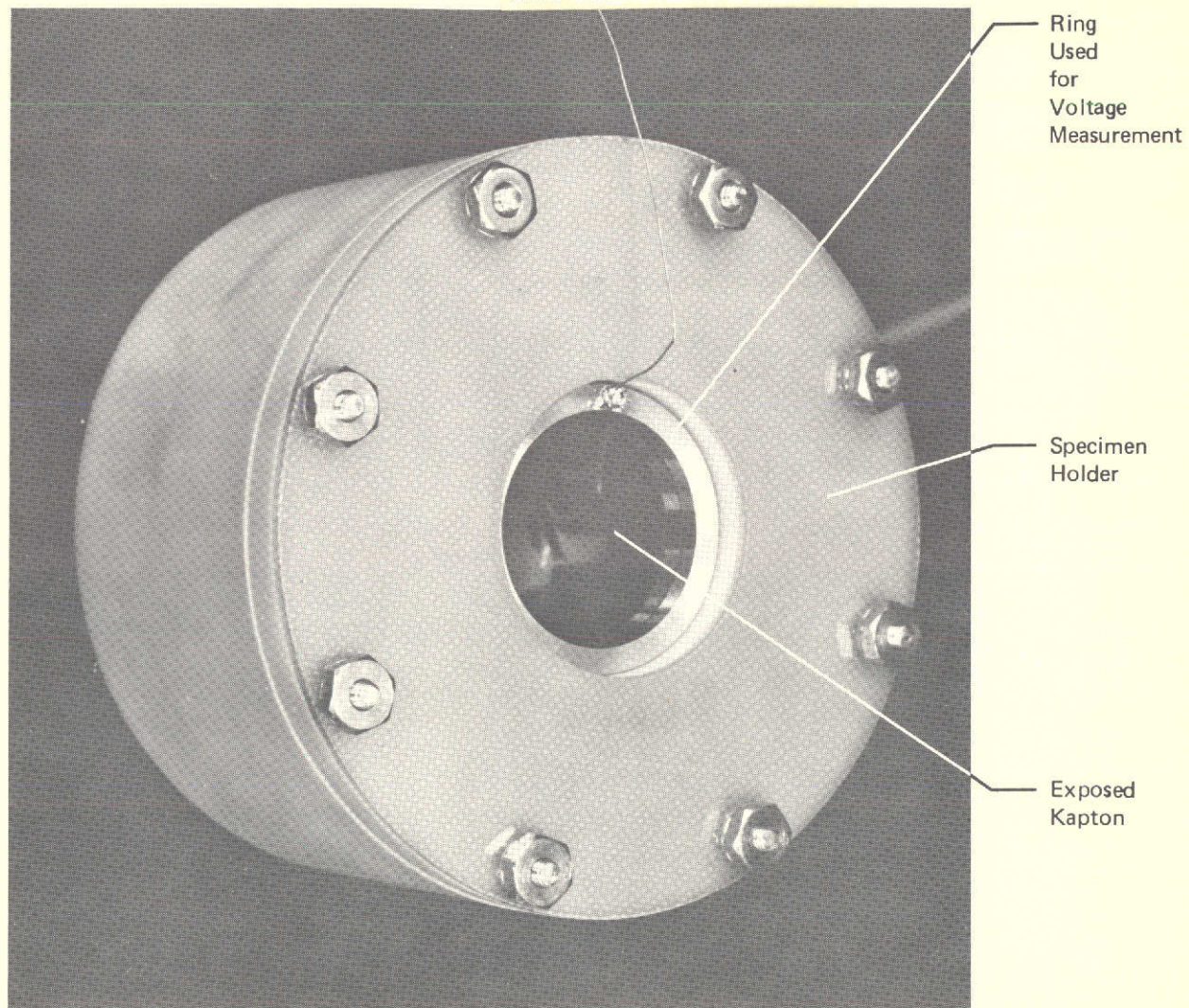


Figure 9: TEST SPECIMEN HOLDER WITH POTENTIAL MEASUREMENT RING

4.0 RESULTS

This section contains test results as well as a detailed description of test specimens, test conditions, and observations made before, during, and after test. Because of the detailed nature of much of this information, the average reader may want to skip this section and turn directly to Section 5.0 for a more concise description of the results and their implications. However for those interested in details of the tests and test results the present section is recommended. For simplicity, this detailed information is presented in four separate subsections:

Subsection 4.1 SPACE PLASMA SIMULATION

Subsection 4.2 PINHOLE CURRENT COLLECTION

Subsection 4.3 SOLAR PANEL CURRENT COLLECTION

Subsection 4.4 DIELECTRICS

4.1 SPACE PLASMA SIMULATION

Test Facility: LPC

Validation of the plasma source as a means of simulating the space plasma was accomplished by means of a spherical probe used as a "standard" test sample. Specifically, 1.27-cm diameter stainless steel sphere was suspended by its high voltage lead in the middle of the test volume of the LPC while voltages up to + 16 kV were applied to the sphere. Plasma current collected by the sphere was measured as a function of voltage at plasma densities ranging from 25 electrons/cm³ to 10⁴ electrons/cm³. The measured data, shown in Figure 10, is in excellent agreement with values predicted from orbit limited spherical probe theory (see Appendix B). Note that at voltages greater than 100 volts the current is proportional to voltage. A replot (Figure 11) of the above data shows that the current is roughly proportional to the ratio of the electron thermal current density (j_e) and the electron average energy (E_e), as predicted by theory.

Although no negative polarity tests were conducted on the sphere in the LPC, measurements were made with a 2.54-cm diameter sphere biased at both positive and negative voltages up to 10 kV in a similar plasma chamber (it was identical to the LPC except all dimensions were approximately doubled). The results, shown in Figure 12, indicate that good agreement between theory and measured data was obtained at both for ion and electron collection.

The good agreement between measured and calculated data suggests that our method of simulating the interaction between high voltage conductors and the space plasma produces fairly accurate data, especially for small test samples.

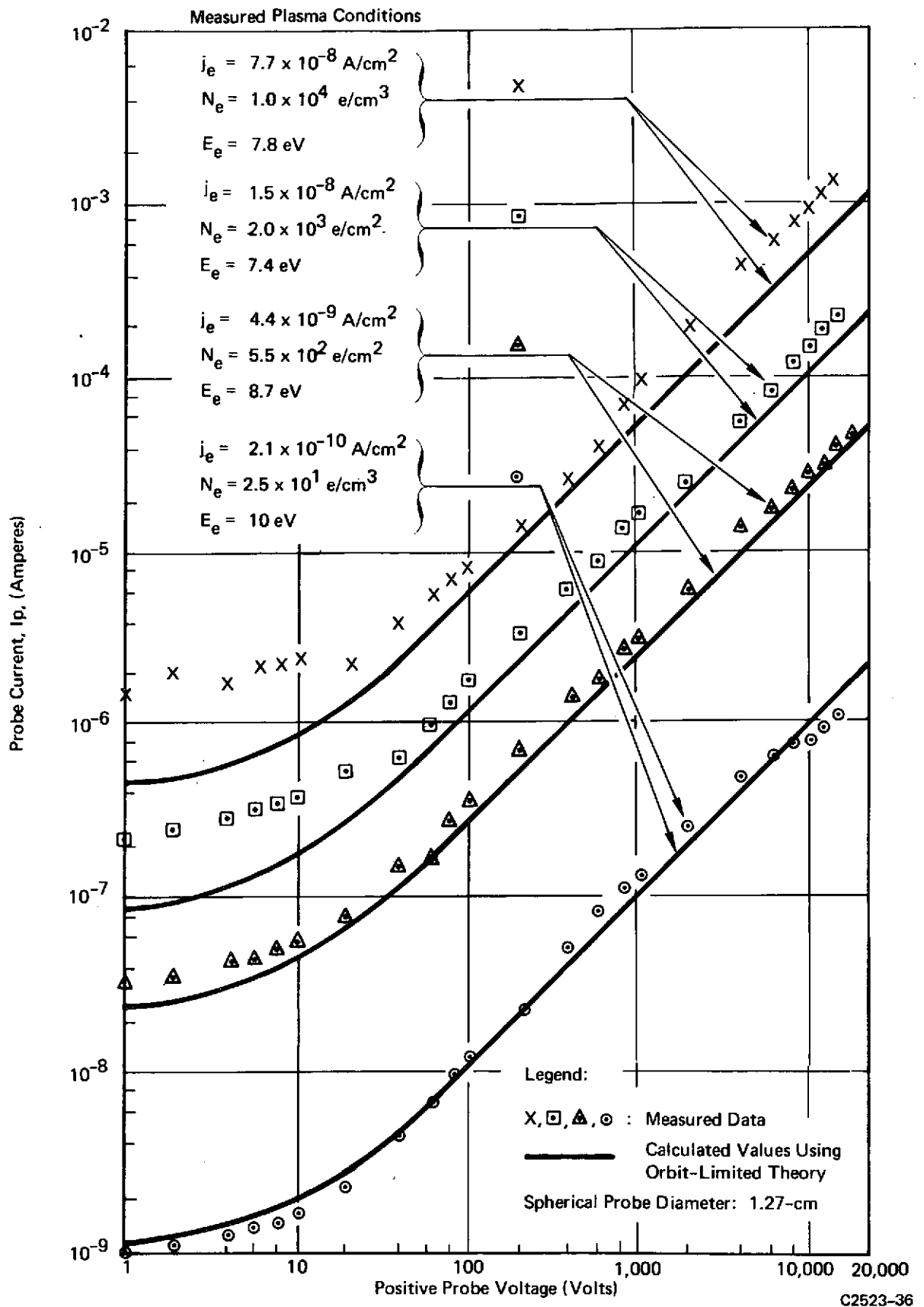


Figure 10: EFFECT OF APPLIED VOLTAGE ON THE LEAKAGE CURRENT COLLECTED BY A SPHERICAL PROBE IMMERSSED IN THE LARGE PLASMA CHAMBER

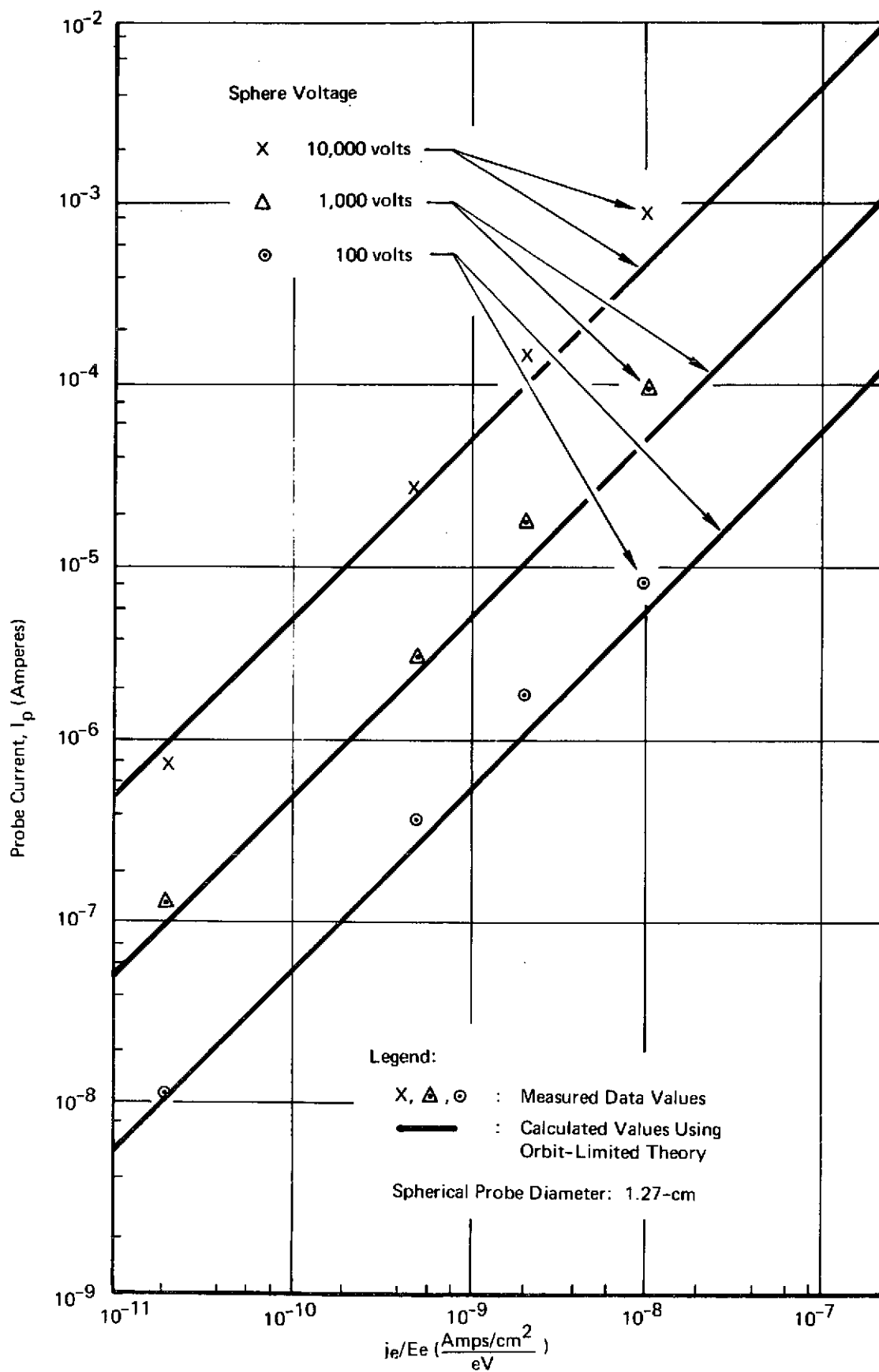


Figure 11: EFFECT OF PLASMA CONDITIONS ON THE LEAKAGE CURRENT COLLECTED BY A SPHERICAL PROBE IMMERSSED IN THE LARGE PLASMA CHAMBER

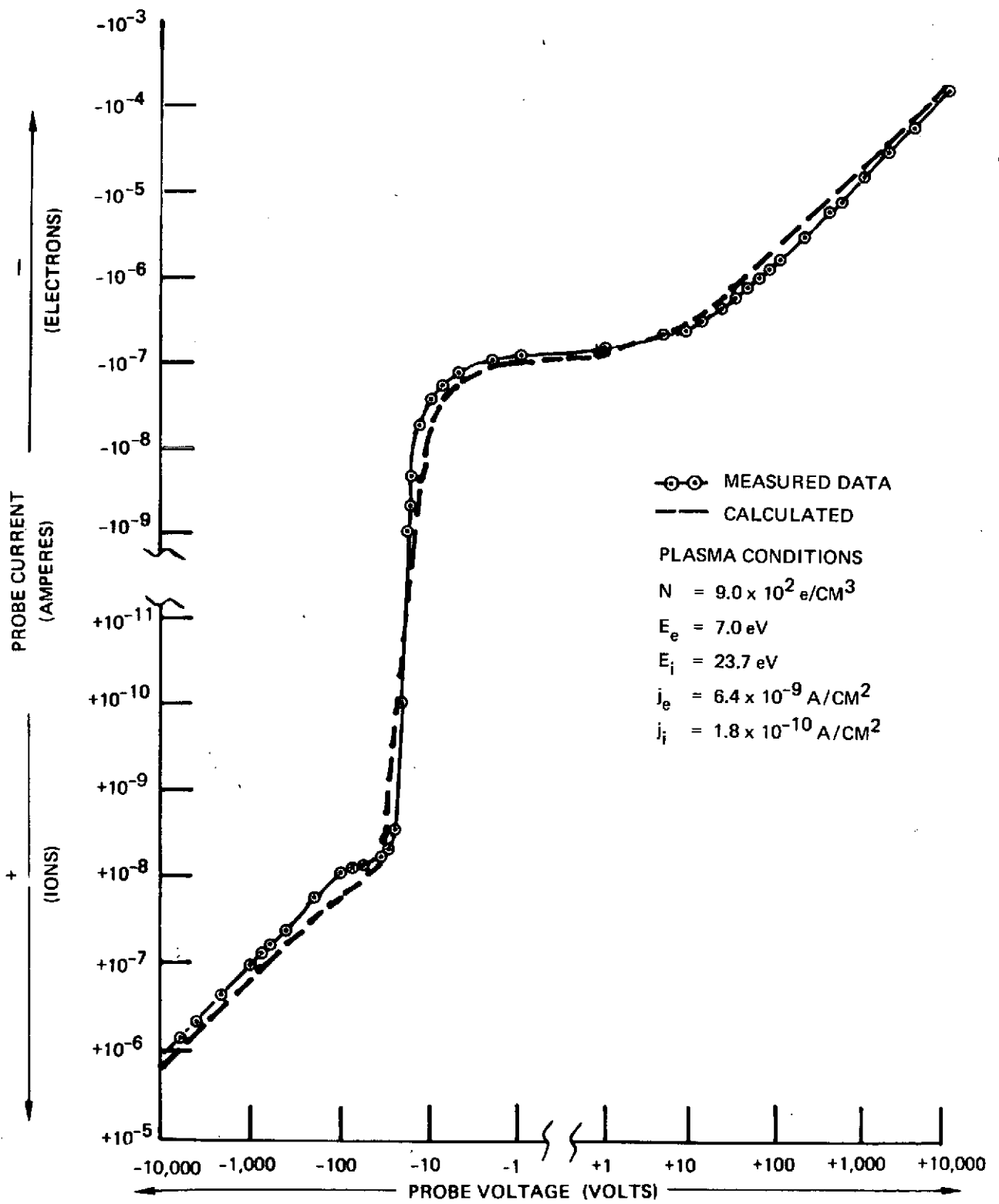


Figure 12: CURRENT-VOLTAGE CURVE OF A 2.54-CM DIA SPHERE IN A PLASMA -
 $N = 9.0 \times 10^2 \text{ ELECTRONS/CM}^3$

4.2 PINHOLE CURRENT COLLECTION

The work described in this section consisted primarily of measuring pinhole currents collected by a wide variety of test specimens in the plasma chamber under various conditions. Specifically, the following test sample parameters were varied: pinhole size, insulation type, area of electrode and surrounding insulation, shape of pinhole and type of insulation adhesive. Environmental and electrical parameters that were varied are: plasma density, voltage level and polarity, length of plasma exposure, and background pressure. In this section detailed descriptions of these tests have been grouped into the following subsections:

Subsection 4.2.1 Effect of Voltage, Pinhole Size, and Plasma Density

Subsection 4.2.2 Large Hole vs Pinhole

Subsection 4.2.3 Type of Insulation

Subsection 4.2.4 Insulation/Electrode Area Effects

Subsection 4.2.5 Slit vs Pinhole

Subsection 4.2.6 Type of Adhesive

Subsection 4.2.7 Short Life Tests

Subsection 4.2.8 Plasma Sheath Equipotential Lines

For an overall discussion of these tests and their implications see Section 5.1.

4.2.1 Effect of Voltage, Pinhole Size, and Plasma Density

Test Facility: LPC

Plasma currents collected by three different size holes in Kapton covering a high voltage disc electrode were measured at voltages up to 20 kV of both polarities. Tests were conducted at four different plasma densities. The Kapton sheet thickness was 0.005-inches (0.0127-cm) with hole diameters of 0.015 inches (0.038-cm), 0.060-inches (0.152-cm), and 0.150 inches (0.381-cm). The Kapton was bonded to a stainless steel disc with conductive epoxy and mounted in the Teflon test holder described in section 3.1.3. This test holder exposed a 3.5-cm diameter disc (9.6 cm² area) of the Kapton surface with the hole in the center facing the ion beam. The following paragraphs separately describe the positive and negative bias tests.

4.2.1.1 Positive Bias

The measured data for all through hole sizes is shown in Figure 13. At low voltages (< 40 volts) Figure 13 shows that the collected plasma currents are strongly dependent upon hole size and nearly independent of voltage. In this voltage range the collected plasma current density of the largest two holes is of the same order of magnitude as the random electron current

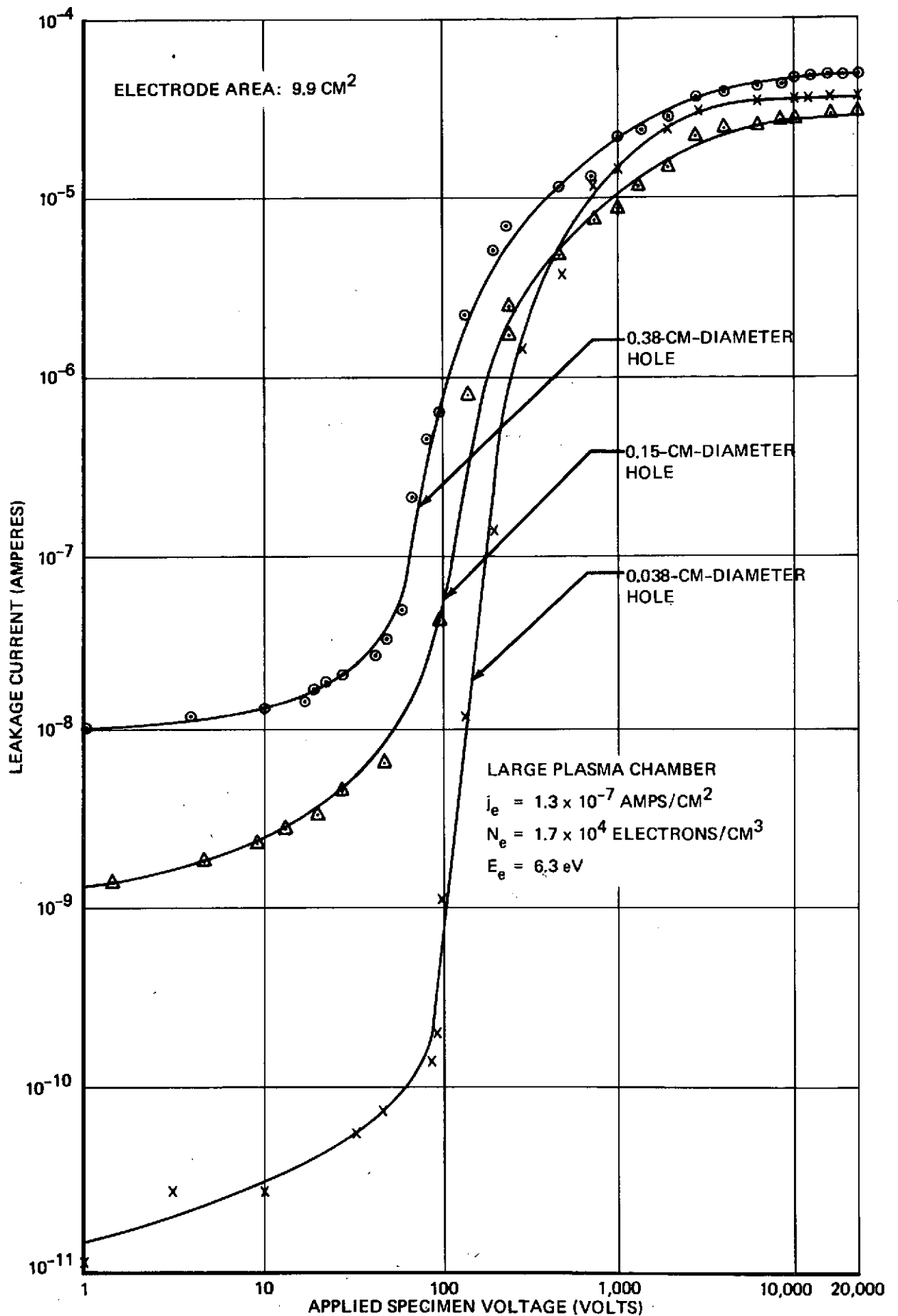


Figure 13 EFFECT OF VOLTAGE AND DEFECT SIZE ON LEAKAGE CURRENT—0.005-INCH-THICK KAPTON—POSITIVE ELECTRODE VOLTAGES

density calculated from Langmuir probe data. The relatively low plasma current density collected by the 0.015-inch diameter defect may be an insulation shielding effect; the hole diameter and depth, being nearly equal, make it a relatively "deep" hole whose walls limit the ability of the applied voltage to collect plasma electrons.

At intermediate voltages (+60 volts to +100 volts) the collected plasma currents start rising rapidly with increasing voltage while the effect of defect size diminishes. At high voltages (+1,000 volts to 20,000 volts) the currents for all three hole sizes are roughly equal and do not increase appreciably as voltage is increased.

The observed current saturation at high voltage was a surprise and at first was thought to be a limitation of the facility; e.g., perhaps the plasma source could provide no more current, or perhaps the limited size of the chamber walls restricted the ability of the holes' plasma sheath to collect current. To check these possibilities, the current collecting behavior of a 1.27-cm diameter sphere was measured under nearly the same plasma conditions with the sphere located close to where the pinhole had been. The result, shown earlier as the upper data in Figure 10, section 4.1, was that the sphere current never saturated and behaved according to theory, even though its current exceeded the pinhole saturation currents by a factor of 50. Thus it appears that the observed pinhole saturation is not a basic limitation of the plasma source or of the chamber size. As will be seen in the other pinhole data, this saturation is a repeatable phenomenon whose level depends primarily upon plasma density and area of insulation surrounding the pinhole.

Another surprise was the high level of the collected current at voltages above about 500 volts. Figure 14 shows that at high voltage the measured current for the smallest pinhole was several orders of magnitude larger than that calculated for a sphere having the same surface area as the pinhole. There is some evidence that this enhancement over what a sphere would collect is due to the presence of the insulation surface surrounding the pinhole (see Section 4.2.4 for a discussion of the "area effect"). It had been suggested that one reason for this is that the voltage from portions of the electrode covered by Kapton are felt by plasma electrons and thereby enhance the pinhole current collection. To test this possibility the above tests were repeated with a Kapton-covered electrode in the same test holder without any pinhole. The region in front of the specimen was investigated with a hot wire probe. With the probe within 0.635-cm of the Kapton surface, no potential could be sensed; specifically, it was still necessary to bias the hot wire probe positive relative to the plasma potential in order to produce electron emission from the hot wire probe. This result makes it seem unlikely that the electrode area under the insulation surrounding a pinhole contributes to the electron-collecting capability of the defect by virtue of electric fields extending through the insulation into the plasma.

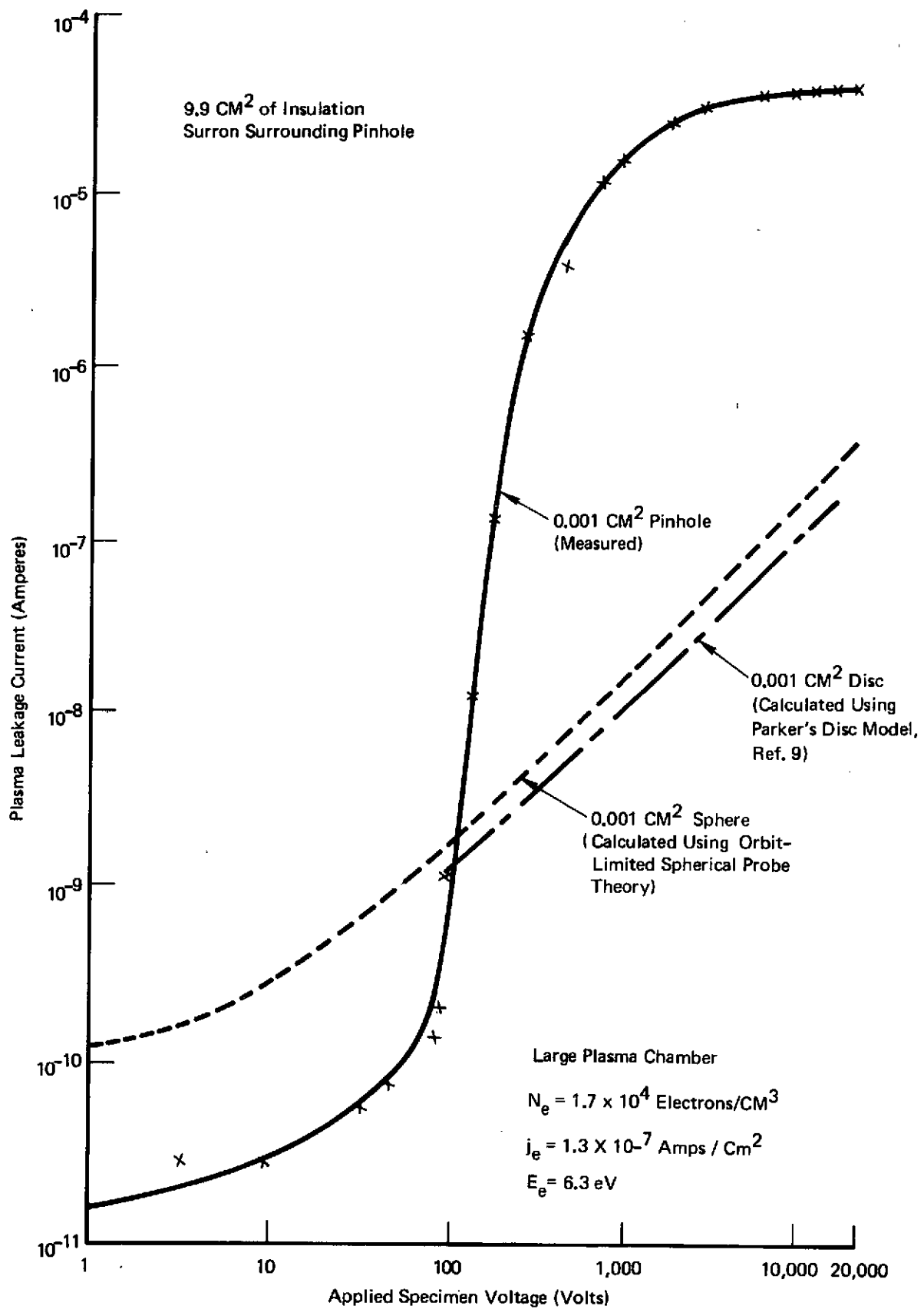


Figure 14: COMPARISON OF EQUAL-AREA PINHOLE AND SPHERE PLASMA LEAKAGE CURRENTS

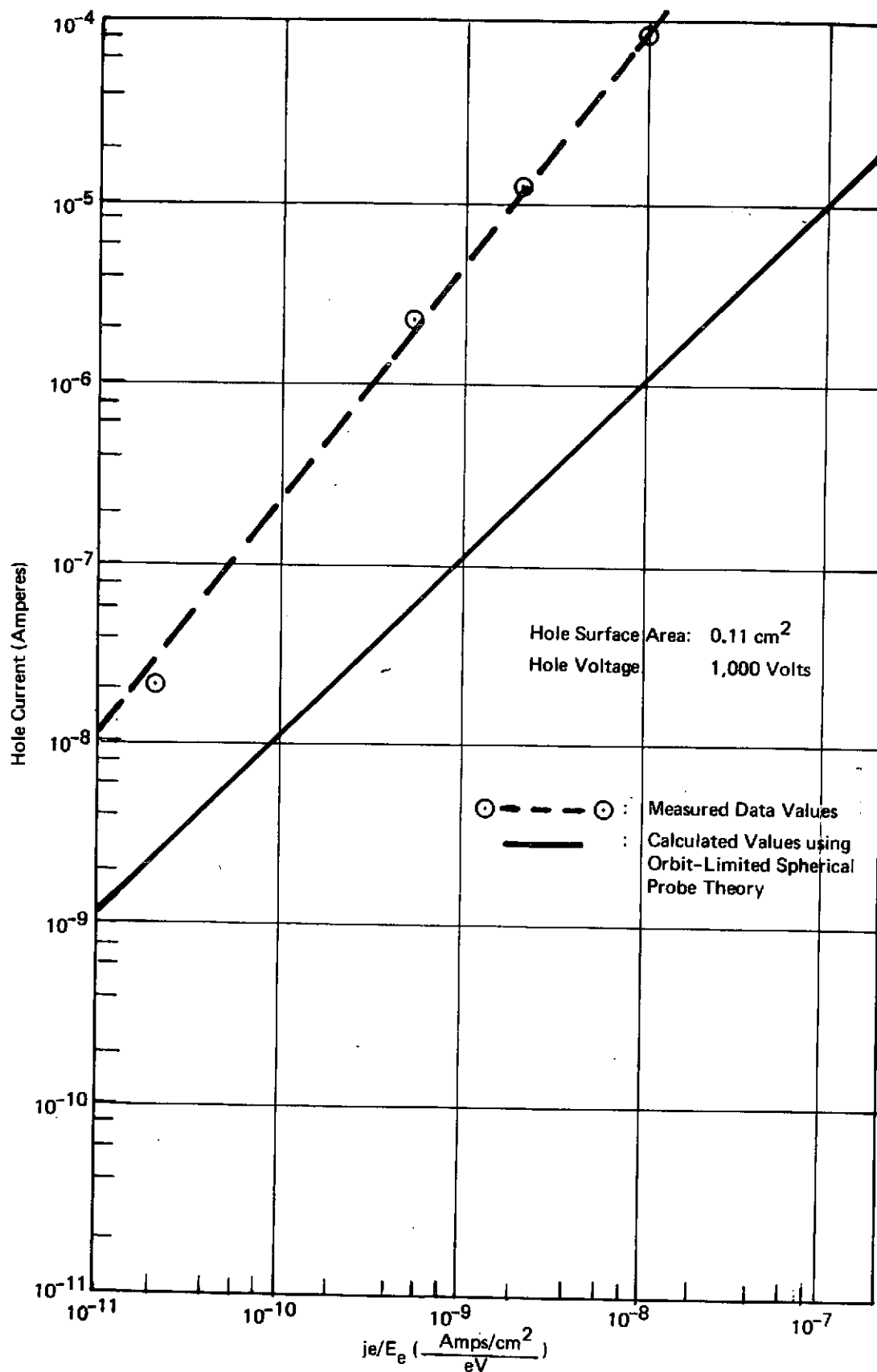


Figure 15 EFFECT OF PLASMA CONDITIONS ON THE LEAKAGE CURRENT COLLECTED BY A 0.38-CM-DIAMETER HOLE IN 0.005-INCH THICK KAPTON — COMPARISON WITH ORBIT-LIMITED SPHERICAL PROBE THEORY

Visual inspection of each defect after testing revealed only slight erosion of the hole. The tests had been run at +16,000 volts for only a few minutes with the plasma power loss at the pinholes being about 0.6 watts. The erosion was most evident in the 0.015-inch diameter hole, probably because the power per unit area dissipated in it was 100 times higher than in the 0.150-inch diameter hole.

Some additional tests were performed on the largest pinhole (0.38-cm diameter) at various plasma densities. The results, shown in Figure 15, indicate that at +1 kV the pinhole current is proportional to $(j_e/E_e)^{1.3}$ and exceeds that calculated for a sphere (with surface area equal to pinhole area) at all plasma density levels.

4.2.1.2 Negative Bias

The above test was repeated with negative bias voltages. A completely different current collecting phenomenon was observed. The data, shown in Figure 16, indicates that the hole size makes no difference even at low voltage, and saturation never occurs at high voltage. Instead, the current rise is in direct proportion to the $3/2$ power of voltage (approximately) over the entire voltage range.

One interpretation of this data is that the leakage current represents space-charge-limited ion flow between the exit screen of the plasma source and the specimen defect. This interpretation requires that an ion space charge sheath of constant thickness be formed around the defect, the thickness presumably being the distance between the specimen and exit screen. The reasoning behind this interpretation is as follows: Geometry is not expected to change the voltage dependence appreciably since the $V^{3/2}$ dependence holds for parallel plane electrodes, concentric cylinders, and spheres of constant separation. Except for geometry our test situation is similar to the simple case of two parallel planes (one emitting ions) separated by a distance d , which have an applied potential V between them. In this sample case, the Child-Langmuir $3/2$ -power law applies:

$$J = \frac{2}{mq}^{1/2} \frac{1}{d^2} V^{3/2} \quad (\text{Child-Langmuir } 3/2\text{-power Law})$$

where j = current density flowing between planes

m = ion mass

q = ion charge

d = distance separating planes

V = voltage between planes

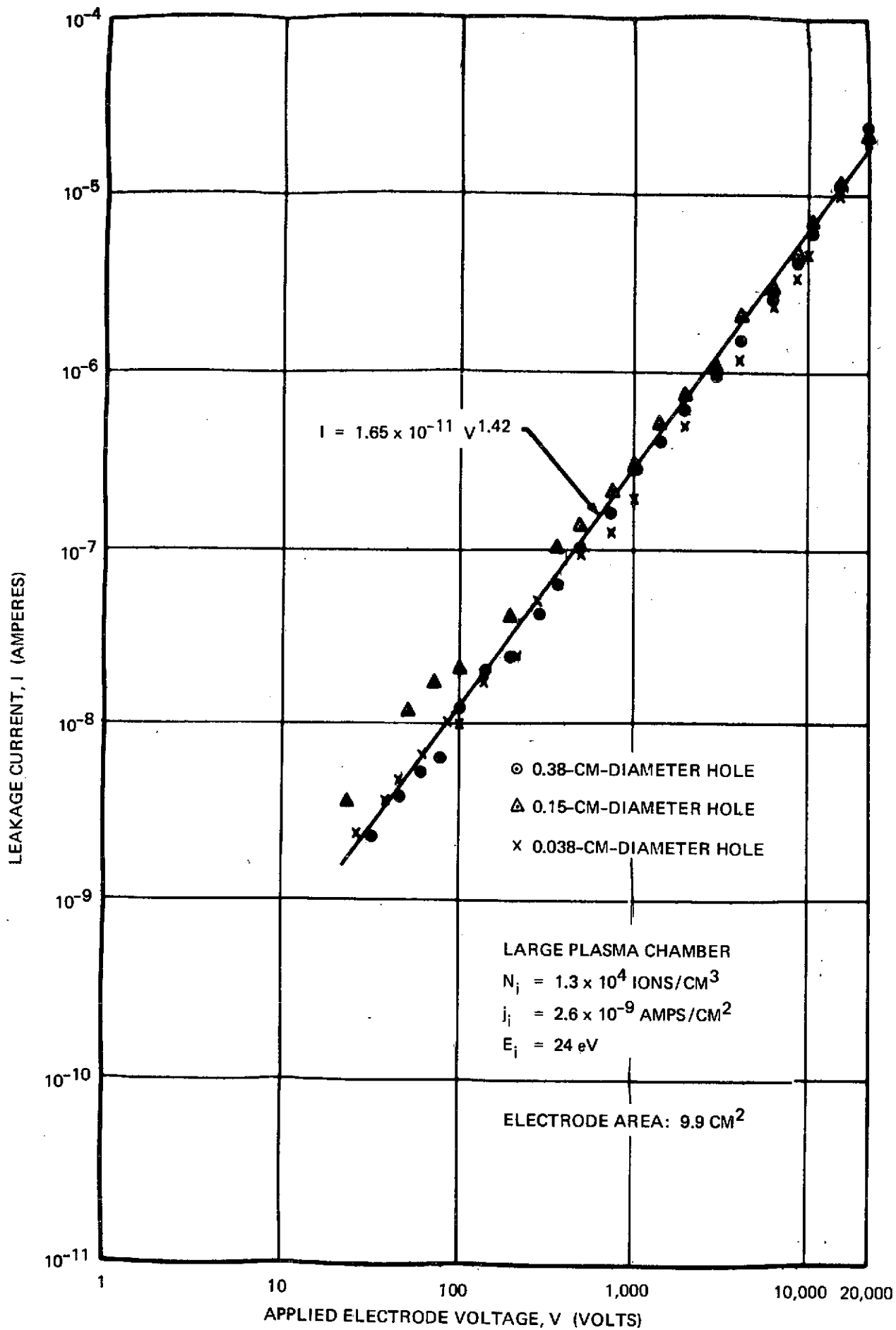


Figure 16 : EFFECT OF VOLTAGE AND DEFECT SIZE ON LEAKAGE CURRENT –
0.005-INCH-THICK KAPTON-NEGATIVE ELECTRODE VOLTAGES

Other possible explanations of the observed data should not be overlooked however.

4.2.2 Large Hole Versus Pinhole Test Facility: LPC

The tests in the preceding subsection indicated that pinhole size does not influence plasma current collection at voltages above about 1 kV. However since the pinhole areas were all insignificant compared with the amount of surrounding insulation area, it was decided to run some tests with a much larger hole (metal disc) where hole area and insulation area were more comparable (insulation area/disc area ≈ 6).

In these tests we measured the plasma currents collected by: (1) a 3.56 cm diameter aluminum disc (large hole) and (2) a 0.38 cm diameter hole (pinhole). These test samples were mounted in the Teflon test specimen holder described in Section 3.1.3. Only positive biases were applied.

Figure 17 shows the results for the pinhole and disc compared with the sphere data shown earlier (Figure 10, section 4.1). At the low voltages (< 40) volts the sphere and disc collect more current than the pinhole, presumably because of their larger surface area. At intermediate voltages (100 volts to 1000 volts) the currents of all three converge. At high voltage (+1,000 to +16,000 volts) the pinhole current saturates whereas the sphere current continues to rise in direct proportion to voltage. The disc current continues to rise but not as rapidly as the sphere current. This data suggests that the saturation has something to do with the relative amount of insulation around the plasma-collecting electrode: The sphere has no insulation and the current rises in proportion to voltage; the disc is surrounded by a small amount of insulation (the Teflon test holder) and its current tends toward saturation at the higher voltages. The pinhole is surrounded by a large amount of insulation (Kapton sheet and the Teflon test holder) and its current saturates very definitely at the high voltages. Similar results were obtained when the tests were repeated at lower plasma densities.

4.2.3 Pinhole Current Versus Type of Insulation Test Facility: LPC

The pinhole tests described in the preceding sections (4.2.1 and 4.2.2) utilized Kapton as the test insulation. In order to see if the results would be significantly different when other materials were used, the tests were repeated with 0.005-inch (0.0127-cm) thick FEP-Teflon and 0.006-inch thick microsheet glass. As in the earlier tests, the test holder described in section 3.1.3 was used. The results, shown in Figures 18 and 19, indicate that the same phenomenon of current saturation at high voltage, rapid rise of current at intermediate voltages, and hole size dependence at low voltage was observed with these materials as was observed in Kapton. A comparison of these figures with Figure 13 shows that the high voltage saturation levels were comparable for all three materials.

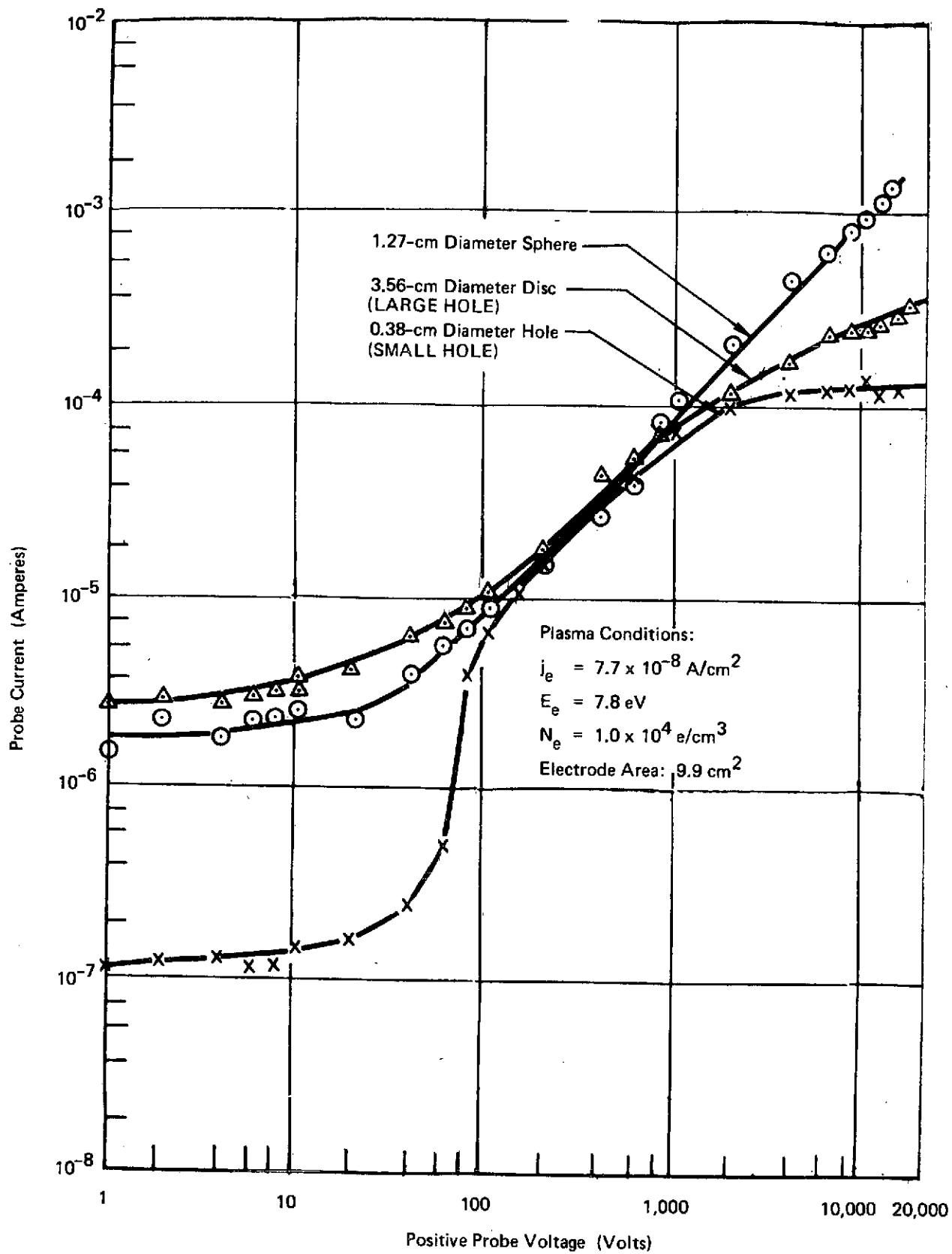


Figure 17: COMPARISON OF I - V CURVES OF A LARGE AND SMALL HOLE IN LARGE PLASMA CHAMBER - PLASMA NUMBER DENSITY: 1.0×10^4 ELECTRONS/ CM^3

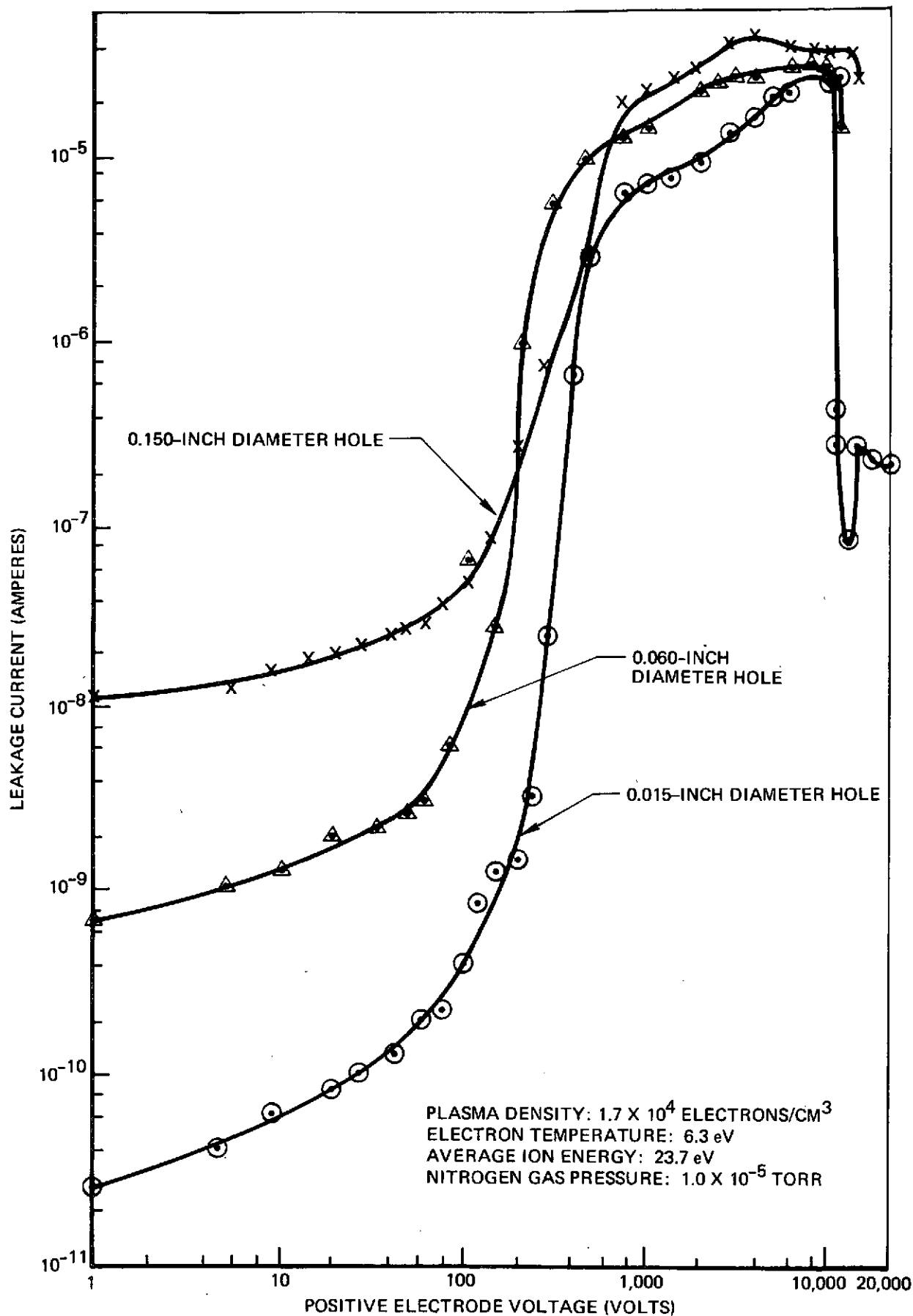


Figure 18: EFFECT OF VOLTAGE AND DEFECT SIZE ON LEAKAGE CURRENT - 0.005 FEP TEFLON

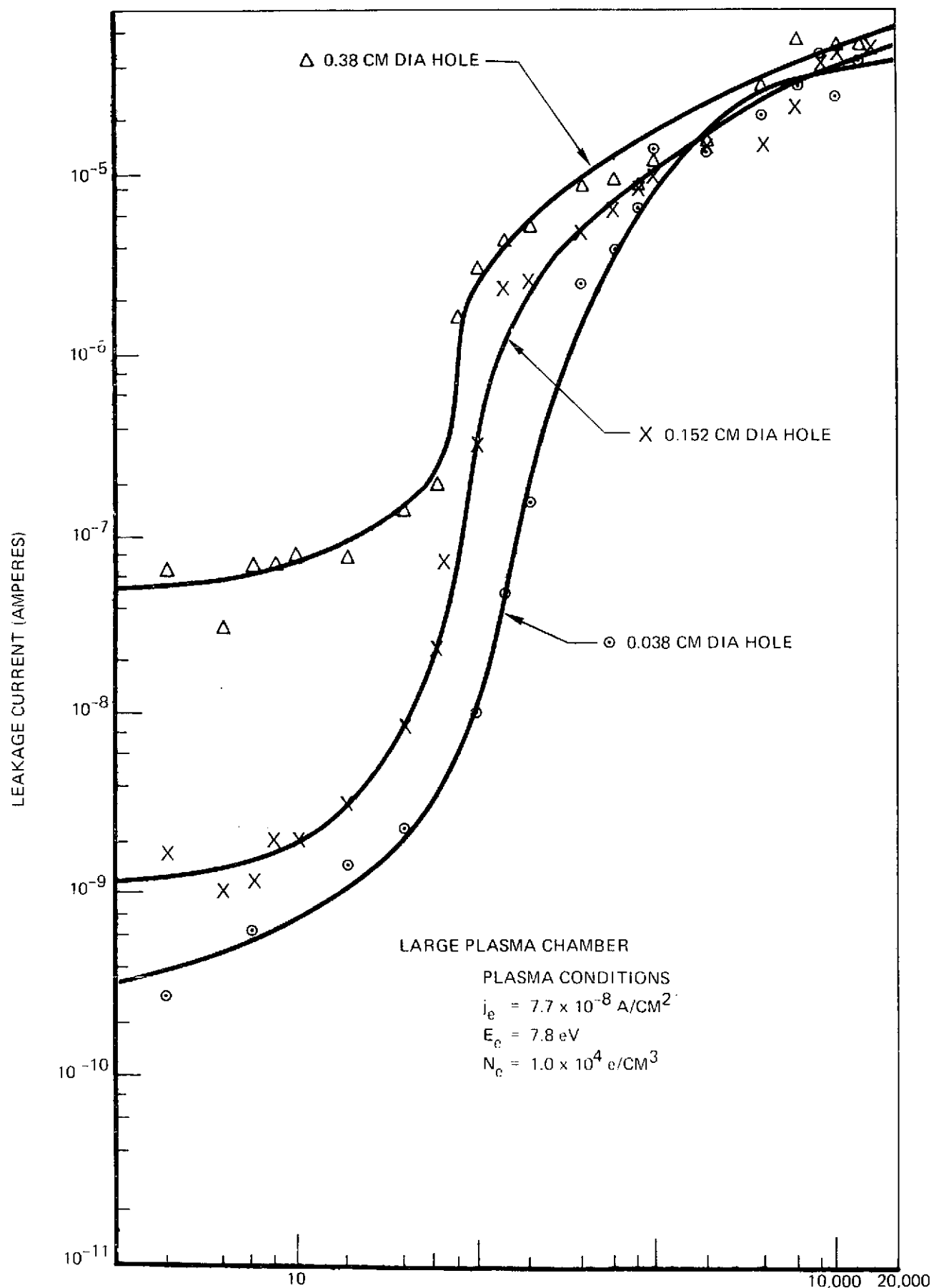


Figure 19: EFFECT OF VOLTAGE AND DEFECT SIZE ON LEAKAGE CURRENT – 0.006-INCH MICROSHEET GLASS

Table II: Leakage Current "Healing" in FEP-Teflon

Hole Diameter (inches)	Power Density at 10 kV (watts/cm ²)	Decrease in Leakage Current (percent)
0.150	3.5	25
0.060	19	57
0.015	307	99.8

Values represent power-per-unit area dissipated at current-collecting hole in Teflon sample when 10 kV was applied to electrode.

Values are given in percent of leakage current measured at 10 kV. The decrease occurred at voltages between 10 and 15 kV.

One difference in the Teflon data (Figure 18) compared with the Kapton data (Figure 13) was that the Teflon samples displayed a "healing" phenomenon (sudden decrease in leakage current) which was not observed with the Kapton samples. One explanation for this "healing" is that at high voltages the power dissipated at the hole is high enough to cause charring of the Teflon, leaving a residue on the exposed electrode which inhibits current collection. Visual inspection of the Teflon samples after test did reveal a black coating on the electrode which was not observed with Kapton samples.

Table II shows that the sample with the smallest hole (0.015-inch diameter) dissipated the most power per unit area (307 watts/cm²) and displayed the most "healing" (a 99.8% drop in current). The largest hole (0.150-inch diameter) dissipated the least power per unit area (3.5 watts/cm²) and displayed the least healing (a 25% drop in current).

4.2.4 Insulator/Electrode Area Effects

In all the pinhole tests described thus far (sections 4.2.1 through 4.2.3) the test specimens have essentially consisted of a 3.56-cm diameter metal disc (9.9-cm² area) covered with test insulation and recessed about .635-cm in a Teflon test holder. Since a pinhole in the substrate of a large area solar array will essentially be surrounded by a large, flat, high voltage electrode (other solar cells) covered by insulation (the rest of the substrate), several pinhole tests were run with larger Kapton-covered electrodes to see if the increased area would make any difference. The tests were limited to positive polarity tests.

4.2.4.1 Large Kapton-Covered Copper Plate Electrode (967 cm² per side) Test Facility: LPC

The test specimen consisted of a 10-inch (25.4-cm) by 15-inch (38.1-cm) copper plate surrounded by a plexiglass frame with 0.005-inch (.0127-cm) Kapton sheet bonded to both sides with R63-489 silicone adhesive. Electrical contact to the plate was made by soldering a high voltage lead to the copper plate through a small hole in the Kapton on the back side. This electrical connection was sealed from the plasma by a Teflon plug filled with R63-489 adhesive. To insure that the entire electrode was well sealed from the plasma, the entire unit was suspended in the plasma and voltages up to +10,000 volts applied. The measured currents (dotted line in Figure 20) correspond to Kapton bulk resistivity values of $>10^{14}$ ohm-cm at voltages between 2Kv and 10kV indicating that no "leaks" existed.

After a 0.038-cm (0.015-inch) diameter pinhole was put in the center of the Kapton surface facing the ion beam, the measured electrode currents (Figure 20) exceeded the values obtained without the pinhole by more than four orders of magnitude at high voltage. For purposes of comparison, a test was run with a smaller (3.5-cm diameter) Kapton-covered electrode having the same size pinhole. The smaller test specimen was held in the Teflon test holder described in section 3.1.3 and located adjacent to the large copper plate, facing the ion beam. Measured pinhole currents for both tests, run within a few minutes of each other, are shown in Figure 21. Note that at voltages above 800 volts the larger electrode collects much more current; at lower voltages the currents are comparable. Also

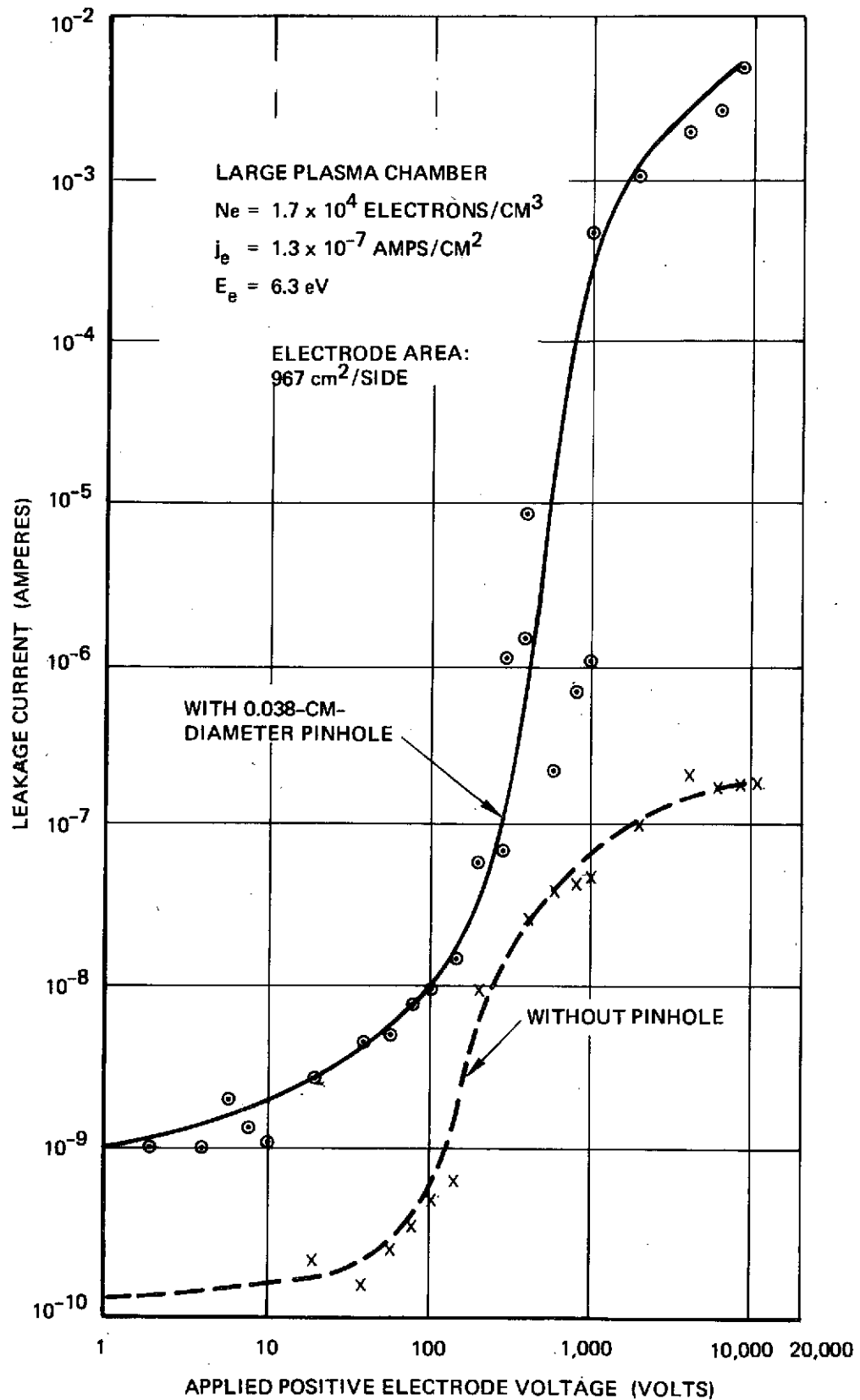


Figure 20: LEAKAGE CURRENT COLLECTED BY A 10-INCH BY 15-INCH COPPER PLATE
 ENCAPSULATED IN 0.005-INCH THICK KAPTON - WITH AND WITHOUT A DEFECT

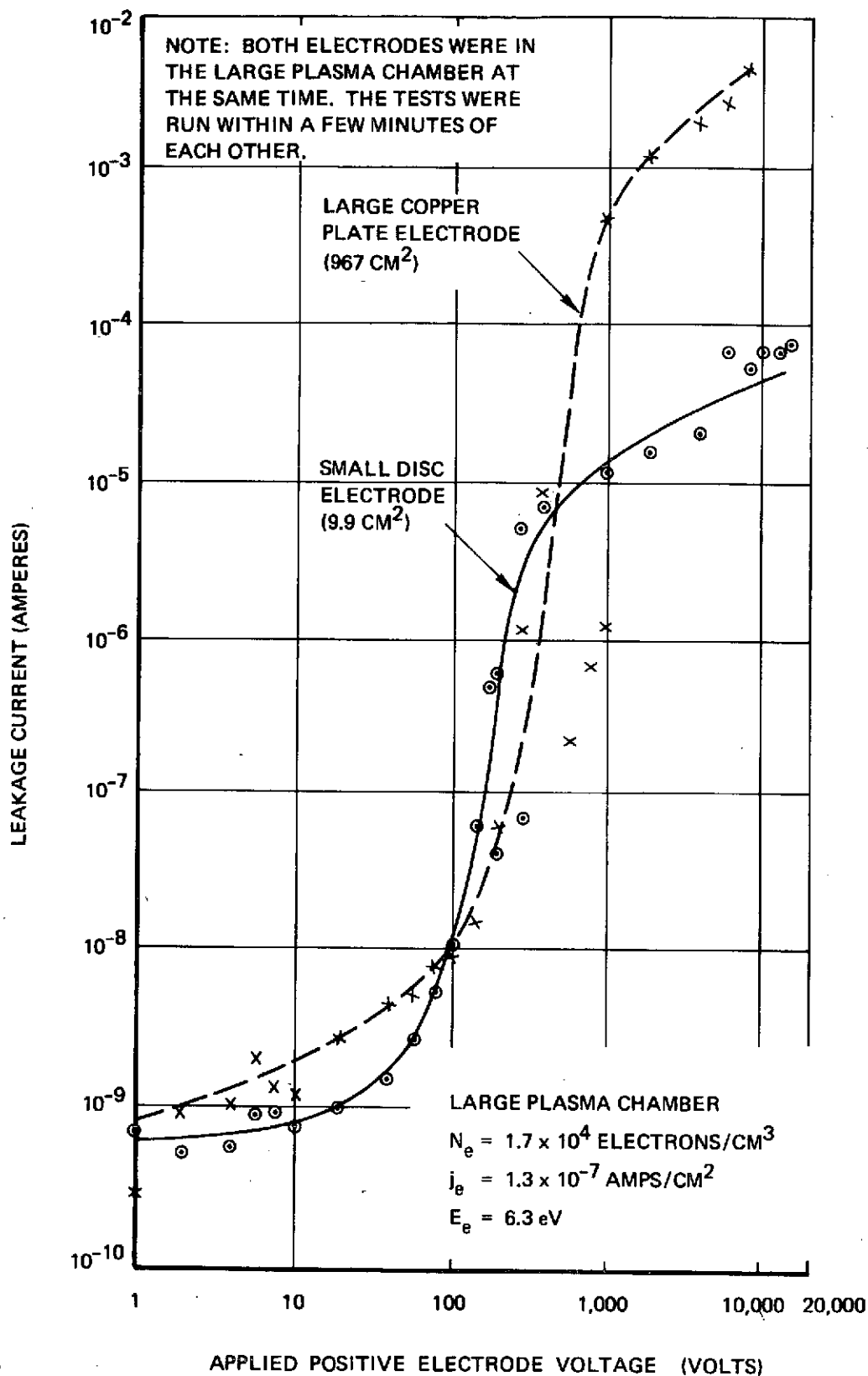


Figure 21: EFFECT OF ELECTRODE SIZE ON THE PLASMA LEAKAGE CURRENT COLLECTED BY A 0.015-INCH-DIAMETER PINHOLE IN 0.005-INCH-THICK KAPTON

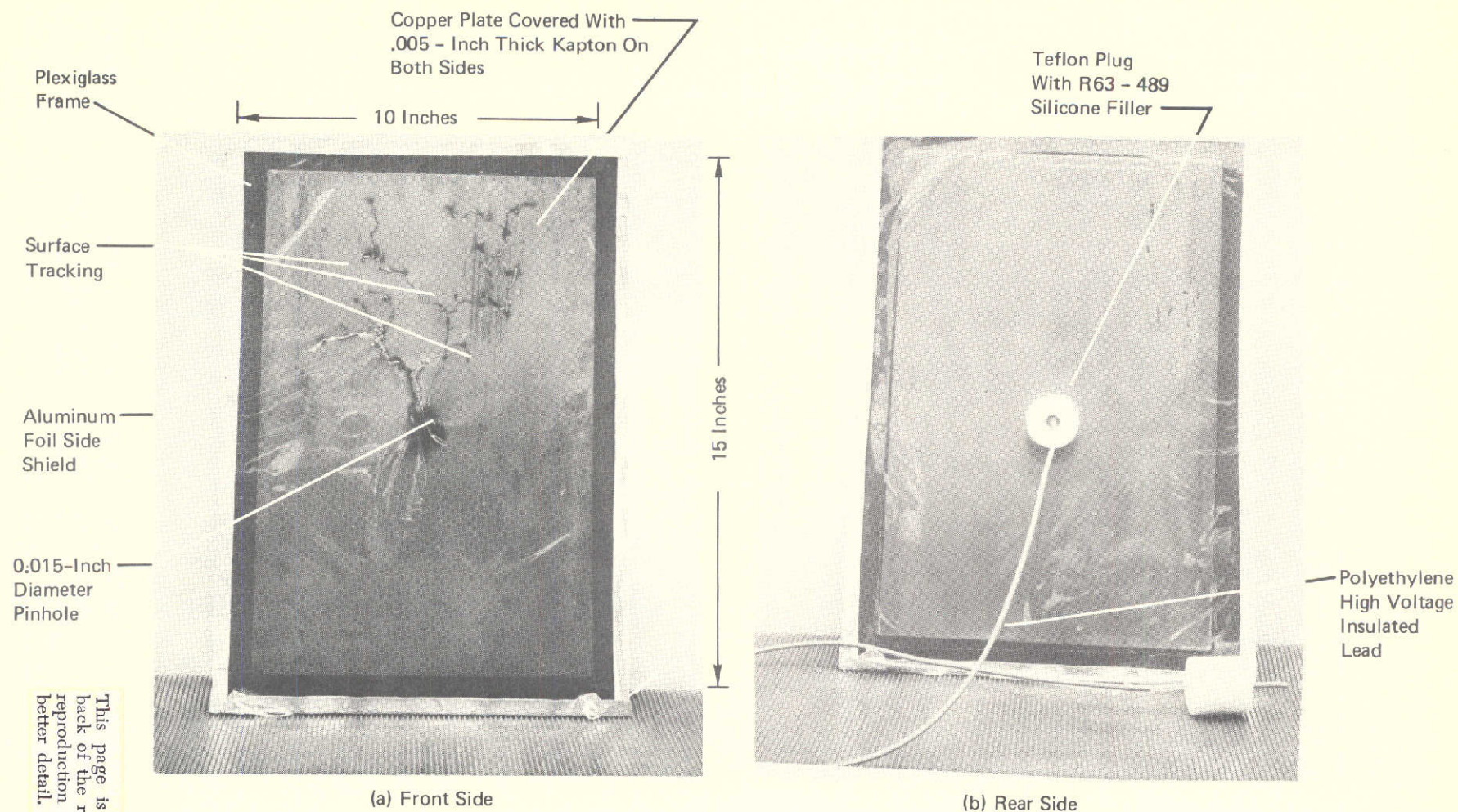


Figure 22: SURFACE TRACKING AROUND A PINHOLE IN KAPTON AFTER 10 MINUTES EXPOSURE TO PLASMA AT A+10,000 VOLT ELECTRODE VOLTAGE

This page is reproduced at the back of the report by a different reproduction method to provide better detail.

note that the smaller test specimen exhibited onset of current saturation at high voltages even though there obviously was more current available from the plasma (as evidenced by the high current collected by the larger sample). It is interesting to note that the ratio of the Kapton-covered electrode areas facing the ion beam for these specimens ($967\text{-cm}^2/9.9\text{-cm}^2 = 98$) is not too different from ratio of the currents at high voltage (e.g., at 10kV: $5 \times 10^{-3} \text{ amps}/7 \times 10^{-5} \text{ amps} = 71$). This raises the important question, as yet unanswered, "Does the amount of surface area surrounding a pinhole increase the pinhole plasma current and, if so, does the effect increase with increasing area?"

Post test examination of the large area electrode revealed heavy surface tracking in the exposed portion of the Kapton surrounding the pinhole (Figure 22). In places along the tracks the Kapton had melted all the way through to the copper electrode. Several other pinholes had developed at random locations along the tracks. This tracking had occurred during a period of about five minutes when the voltage was above 1,000 volts (the entire test on the large electrode only lasted 15 minutes). Observations through the vacuum chamber window during the high voltage portion of the test had revealed a bright red spot at the pinhole site and the dark track had been seen growing from there along the Kapton surface. It is not too surprising that this tracking occurred since at +10kV the power dissipated in the vicinity of the pinhole was 50 watts (or $50,000 \text{ watts/cm}^2$ if dissipation is confined to pinhole area).

4.2.4.2 Large Kapton-Covered Aluminum Electrode (506 cm^2 per side) Test Facility: LPC

It has been suggested that uncured adhesive and the observed heavy tracking observed in Kapton in the large-electrode test described in the preceding section (4.2.4.1) was the cause of the excessively high currents observed. Therefore, another large electrode test was performed with extra care taken to insure that the test specimen contained no uncured adhesive. Also, the test was conducted at a lower plasma density to lessen the possibility of tracking so that the main difference between this test and other small electrode tests was the electrode area size.

The new test specimen consisted of an aluminum foil disc (506 cm^2 surface area per side) encapsulated between two sheets of 0.005-inch (0.0127-cm) Kapton having 929 cm^2 of surface area per side. Figure 23 shows the leakage current with and without a 0.015-inch (0.038-cm) diameter pinhole with positive voltage applied. Clearly a good plasma seal had been obtained prior to creation of the pinhole. Figure 24 compares this pinhole data with data taken under similar conditions with a smaller electrode. As in the results described in the preceding section (4.2.4.1), the larger electrode collects more current. Also it is noted that the ratio of the Kapton-covered electrode areas facing the ion beam for these specimens ($506 \text{ cm}^2/9.9 \text{ cm}^2 = 50$) is not too different from the ratio of the currents at high voltage (e.g., at 10kV: $3 \times 10^{-4} \text{ amps}/1.5 \times 10^{-3} \text{ amps} = 20$).

Post test examination of the large area electrode revealed a small amount of darkening around the pinhole and the existence of a single surface track which started at the pinhole and wandered outward for a total track length of about 6-cm (see Figure 25).

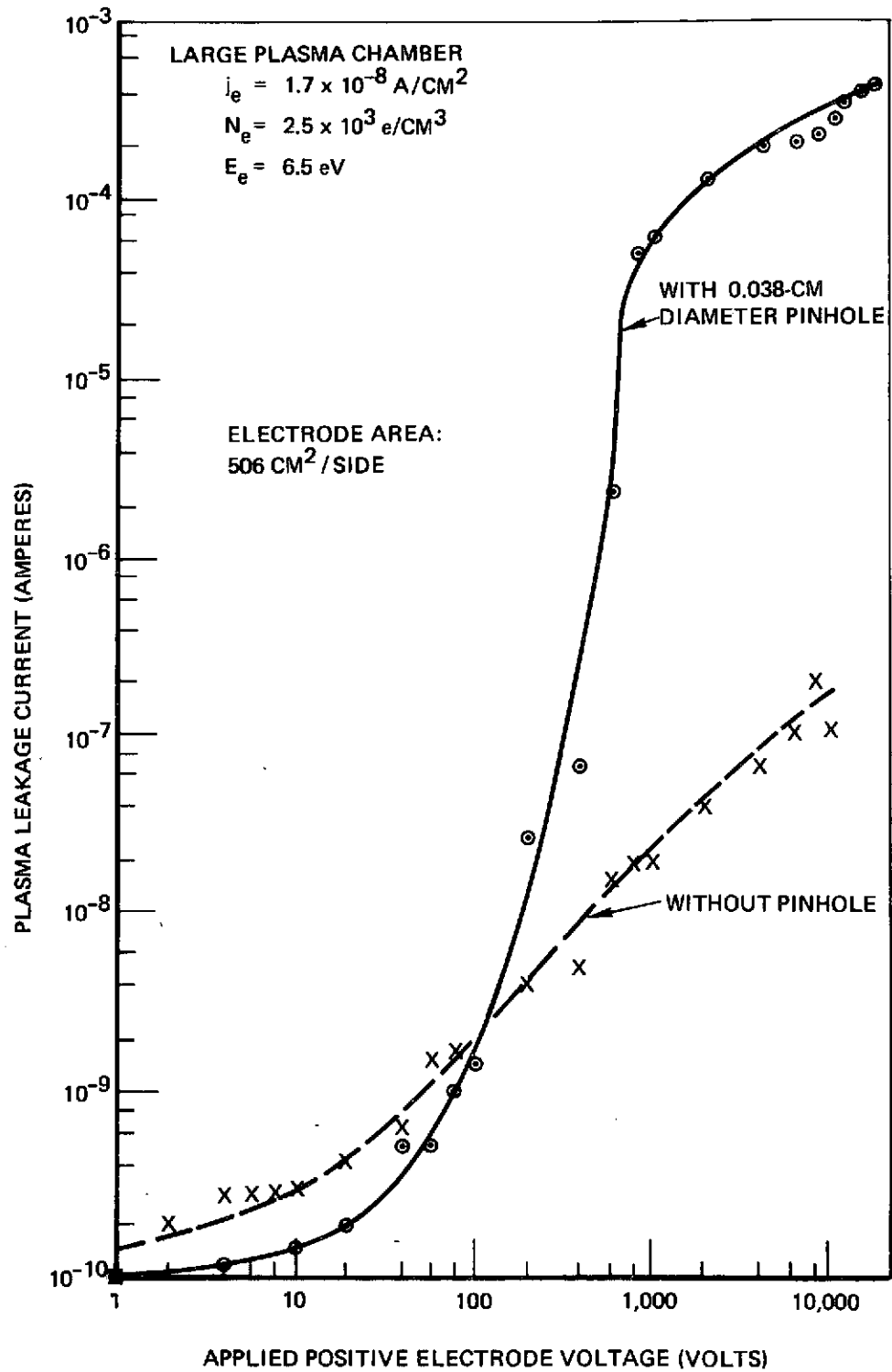


Figure 23 LEAKAGE CURRENT COLLECTED BY A 10-INCH DIAMETER ALUMINUM DISC ENCAPSULATED IN 0.005-INCH THICK KAPTON – WITH AND WITHOUT A DEFECT

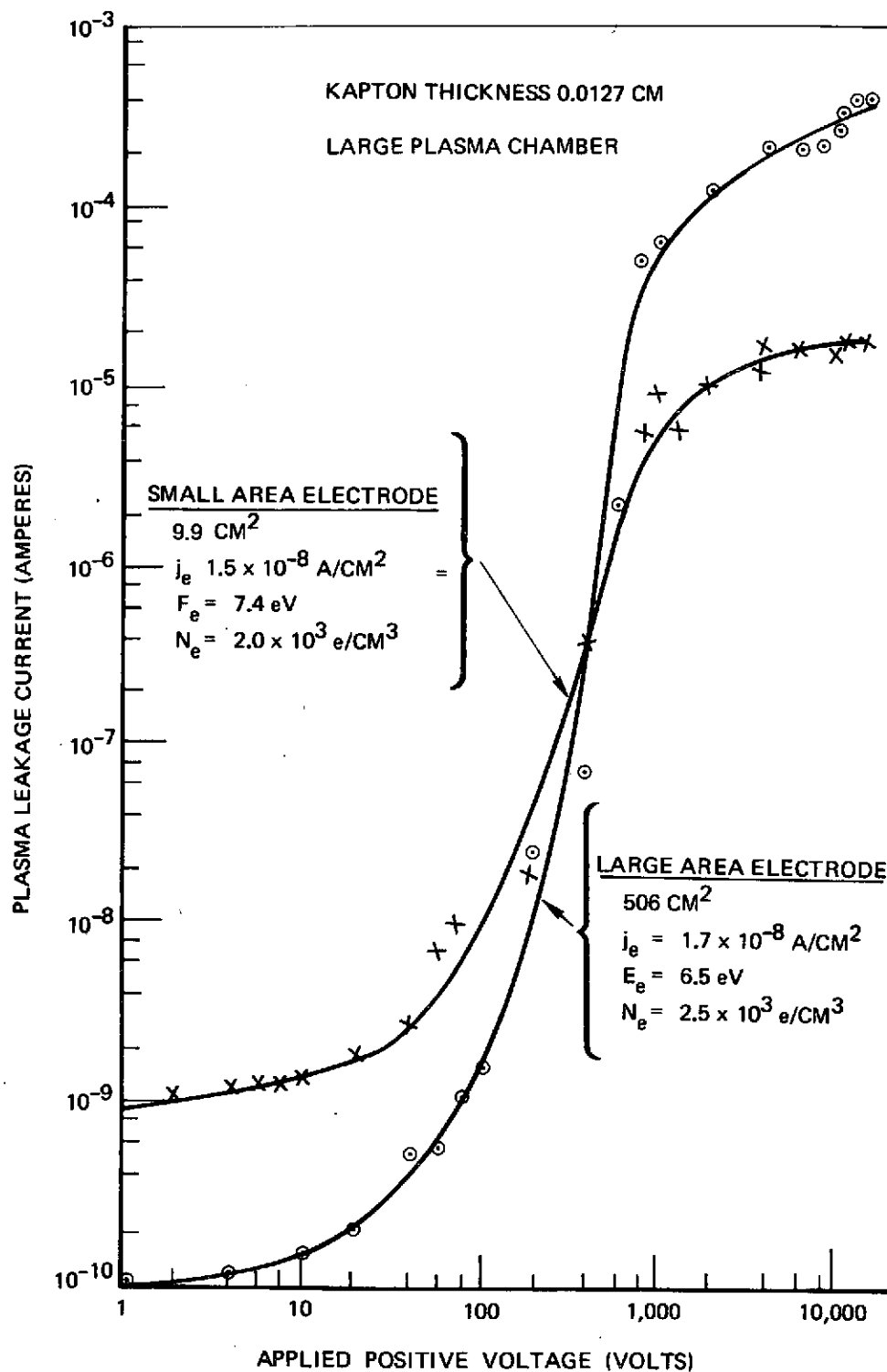


Figure 24 PLASMA LEAKAGE CURRENT COLLECTED BY 0.038-CM PINHOLES
IN LARGE- AND SMALL-AREA KAPTON-COVERED ELECTRODES

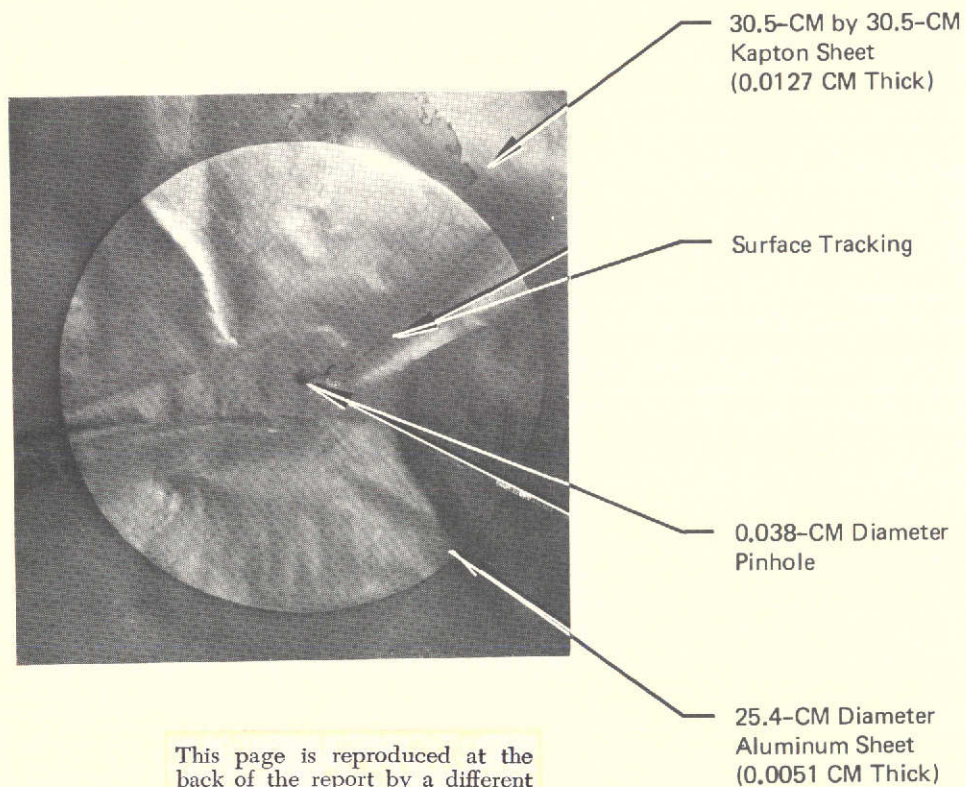


Figure 25: PHOTOGRAPH OF LARGE AREA DISC ELECTRODE

4.2.5 Slit vs. Pinhole Current Collection

Test Facility: LPC

The tests described in section 4.2.1 showed how different size pinholes in Kapton collected plasma current. A test was repeated with the identical test setup and identical test specimens except that the pinhole was replaced by a 0.5-cm long slit made with a surgical knife. The resulting currents collected by the slit are compared in Figure 26 with those obtained earlier with a .015-inch diameter pinhole. Apparently, the form of small defects does not affect their current collecting capability significantly. A track on the exposed surface of the Kapton was observed after only a few minutes of high voltage exposure. The observed track started at one end of the slit and terminated at the outside boundary of exposed portion of the Kapton. No such tracking had been observed in the pinhole samples tested at this same plasma density. It is possible that the slit opening is so small that the resulting power density per unit area is higher than in the small pinhole, this causing localized heating which promoted the tracking.

4.2.6 Effect of Adhesive

In most of the small electrode pinhole tests described in the preceding sections the Kapton insulation was bonded to the electrode with a conductive epoxy. However, in the large electrode tests R63-489 silicone adhesive was used as the bonding agent. To see if there was a difference due to adhesive, a small electrode pinhole test was conducted with the R63-489 used as the Kapton adhesive. Test conditions were identical to those described in section 4.2.1. As seen in Figure 27, the collected current was not affected by the type of adhesive used.

4.2.7 Short Life Tests

Several short life tests were conducted on pinhole test samples. Table III summarizes the results for Kapton indicating that tracking and darkening started at power levels between 0.5 and 5 watts. FEP Teflon showed a greater resistance to darkening and tracking. Details of the tests are described below.

4.2.7.1 Large Plasma Chamber Test

Two identical life tests were conducted in which a Kapton-covered disc having a 0.015-inch (.038-cm) diameter pinhole in the Kapton was maintained at +3,000 volts in the LPC at a fixed plasma density. In both tests the Teflon test holder described in section 3.1.3 was used with the pinhole facing the ion beam. The leakage current was monitored approximately once every two hours. Figure 28 shows that in neither test was there a catastrophic increase in current. On the average, the leakage current in Sample No. 1 increased by about a factor of 2; in Sample No. 2 the leakage current remained fairly constant. Post test inspection of both samples revealed erosion of the original 0.038-cm diameter pinhole resulting in a larger 0.229 cm (0.090-inch) hole.

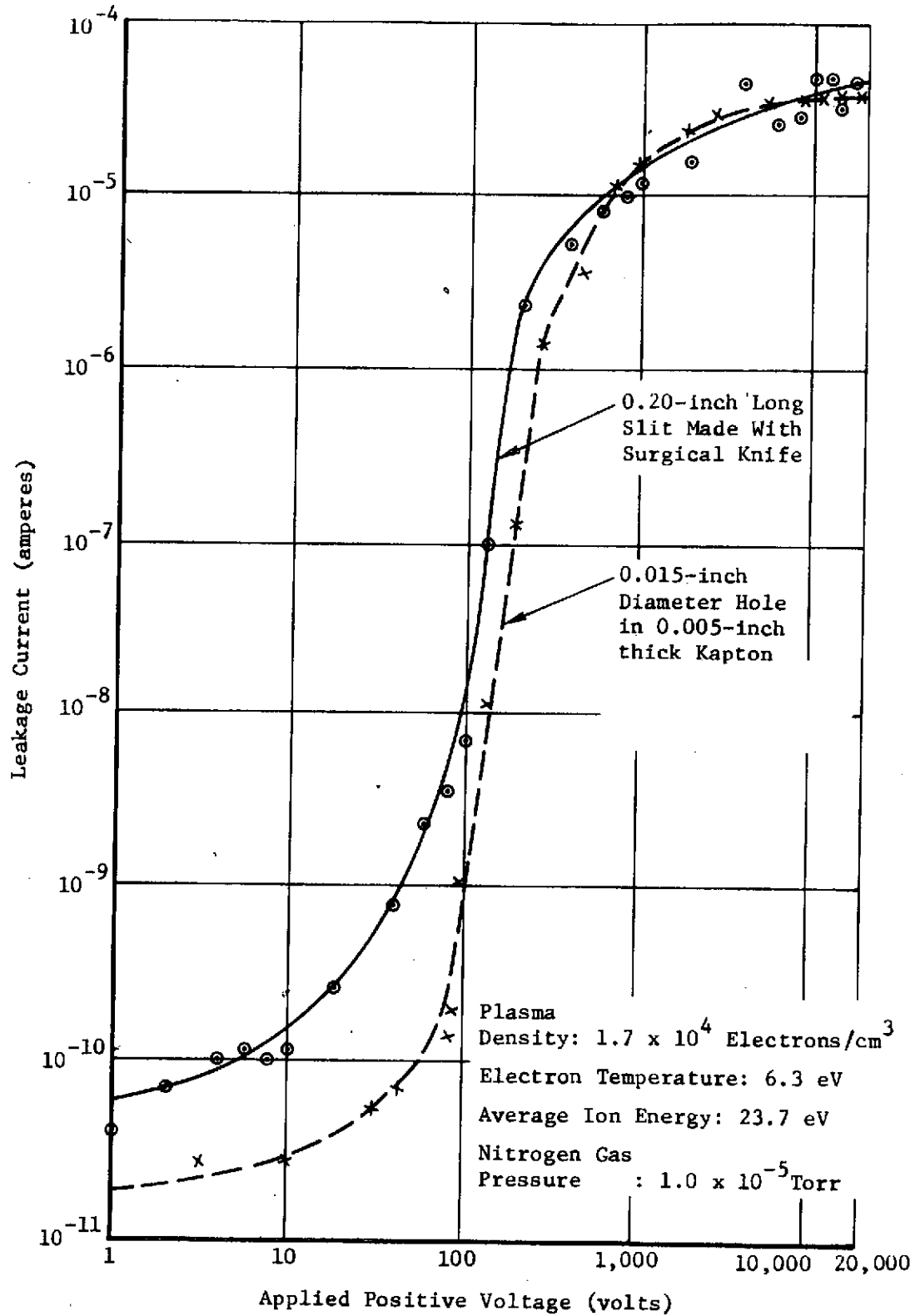


Figure 26: LEAKAGE CURRENT COLLECTED BY A SLIT IN 0.005-INCH THICK KAPTON IN THE LARGE-SCALE PLASMA SIMULATOR

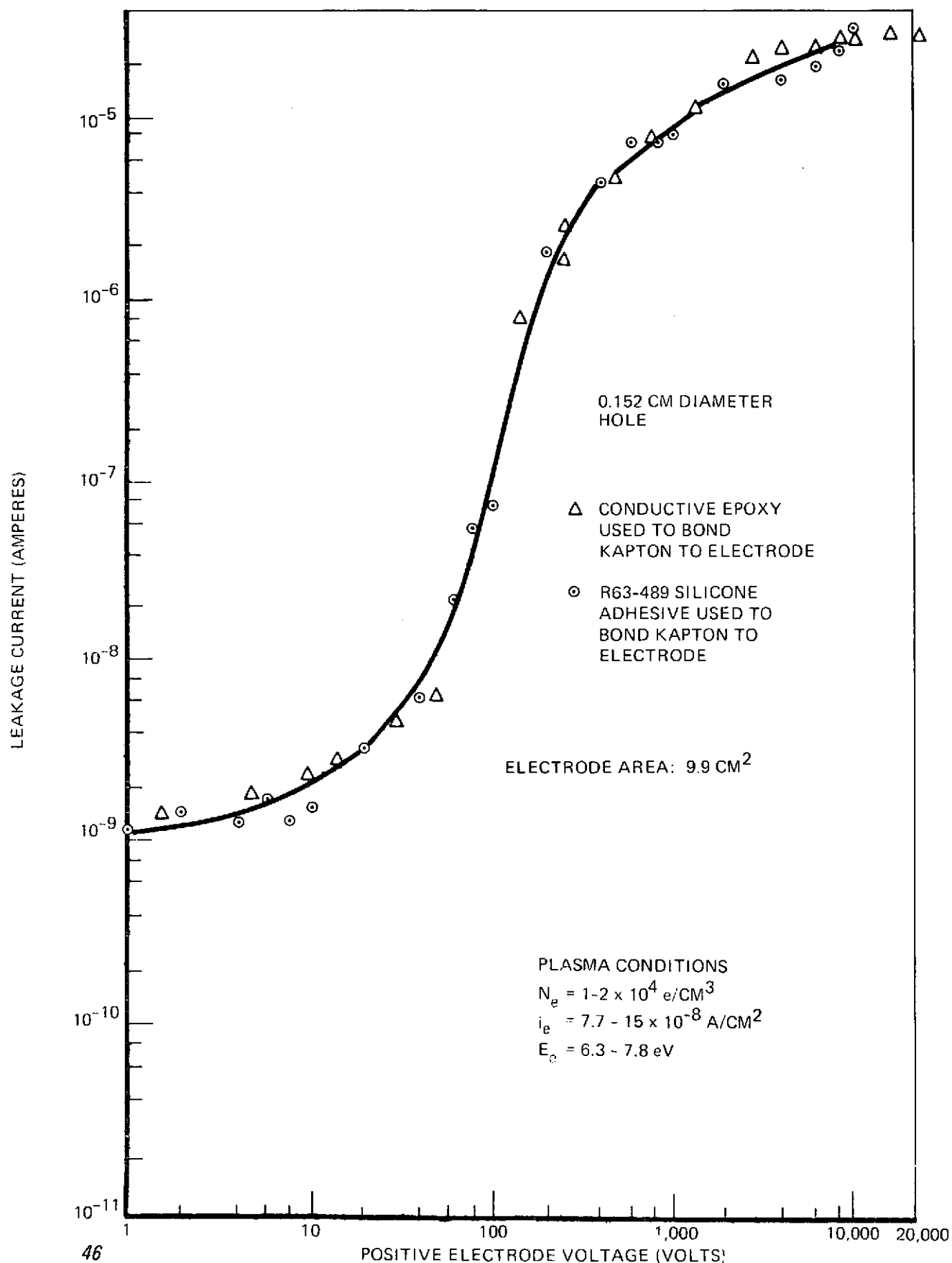


Figure 27 COMPARISON OF PLASMA LEAKAGE CURRENT TO PINHOLES IN KAPTON BONDED TO ELECTRODES WITH DIFFERENT ADHESIVES

TABLE III: DAMAGE DUE TO PINHOLE CURRENTS

POWER (WATTS)	VOLTAGE (VOLTS)	CURRENT (AMPS)	DURATION	DEFECT	TRACKING	DARKENING
50	+10,000	5×10^{-3}	FEW MINUTES	0.15"-DIA HOLE	HEAVY	YES
5	+10,000	5×10^{-4}	FEW MINUTES	.015"-DIA HOLE	MILD	YES
1	+10,000	1×10^{-4}	3 DAYS	.015"-DIA HOLE	NONE	YES
0.5	+10,000	5×10^{-5}	FEW MINUTES	SLIT	MILD	NO
0.01	+10,000	1×10^{-6}	11 DAYS	.015"-DIA HOLE	NONE	NO

FOR SMALL HOLES, TRACKING STARTS AT 0.5 TO 5 WATTS

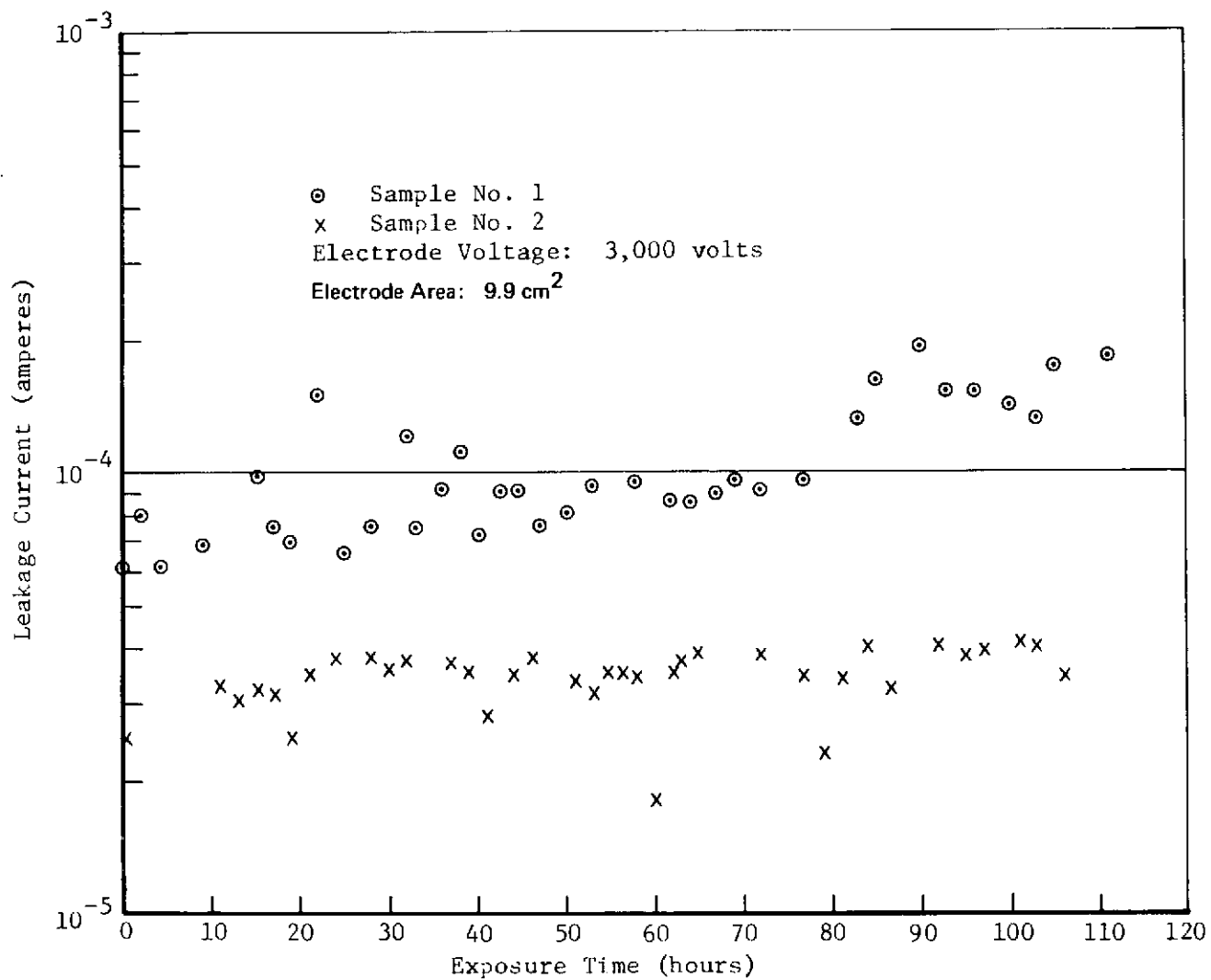


Figure 28 PLASMA LEAKAGE CURRENT VS TIME COLLECTED BY A 0.015-INCH-DIAMETER PINHOLE IN 0.005-INCH THICK KAPTON - POSITIVE ELECTRODE VOLTAGE

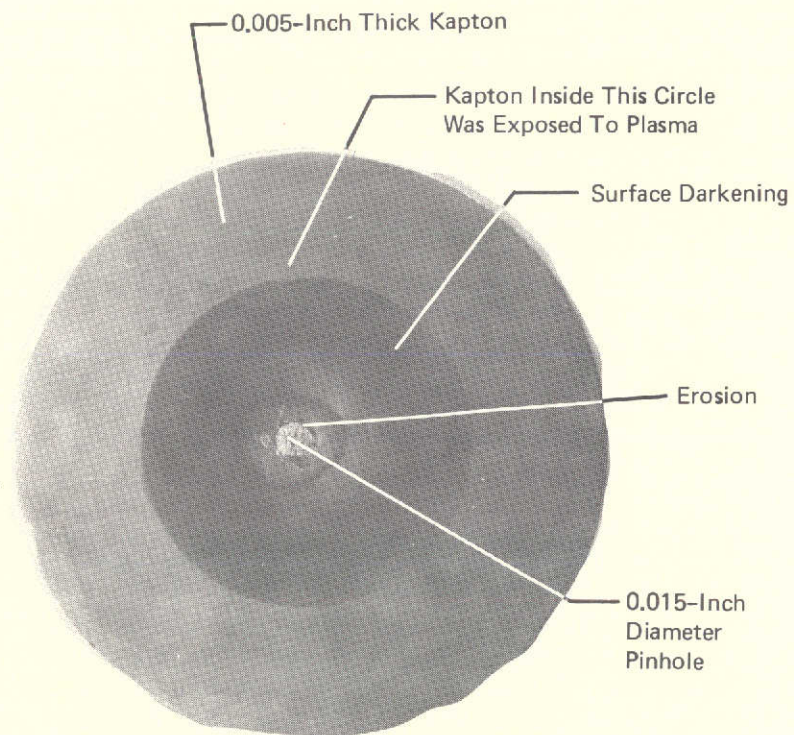


Figure 29: EROSION AND SURFACE DARKENING AROUND A PINHOLE IN KAPTON AFTER MORE THAN 4 DAYS EXPOSURE TO PLASMA WITH A +3,000-VOLT ELECTRODE VOLTAGE

This page is reproduced at the back of the report by a different reproduction method to provide better detail.

In addition, a darkening of the entire exposed surface was observed in both samples although no surface tracking was evident (Figure 29). An infrared analysis of the samples indicated that most of the darkening was a layer of carbon from an unknown source. Near the hole the Kapton itself had turned black.

4.2.7.2 Small Plasma Chamber Test

Two pinhole test specimens (Figure 30) were subjected to a plasma life test. One specimen utilized .0127-cm thick FEP Teflon test insulation bonded to the electrode with Dow Corning 93-072 silicone adhesive. The electrode voltage was maintained at +10kV while the pinhole current was maintained at 1×10^{-4} amperes. After 69 hours of exposure, the hole in the Teflon had enlarged to 0.64 cm diameter and the entire outer surface of Teflon (an 8.3 cm diameter disc) had become coated with a grayish film that could be dissolved and washed away with methyl ethyl ketone (MEK). The Teflon under the film appeared to be unaffected by the life test. During the test, bright red spots in the vicinity of the pinhole could be seen and it is nearly certain that the observed grayish film was comprised of FEP Teflon or 93-072 adhesive vaporized from the hot pinhole region and redeposited on the surrounding Teflon surface. That the grayish film did not come from another part of the vacuum chamber is substantiated by the fact that (1) no such film could be found on any other surfaces in the chamber and (2) the film was darker near the pinhole region.

Concurrent with this test, an identical experiment was conducted in the same vacuum chamber with Kapton test insulation and a larger pinhole (0.38-cm diameter). Because the pinhole was larger, the power per unit area dissipated at the pinhole was less than the Teflon experiment and pinhole did not become bright red. No deposited film was found on the Kapton (presumably because the pinhole did not become hot enough to vaporize), however, the entire outside Kapton surface surrounding the hole had turned completely black after the 69 hour exposure (@ +10kV and 1×10^{-4} ampere pinhole current).

4.2.8 Plasma Sheath Equipotential Lines Test Facility: LPC

As a means of providing additional insight to the current-collecting behavior of pinholes, discs and spheres a hot wire probe was used to measure the equipotential lines surrounding these electrodes while they were collecting plasma current at the levels shown in Figure 17 at +10,000 volts. Figure 31 shows the resulting sheath voltages plotted as a function of distance from each electrode. Note that the voltages from the sphere extend farther into the plasma than those for the disc which, in turn, extend farther than those of the pinhole. Thus, it is not strange that the current collected by the electrode follows the same pattern with the sphere current being highest (3×10^{-5} amperes), the disc current being next (7×10^{-6} amperes), and the pinhole current being lowest (5.5×10^{-6} amperes).

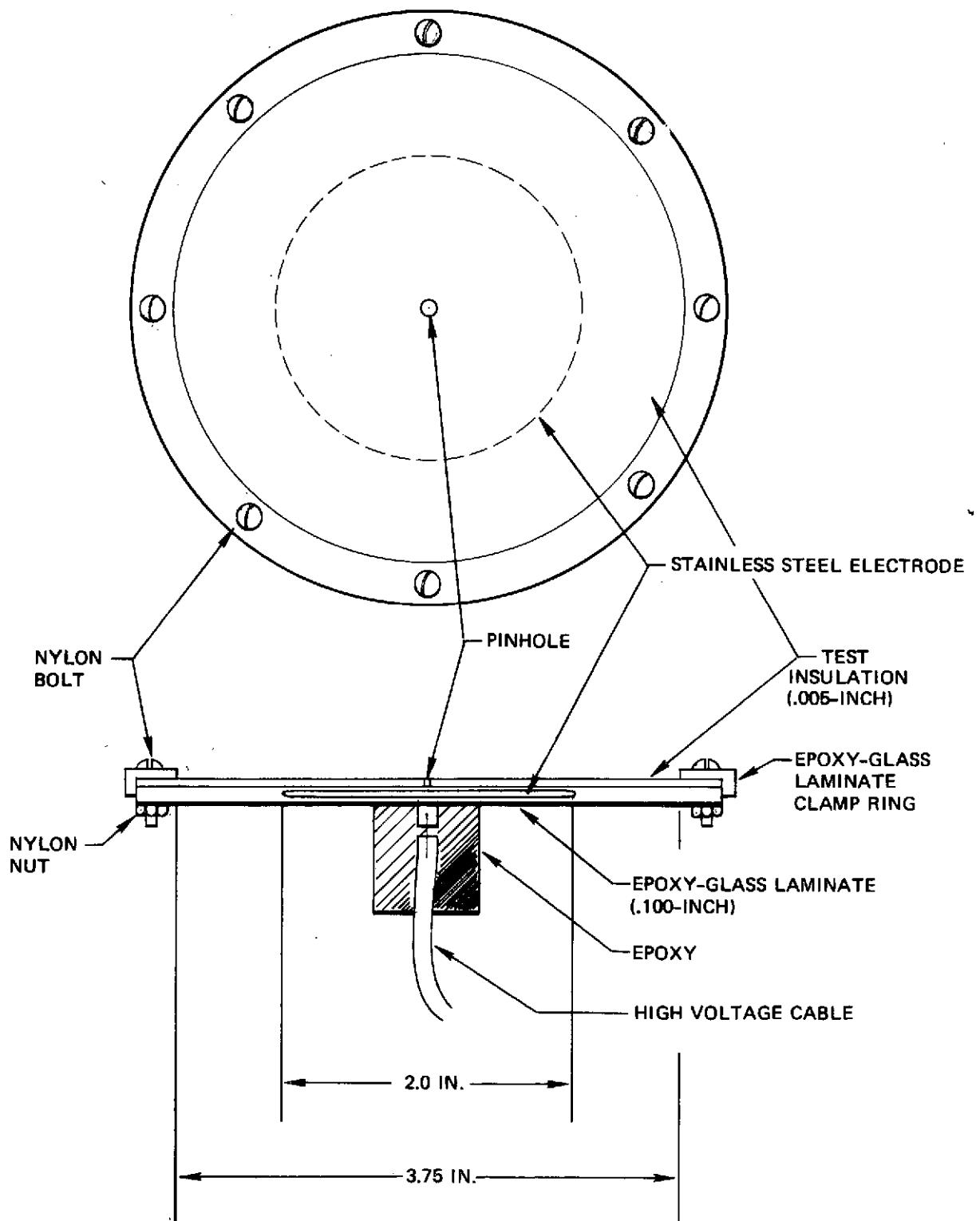


Figure 30: PINHOLE TEST SPECIMEN

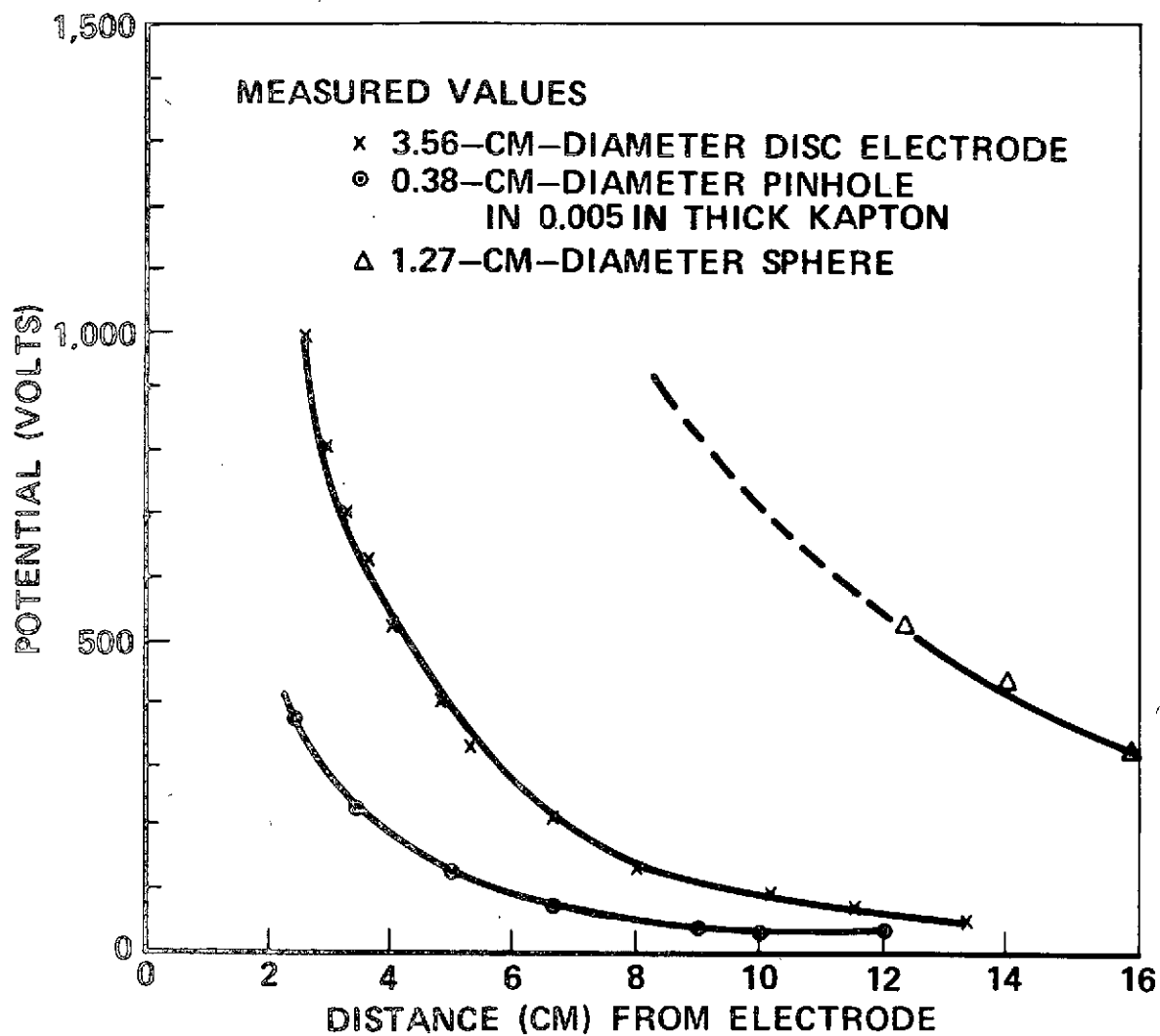
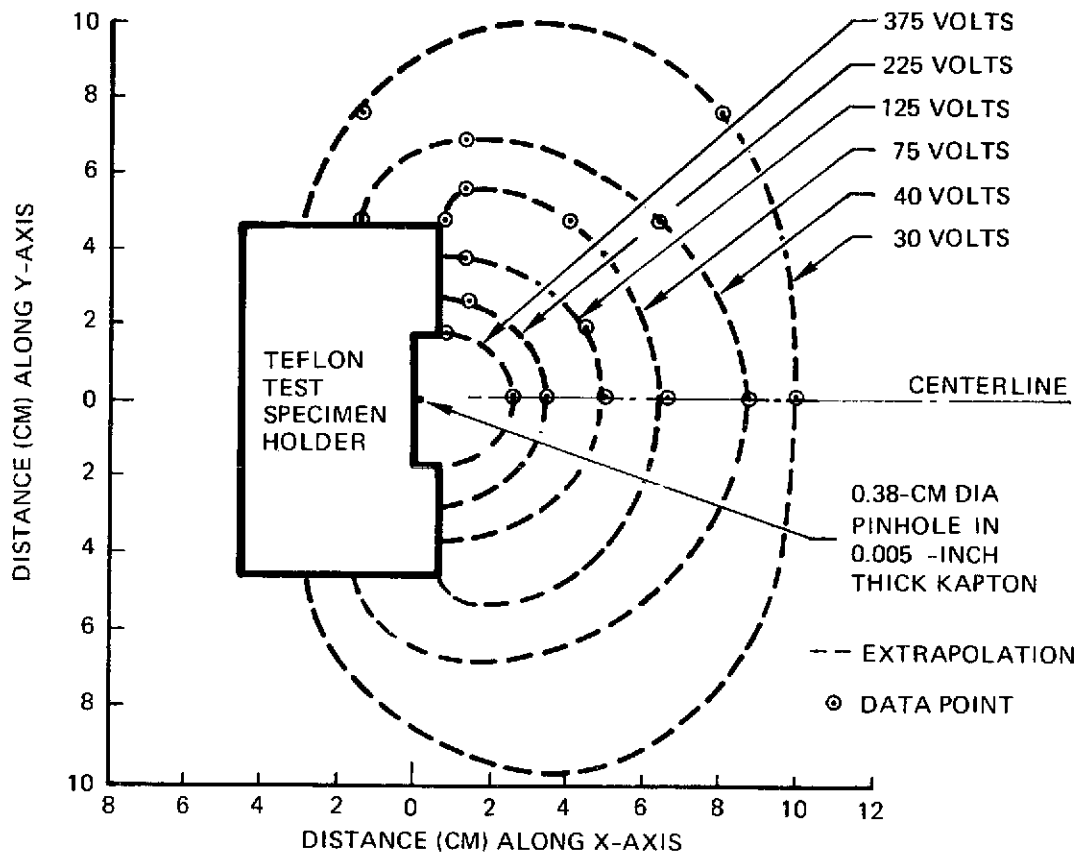


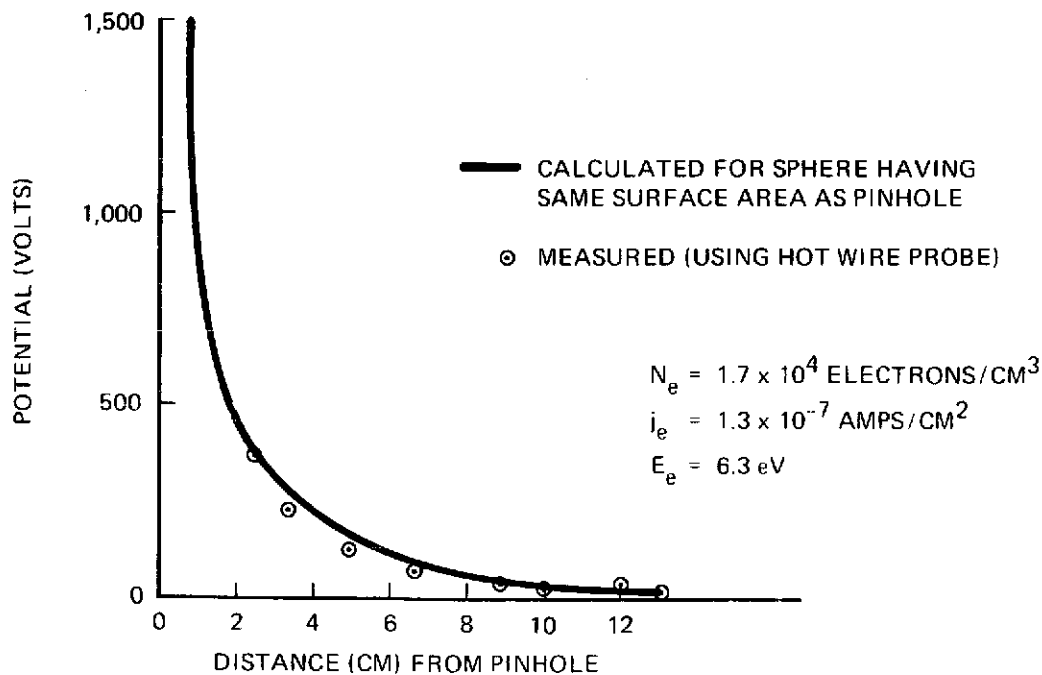
FIGURE 31: COMPARISON OF MEASURED POTENTIAL DISTRIBUTION AROUND A PINHOLE, DISC AND SPHERE AT +10,000 VOLTS

Figure 32a shows the shape of equipotential lines around the pinhole, and Figure 32b compares the measured potentials with those calculated for a sphere with the same surface area as the pinhole in vacuum, indicating excellent agreement.

Figure 33a shows the shape of equipotential lines around the disc and Figure 33b compares the measured potentials with those calculated for a sphere (with the same surface area as the disc) in vacuum. The fact that the calculated disc potentials extend farther from the surface than the measured values is in agreement with the fact that the measured disc currents are less than what one would predict for a sphere of the same area.

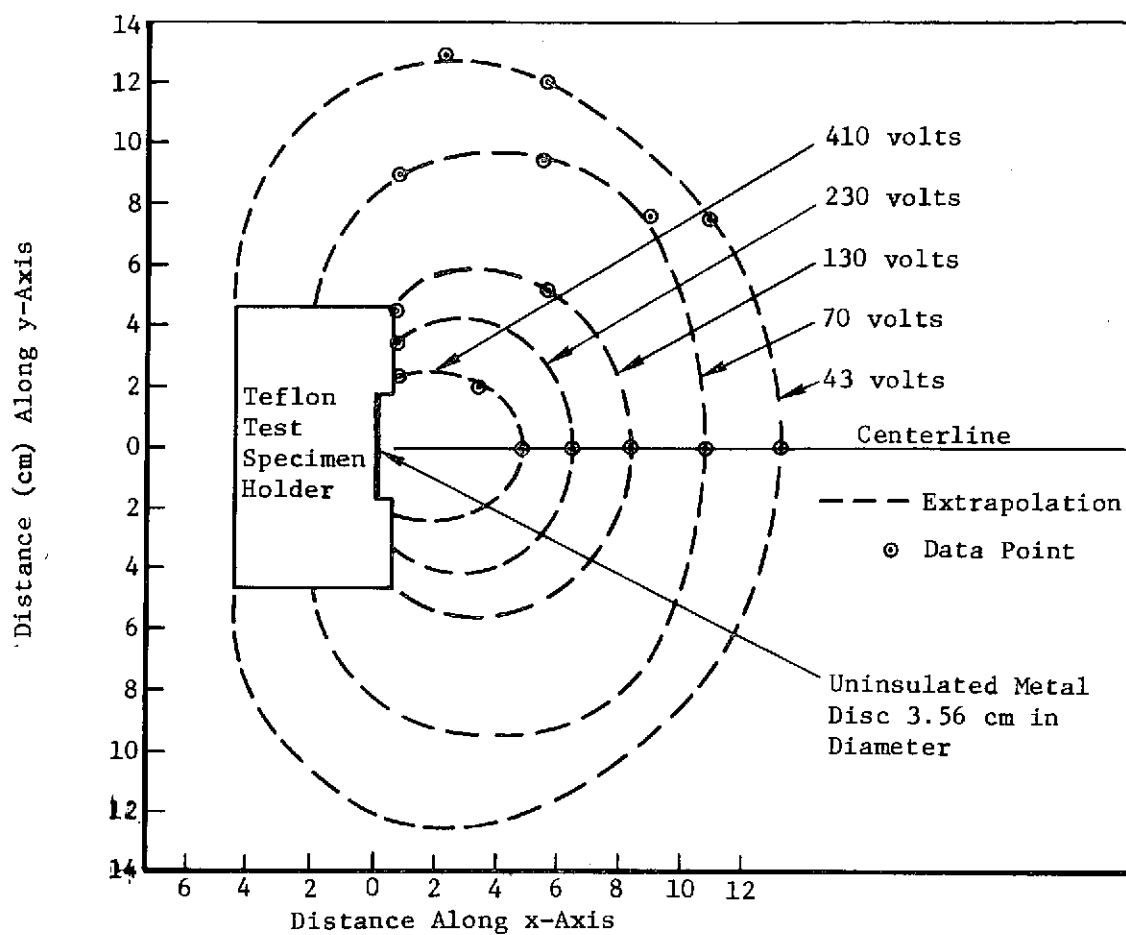


(A) TOP VIEW OF EQUIPOTENTIAL LINES

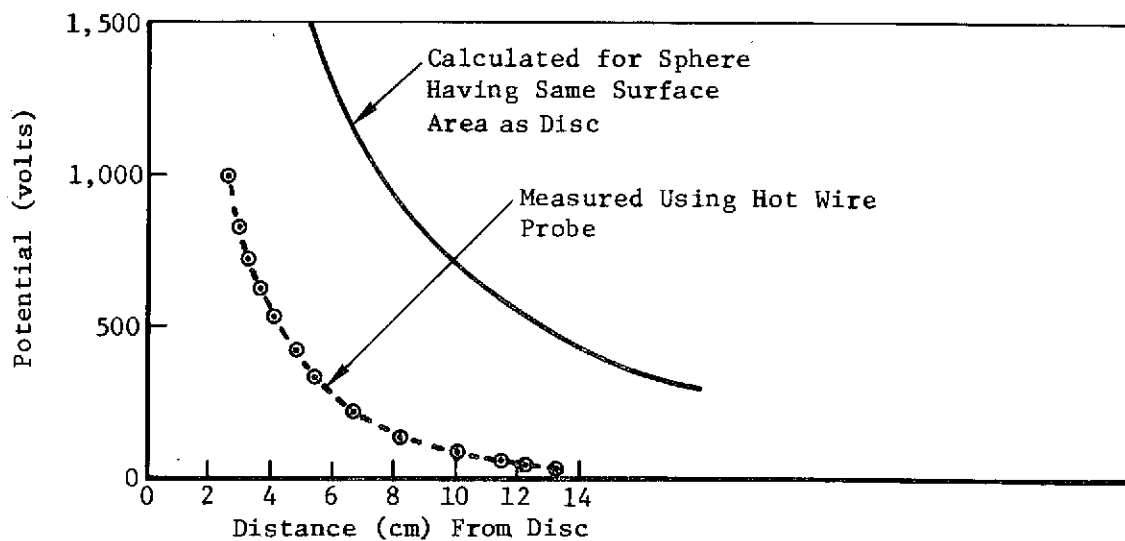


(B) POTENTIAL DISTRIBUTION ALONG CENTERLINE (Y = 0)

Figure 32 POTENTIAL DISTRIBUTION AROUND A 0.38-CM DIAMETER PINHOLE AT 10,000 VOLTS IN LARGE PLASMA CHAMBER



(A) Top View of Equipotential Lines



(B) potential Distribution Along Centerline ($y=0$)

Figure 33 POTENTIAL DISTRIBUTION AROUND A 3.56-CM-DIAMETER DISC ELECTRODE AT +10,000 VOLTS IN LARGE PLASMA CHAMBER

4.3 SOLAR PANEL CURRENT COLLECTION

Three categories of solar panels were tested: (1) conventional solar panels having exposed interconnects; (2) completely insulated solar panels; and (3) a screen-shielded solar panel. Figure 34 shows the specific panel configurations that were tested. The panels varied in size between 0.1 ft^2 to 1 ft^2 and were subjected to various plasma conditions while biased at high voltage. The results are grouped in this section as follows:

4.3.1 Conventional Panels (Bare Interconnects)

- 4.3.1.1 One ft^2 Panel
- 4.3.1.2 Short Life Test

4.3.2 Completely Insulated Panels

- 4.3.2.1 Conventional Solar Cells
- 4.3.2.2 Wrap-Around Solar Cells
- 4.3.2.3 FEP-Teflon Encapsulation
- 4.3.2.4 Aluminum Dummy Cells

4.3.3 Screen-Shielded Panel

4.3.1 Conventional Panels (Bare Interconnectors)

- 4.3.1.1 Solar Panel ($\sim 1 \text{ ft}^2$) with Bare Interconnectors
Test Facility: LPC

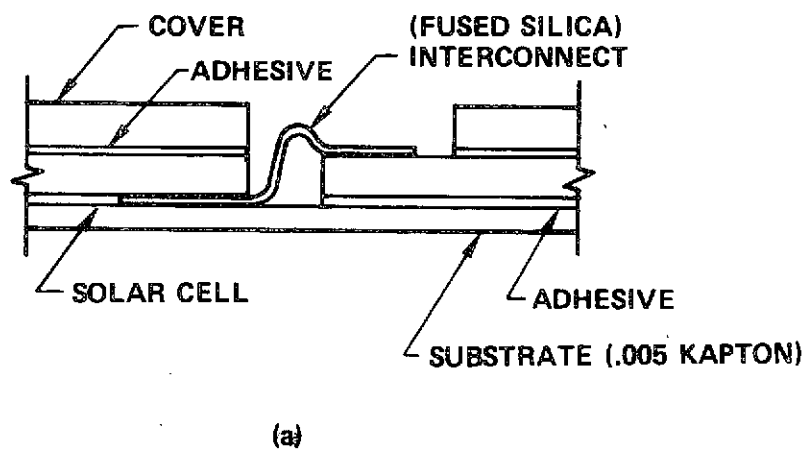
The plasma leakage current collected by a positively and negatively biased solar panel at plasma densities varying from 26 electrons/ cm^3 to 1.7×10^4 electrons/ cm^3 was measured at positive and negative voltages up to 16 kV.

The solar panel tested was one of a two-section solar panel (Figures 35 and 36). Each section consisted of 238 two cm by two cm silicon solar cells in a 14 cell-by-17 cell matrix. Fronts of the cells were covered with .006-inch (.015-cm) thick microsheet covers and the backs of the cells were completely insulated with R63-489 silicone adhesive to prevent any current collection to the back side. Uninsulated silver mesh interconnectors comprised approximately 10% of the front surface area. Total interconnector area (A_i) was 106 cm^2 and total front surface area (A_p) was 1058 cm^2 .

4.3.1.1.1 Positive Bias

The measured leakage current data at the highest plasma density (Figure 37), shows that with the panel biased slightly positive (+1 to +20 volts depending on the plasma density) the panel collected a plasma leakage current equal to the product of the plasma thermal electron current density, j_e , and the total interconnector area A_i . As the panel voltages were increased, the leakage current increased also, becoming equal to the product of j_e and the total panel area, A_p , at voltages between 30 and 60 volts. Thus in the voltage range of 30 to 60 volts the panel behaved as if a thin electron

CONVENTIONAL DESIGN



OTHER DESIGNS

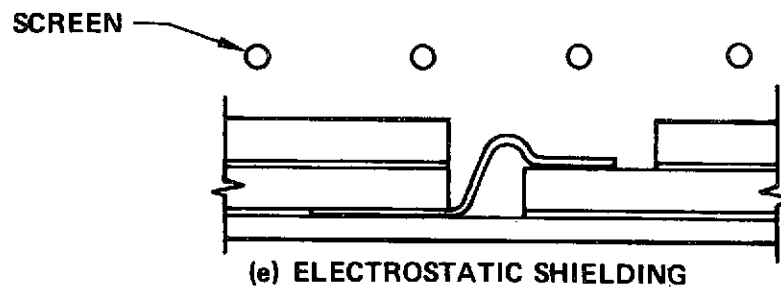
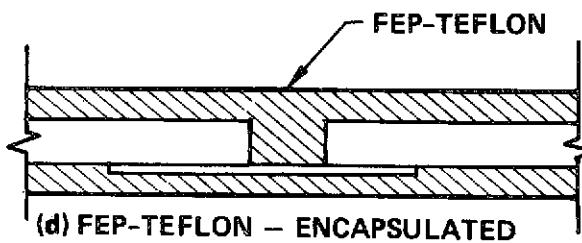
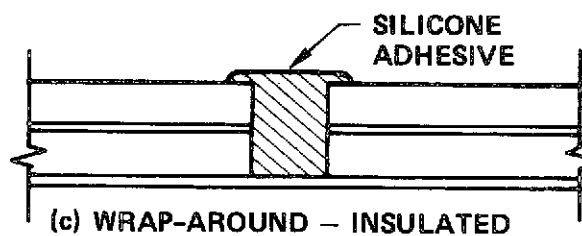
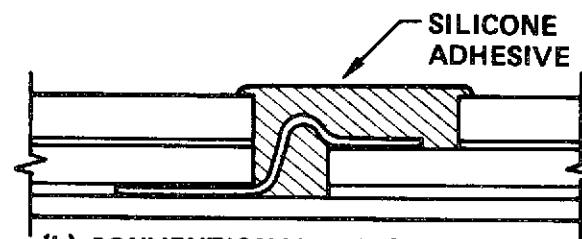


Figure 34 HIGH VOLTAGE SOLAR DESIGN CONCEPTS

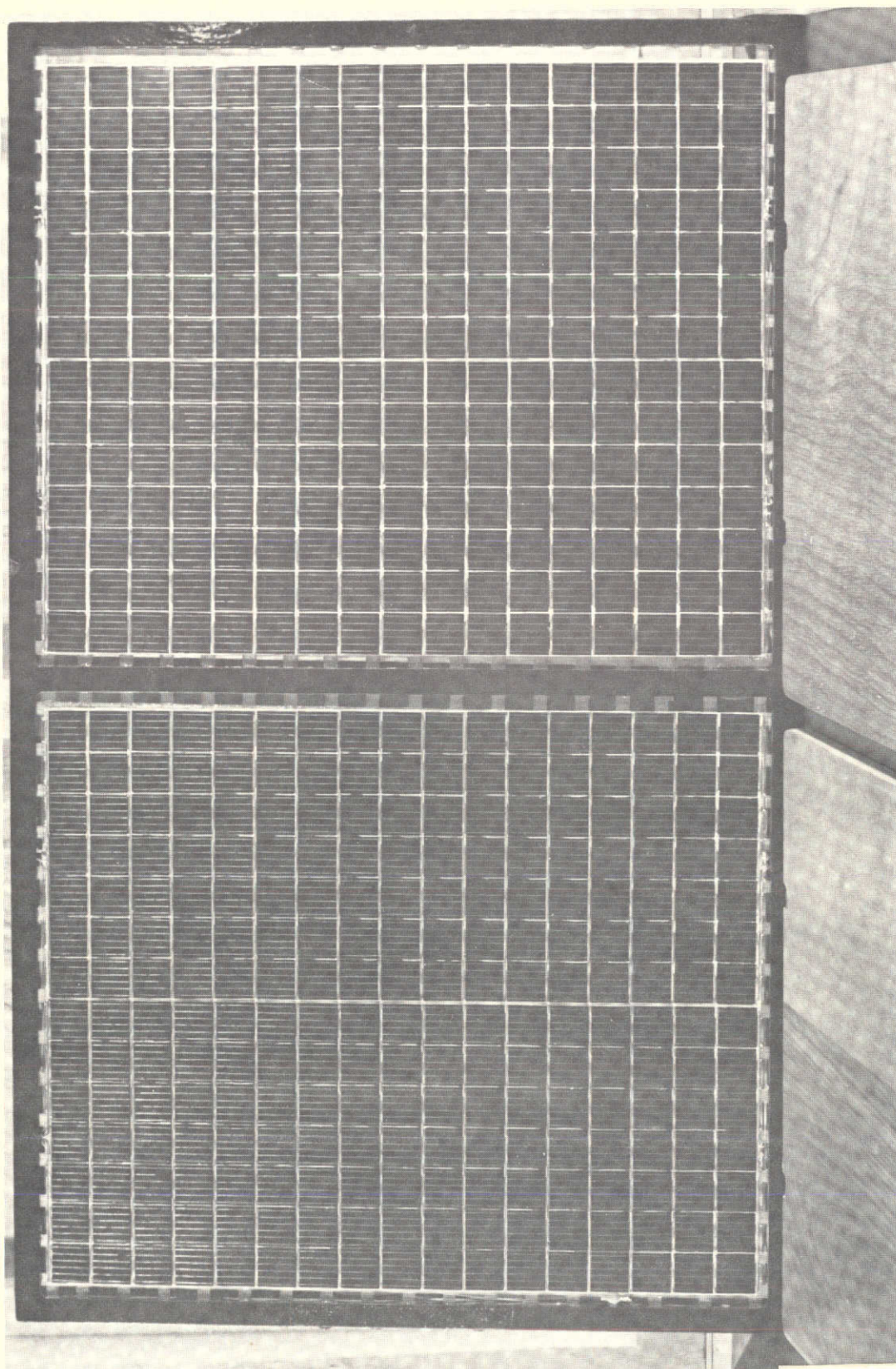


Figure 35: SOLAR ARRAY-UNINSULATED

This page is reproduced at the back of the report by a different reproduction method to provide better detail.

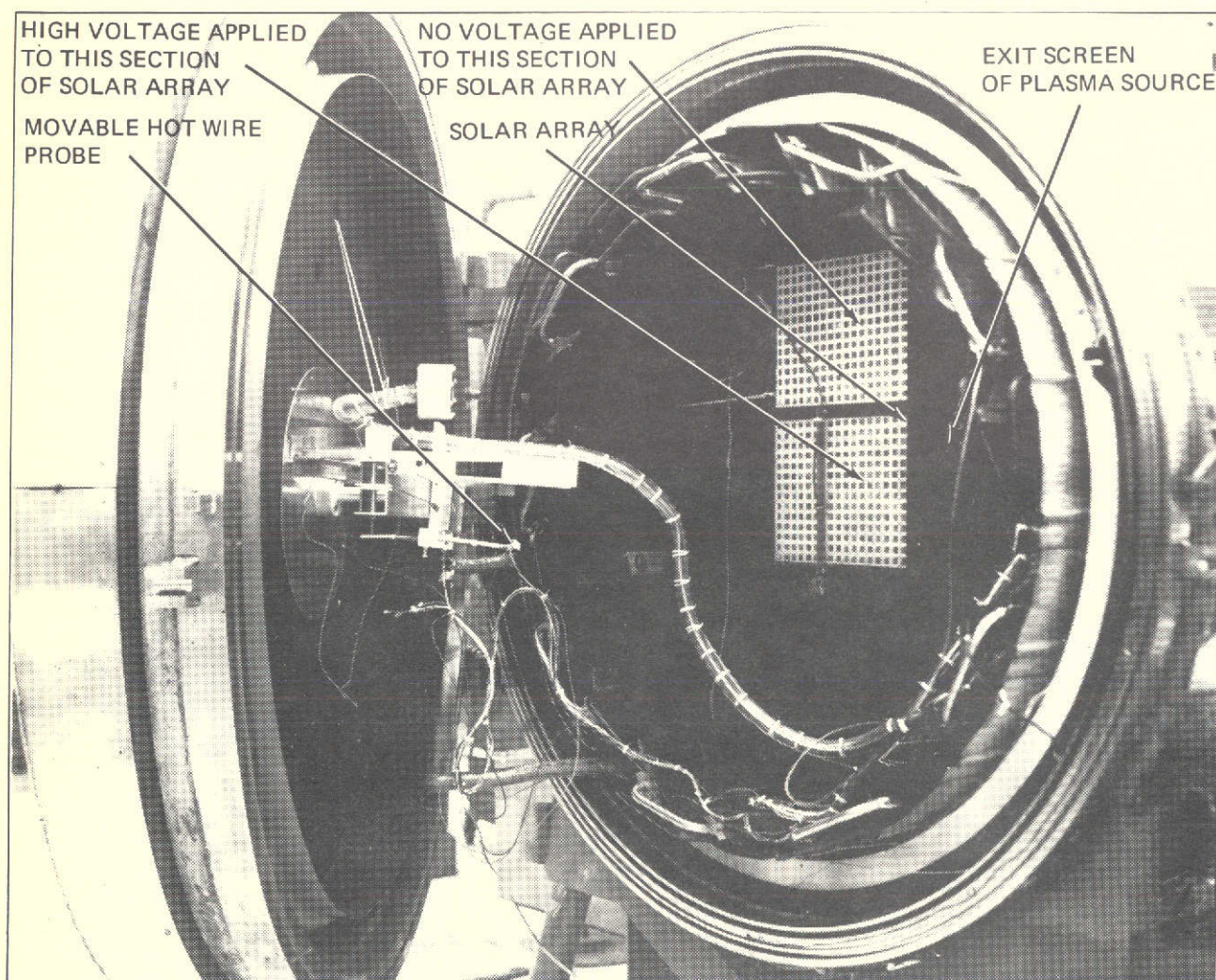


Figure 36: PHOTOGRAPH OF SOLAR ARRAY IN LARGE PLASMA CHAMBER

This page is reproduced at the back of the report by a different reproduction method to provide better detail.

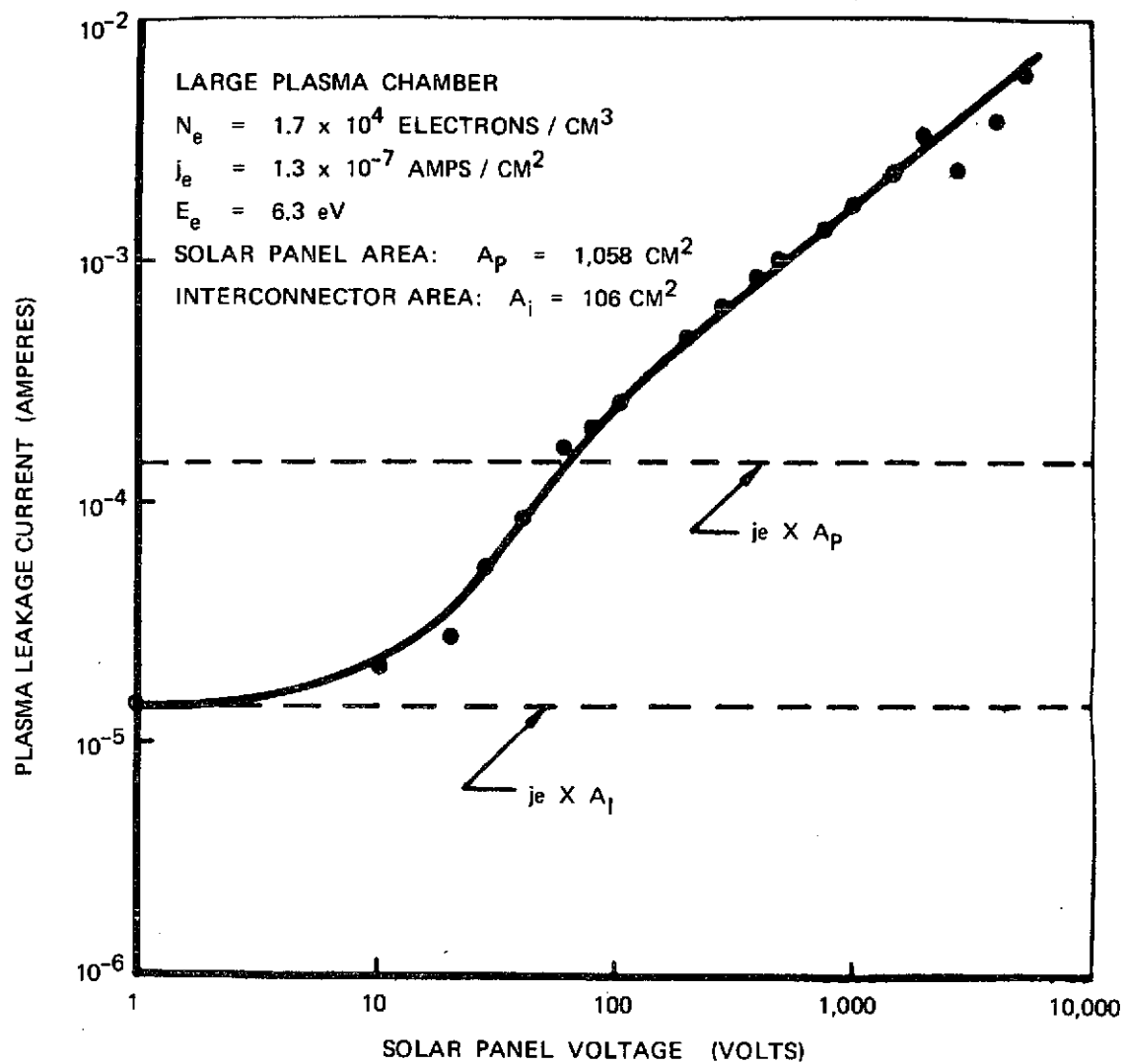


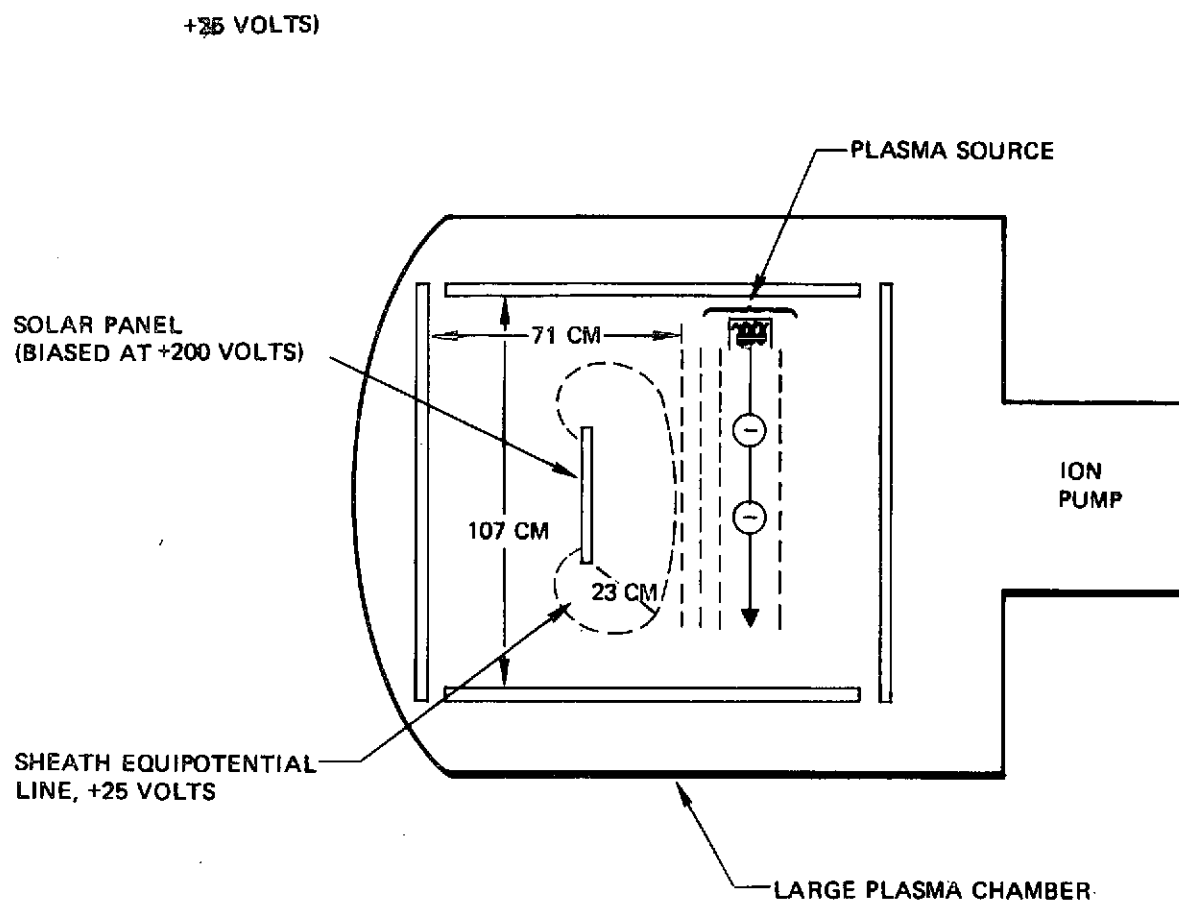
Figure 37 PLASMA LEAKAGE CURRENT COLLECTED BY A SOLAR PANEL WITH UNINSULATED INTERCONNECTORS

sheath were formed over the entire front surface of the panel and all plasma electrons encountering this sheath were collected by the panel. As the panel voltages were increased even further, the leakage currents exceeded the product $j_e \times A_p$, indicating that the sheath surface area exceeded that of the front surface of the panel (i.e., thin sheath theory no longer applies). In order to see if the sheath thickness had, indeed grown, a movable hot wire probe was used, as described earlier in Section 3.1.4, to determine the positions at which the potential around the panel had dropped to within 25 volts of plasma potential. The resulting 25-volt equipotential line when the panel voltage was 200 volts is shown in Figure 38, indicating that the sheath thicknesses exceeded 23 cm. With a sheath thickness of this magnitude, the sheath surface area exceeds the panel surface area due to edge effects and thin sheath theory no longer applies. The product of j_e and sheath surface area can account for the increase in panel current observed in Figure 37 up to about 200 volts.

At panel voltages higher than approximately 200 volts the sheath dimensions become comparable to test chamber dimensions (Figure 38) and the continued rise in panel current with increased voltage observed in Figure 37 cannot be explained simply by a growth in sheath area. It may be that at these higher voltages the panel voltage is coupling directly with the plasma source. This does not necessarily mean that the measured currents are larger than what would be expected under idealized conditions. Indeed, remarkable agreement between measured currents and those calculated based on a partially insulated spherical probe model (described in Appendix C) were obtained over the entire range of plasma densities (Figure 39). The agreement between calculated and measured values at voltages above 200 volts may be only a coincidence since the chamber size limits the natural plasma sheath expansion of the biased panel. However, this "coincidence," plus the fair agreement noted at lower voltage where the chamber size is not a limiting factor, suggests that this model may be a reasonable one.

The calculations or the measured values in Figure 39 should not be used as a basis for predicting currents for a larger array on a current per unit area basis. This is because theory predicts that the plasma current per unit area collected by a solar panel decreases as the panel area is increased (see Appendix C). Using data directly from Figure 39 will therefore result in erroneously high current predictions. Appendix C describes how one might estimate plasma currents for large area solar arrays.

It was possible to observe the front surface of the solar panel when plasma current collection was taking place through a quartz window in the vacuum chamber. At plasma densities of 3.6×10^{12} electrons/cm³ and higher, a blue glow over the front surface of the panel could be observed when the panel was above 5,000 volts. At the two highest plasma densities, bright red and white spots could be observed at various points on the bare interconnectors when voltages were raised above 5,000 volts. Occasionally these spots would be surrounded by a momentary blue discharge which extended about 10 cm from the panel front surface. These discharges were accompanied by large bursts in current collected by the panel, suggesting that local ionization produced great quantities of electrons available temporarily for attraction to the high voltage interconnectors. The red and white spots



(1/20 SCALE)

Figure 38 ELECTRON SHEATH EQUIPOTENTIAL LINE AROUND 1 FT² SOLAR PANEL WITH BARE INTERCONNECTORS

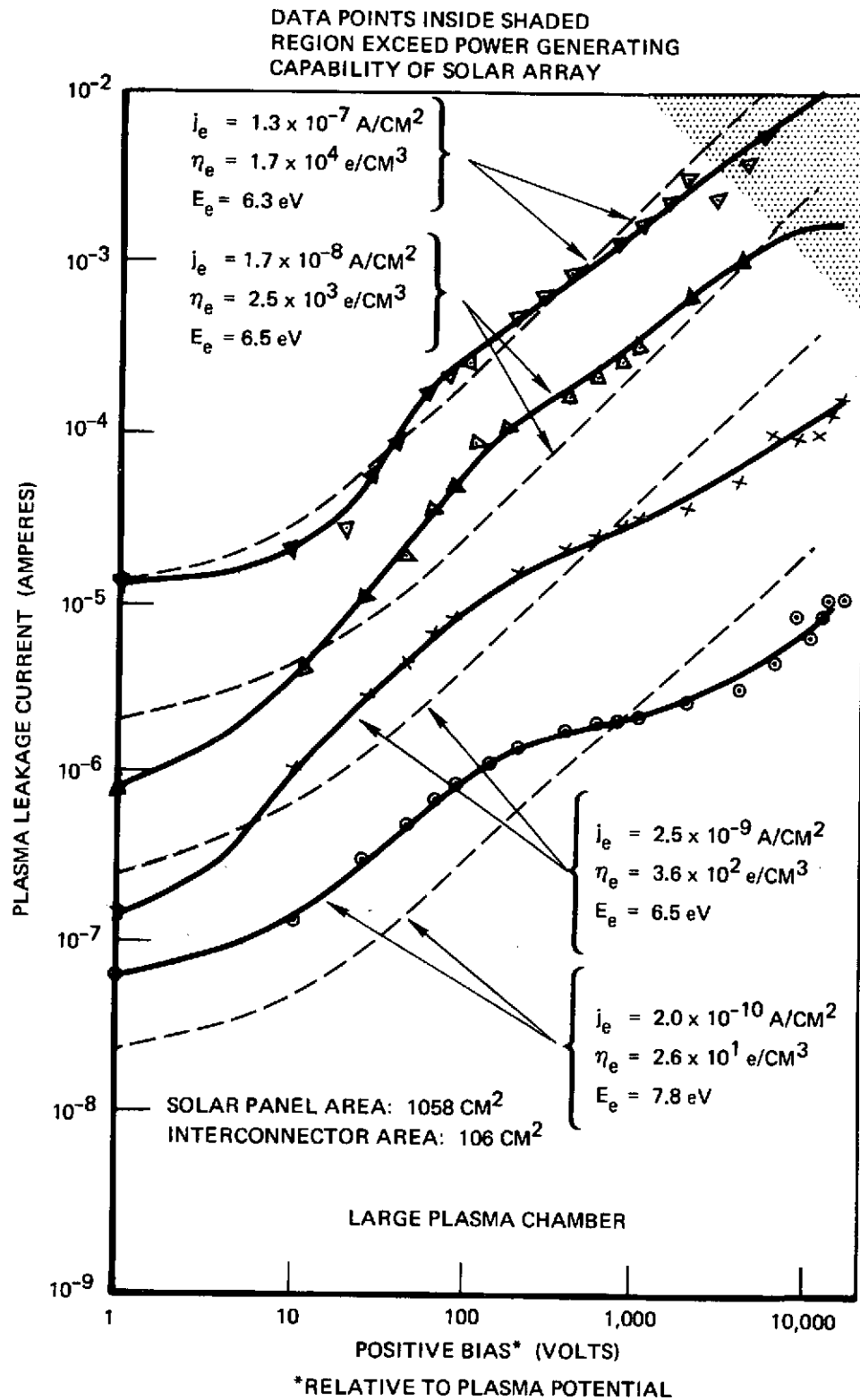


Figure 39 EFFECT OF PLASMA CONDITIONS ON THE PLASMA LEAKAGE CURRENT COLLECTED BY A POSITIVELY-BIASED SOLAR PANEL WITH BARE INTERCONNECTORS

and the blue glows could be made to disappear instantly by turning off the plasma source, indicating that the heating and localized ionization required a continual source of electrons to sustain itself. An alternate method of making the red and white spots disappear was to reduce the voltage from > 5,000 volts to 1,000 volts. If the bright spots and large currents had been due to vapor arcs at the interconnector surfaces, which according to ref. 1, p. 36, should continue to burn at voltages between 4 and 100 volts, one would have expected the spots to glow even at the reduced voltage level. The implication is that the bright spots were caused by heating due to large currents coming from the surrounding plasma rather than from local discharges around the bare interconnectors.

Post-test examination of the panel did reveal damage to the interconnectors. A good portion of the exposed silver mesh interconnector material was gone in regions where silicone adhesive (R63-489) from the backside had spilled onto the mesh. Apparently the presence of this silicone in layers too thin to prevent current collection caused excessive heating in these areas which resulted in vaporization of the silver mesh. Places where the silver mesh had been soldered to the solar cell were still intact, presumably because the solar cell acted as a heat sink, therefore preventing overheating of the mesh.

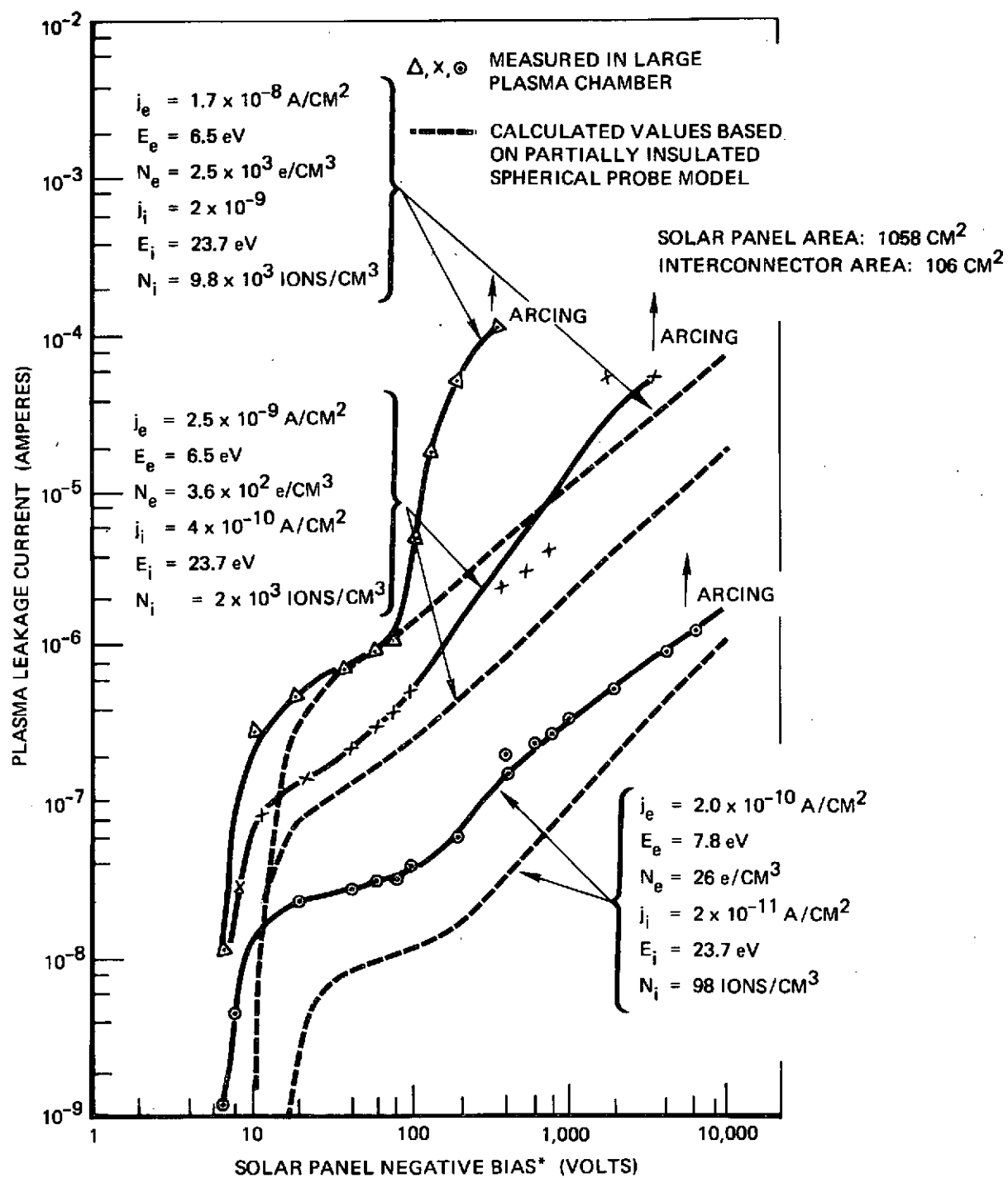
4.3.1.1.2 Negative Bias

The measured plasma current collected by the panel at several different ion densities is shown in Figure 40 along with calculated values based on the partially-insulated spherical probe model described in Appendix C. Fair agreement is noted at the higher voltages in the lowest ion density case, however at the higher densities the collected ion current rose rapidly at voltages above about 100 volts at a rate much faster than expected. Because it is expected that the sheath thickness voltages above 100 volts exceed the chamber dimensions it is not too surprising that the measured current values at high voltage do not agree with calculated values. In the highest ion density case it was observed that heavy discharges started at voltages as low as 400 volts. These discharges consumed enough current to trip off the high voltage power supply when it was set at a 20 mA shut-off threshold. In the positive polarity tests of the same panel such discharging did not start until voltages well above 5,000 volts were applied and much higher current levels were attained. In all the negative bias tests there were noticeably more discharges at much lower voltages than in the positive bias tests.

4.3.1.2 Solar Panel ($\sim 1/10 \text{ ft}^2$) with Bare Interconnectors - Short Life Tests Test Facility: SPC

4.3.1.2.1 Positive Bias - First Test

A small solar panel with bare interconnectors was biased at +4000 volts and the plasma adjusted such that the current collected was 1×10^{-5} amperes and allowed to run at these conditions for 114 hours. The purpose of the test was to see what effects, if any, this level of plasma power loss ($\sim .4 \text{ watts/ft}^2$) have on a solar panel with bare interconnectors. This



*MEASURED RELATIVE TO PLASMA POTENTIAL

Figure 40 EFFECT OF PLASMA CONDITIONS ON THE PLASMA LEAKAGE CURRENT COLLECTED BY A NEGATIVELY BIASED SOLAR PANEL WITH BARE INTERCONNECTORS

power level was chosen low enough compared with the output capability of an array (10 watts/ft²) that it is not of concern from a power loss standpoint.

The solar panel was comprised of 24 series connected 2-cm by 2-cm silicon solar cells having conventional contacts, silver mesh interconnectors, and .012-inch (.030-cm) thick fused silica coverslides. The cells were each bonded to a .005-inch (.0127-cm) thick sheet of Kapton with a small dot of 93-500 silicone adhesive. The Kapton was, in turn, bonded to a sheet of 0.125-inch thick epoxy-glass laminate to insure that current collection was limited to the front side of the panel. Care was taken to insure that no adhesive spilled onto the interconnects to minimize the possibility of hot spot vaporization of interconnectors such as occurred during the tests described in section 4.3.1.1.

Observation made through a window in the vacuum chamber during the test indicated no glowing or other evidence of burning on the front surface of the panel (actually no glows were expected since in the tests described earlier in section 4.3.1.1 blue glows were not observed until the plasma power loss was up to about 5 watts/ft²).

After the 114 hour test was complete the solar panel was inspected. All interconnectors had darkened considerably (they looked dark gold, rather than bright silver) and one could also detect a slight darkening of the coverslides.

Current-voltage curves of the illuminated solar panel output measured before and after the plasma exposure (Figure 41) showed a 7 percent decrease in short-circuit current, an indication that the transmission of the coverslides had been reduced by this much, due to the observed darkening.

It has not yet been determined if the darkening was caused by a contaminate from the plasma source, vacuum chamber, or solar panel. There is evidence, however, that the contaminate is a negative ion which is attracted to the high voltage solar panel interconnectors and neutralized upon impact, forming a deposit on the interconnector (and also on the coverslides, because some ions would impact the coverslide first, even though attracted towards the interconnector). The prime evidence is that no darkening of any kind was observed in the fully insulated solar panel located adjacent to the panel under discussion. Although the fully insulated panel (see section 4.3.2.2) was biased at +4kV also, it drew no current. If the contaminate were a neutral particle caused by condensation of materials outgassing in the chamber one would have expected both panels to darken equally.

Whatever the cause of the darkening, it is important that it be determined whether it is a chamber-related phenomenon or a feature of positively-biased high voltage solar panels. A seven-percent loss in power output in 4-3/4 days (114 hours) extrapolates to a 50-percent loss in 34-days, clearly an intolerable degradation. It is therefore recommended that future work include life tests such as the one described here with special emphasis placed on isolating causes of contamination to determine if they are of concern to space-flight arrays.

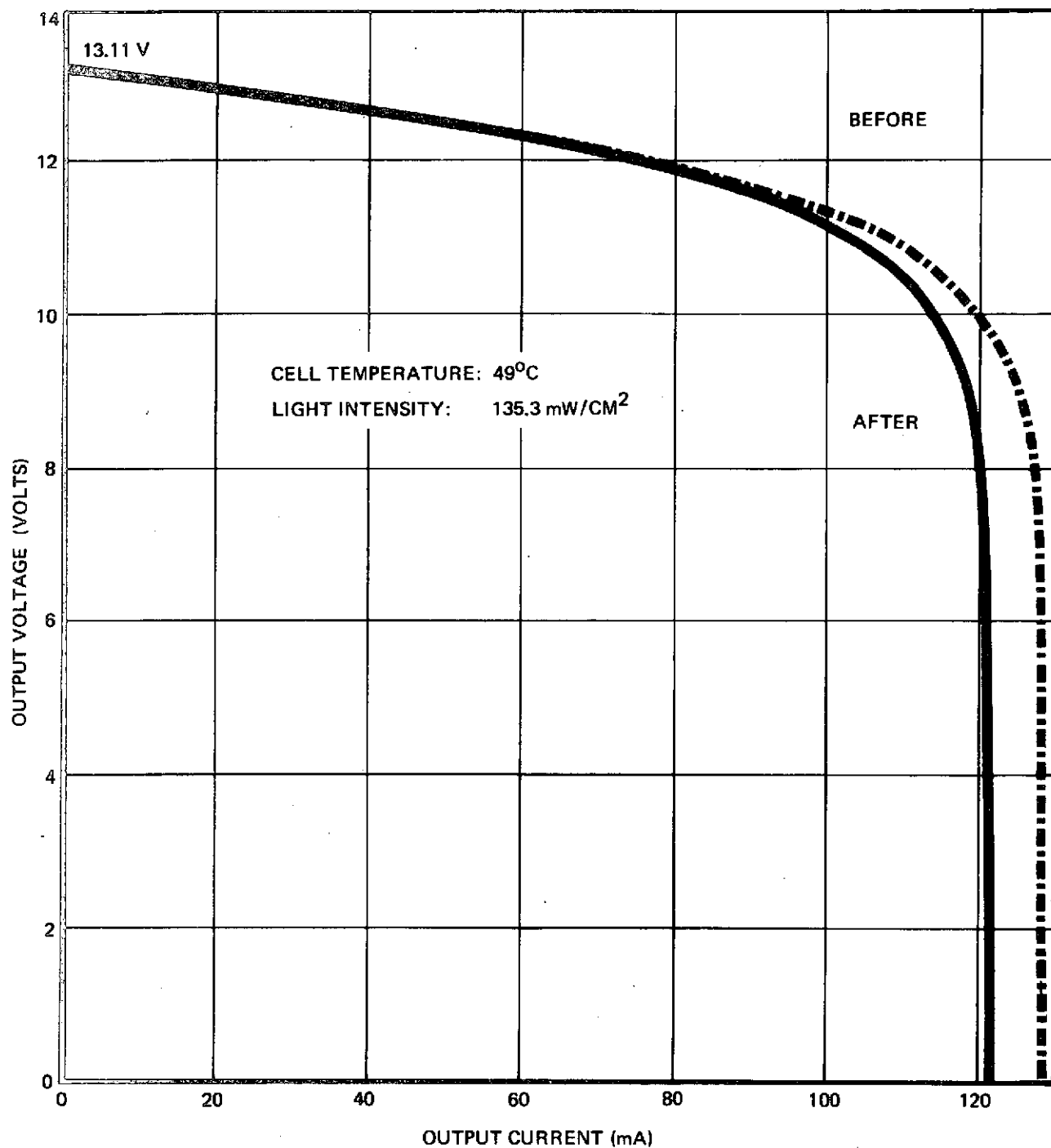


Figure 41 EFFECT OF 114-HOUR EXPOSURE TO PLASMA ON SOLAR PANEL WITH BARE INTERCONNECTORS AT +4 kV

4.3.1.2.2 Positive Bias - Second Test

After the test described in the preceding section (4.3.1.2.1) was completed, the solar panel was put back in the plasma chamber at +5kV and the plasma density was increased so that plasma current was 6×10^{-4} amperes and power loss was ~ 30 watts/ft². Although a blue glow could be seen over the front surface of the panel, no bright red or white spots could be seen.

This is in marked contrast to the observations made in the test described in section 4.3.1.1 where plasma power losses above 5 watts/ft² resulted in numerous bright spots along the interconnectors. It is believed that the difference is due to the fact that adhesive had spilled onto the interconnectors in the earlier described test whereas the interconnectors in this test were "clean" and therefore did not lend themselves to the creation of "hot spots."

4.3.1.2.3 Negative Bias

A panel identical to that discussed in section 4.3.1.2.1 (24 series-connected 2 cm by 2 cm silicon solar cells with bare interconnects) was initially biased at -16,000 volts with the plasma adjusted such that the collected current was 1×10^{-7} amps. Testing could not be continued at this voltage level because of continued arcing which kept shutting off the high voltage power supply. The voltage was then reduced to -10kV and the plasma current again adjusted to 1×10^{-7} amps and allowed to run for 140 hours. During this time it was noticed that even though the plasma density was never changed, the solar panel current would increase by an order of magnitude (up to $> 10^{-6}$ amperes) in a period of about five minutes. It would then arc (flashes all over the interconnectors and cell edges could be seen) and the current would drop back to the originally established value of 1×10^{-7} or even lower. After about 24 hours of operation, the frequency of this arcing was reduced from once every five minutes to once every fifteen minutes. The phenomenon continued throughout the remainder of the test. One possible explanation of this phenomenon is that the coverslides built up an accumulation of charge which then were discharged to the interconnectors. After the plasma exposure, evidences of arcing could be seen around the edges of the cells.

Current-voltage curves of the illuminated panel output measured before and after the plasma exposure indicated no change in power output capability.

4.3.2 Completely-Insulated Panels

4.3.2.1 Solar Panel ($\sim 1/10$ ft²) with Insulated Interconnectors (Conventional Solar Cells) Test Facility: SPC

The purpose of the test described here was to see if a small solar panel with conventional solar cells could be completely insulated against a plasma when biased to high voltage. The panel consisted of 24 series connected 2 cm by 2 cm, .012-inch (.030-cm) thick silicon solar cells having conventional contacts, .012-inch (.030-cm) fused silica coverslides, and silver

mesh interconnectors. The cells were bonded to a .005-inch (.0127-cm) thick sheet of Kapton with 93-500 silicone encapsulant which was allowed to ooze up between cells to the top level of the coverslides, thereby covering the interconnectors (Figure 34b). Prior to curing, the encapsulant was outgassed under vacuum, then inspected for voids which were subsequently filled with more 93-500 encapsulant by means of a syringe. After curing, another layer of encapsulant was applied with the syringe along the interconnector regions, outgassed and then cured. The edges of the outer cells were protected by means of a "dam" of 93-500 which surrounded the panel. The Kapton substrate was bonded to a sheet of 0.125-inch thick epoxy-glass laminate to insure that current collection was limited to the front side of the panel. Care was taken to insure that the high voltage cables were insulated at all joints to insure that if any plasma leakage was found it could be attributed to the panel front surface.

In order to check for plasma leakage, the SPC plasma density was set at a level high enough ($\sim 10^{-4}$ electrons/cm³) that pinhole currents could easily be detected. Positive voltage was then applied in small steps. Leakage current was less than 1×10^{-10} amperes at voltages up to + 400 volts. However, when the voltage exceeded + 400 volts, the current suddenly jumped up to 2×10^{-6} amperes indicated a dielectric breakdown and subsequent collection of a plasma pinhole current. As the voltage was raised further, the current increased (at + 2,000 volts the current had increased to 4×10^{-5} amps). At the + 2,000 volt level red and white spots could be seen all over the interconnector regions and frequent flashes occurred at these spots. The implication is that the spots were at pinhole sites in the 93-500 encapsulant caused by dielectric breakdown and the localized heating was caused by high power densities being dissipated at the pinholes.

It is interesting to note that the observed hot spots and flashing occurred at a plasma power loss of ~ 0.8 watts/ft @ 2 kV with this insulated panel whereas the uninsulated panel test described in section 4.3.1.2.2 gave no indication of hot spots at a plasma power loss of up to ~ 30 watts/ft² at 5 kV. Since hot spots can do damage (see discussion in section 4.3.1.1.1), this test indicates the seriousness of pinholes even at relatively low overall plasma power loss levels.

4.3.2.2 Solar Panel ($\sim 1/10$ ft²) with Insulated Interconnectors (Wrap-around Contact Solar Cells) Test Facility: SPC

Two small solar panels with wrap-around contact solar cells were completely insulated and tested in a plasma for leakage. One test was conducted at + 4kV and the other at -10 kV.

The panels consisted of 24 series-connected, 2 cm by 2 cm, .012-inch (.030-cm) thick silicon solar cells having wrap-around contacts, .012-inch (.030-cm) fused silica coverslides and silver mesh interconnectors. The interconnectors were insulated in the manner depicted in Figure 34c. The cells were bonded to a .005-inch (.0127-cm) thick sheet encapsulant and the adhesive allowed to ooze up between cells to the top level of the coverslides,

thereby covering the interconnectors with .024-inches (.061-cm) of insulation. Prior to curing, the applied encapsulant was outgassed under vacuum, then inspected for possible voids which were subsequently filled with more 93-500 encapsulant by means of a syringe. After another outgassing, the panel was cured, then the panel was again inspected for voids which were filled and a whole additional layer of 93-500 was applied to the interconnector region, outgassed, then cured. The Kapton substrate was bonded to a sheet of 0.125-inch thick epoxy glass laminate to insure that current collection was limited to the front side of the panel. Care was taken to insure that the high voltage cables were well insulated at all connections to insure that if any plasma leakage was found, it could be attributed to the panel front surface.

4.3.2.2.1 Positive Bias

The first attempt to bias the panel at positive voltages in a plasma of about 10^4 electrons/cm³ resulted in a breakdown at about 1 kV (the current jumped from $< 3 \times 10^{-10}$ amps to 1×10^{-6} amperes). Since only one bright spot appeared, the test was discontinued and the panel was repaired by adding 93-500 at the point where the bright spot had appeared. When the test was resumed, the currents remained less than 1×10^{-9} at voltages up to + 4kV. To verify that this current level was due to the insulation resistance of the panel rather than a plasma leakage current, the plasma density was varied between 10^4 and 10^2 electrons/cm³ with no observed change in panel current. Only when the plasma was turned off did the plasma current drop to $< 1 \times 10^{-10}$ amperes.

With the panel adequately sealed against a 10^4 electron/cm³ plasma at + 4 kV, the test was continued for 114 continuous hours during which time no rise in current was observed. This was the first time we had had success in completely insulating a solar panel against plasma at voltages above a few hundred volts. Simultaneous with this test, we operated an uninsulated panel of the same size (section 4.3.1.2.1) at + 4 kV. It was a striking comparison to see the panels side by side, the uninsulated one drawing up to 6×10^{-4} amperes and the completely insulated one drawing $< 1 \times 10^{-9}$ amperes. Post-test inspection of the insulated panel revealed no evidence of damage or discoloration of any kind. A comparison of illuminated current-voltage curves indicated no change in power generating capability.

The above described success in insulating the panel must be tempered with the observation that it was an extremely difficult task which may have to be modified for volume production. Numerous 100-percent inspections of interconnector encapsulant were required. Even after this was done, a plasma leak checked revealed a weak point that had to be repaired. Also, as has been pointed out several times in this report, even a completely insulated panel can eventually develop pinholes due to micrometeoroid punctures or thermal stresses. Once such pinholes occur, hot spots develop at relatively low plasma current levels due to the "focusing" of the current into such a small area.

4.3.2.2.2 Negative Bias

The above test was repeated with another panel insulated in the same manner but biased at negative potentials up to -10kV and left for 95 hours without breakdown (the collected current was less than 3×10^{-9} amperes). (For purposes of comparison, it may be noted that an uninsulated panel of similar construction at -10kV under similar conditions collected between 1×10^{-7} and 1×10^{-6} amperes and sustained arcing every 5 to 15 minutes. See section 4.3.1.2.3).

After the above 96 hour exposure was completed, an attempt was made to increase the voltage to -16kV. At -14kV a breakdown occurred and the current jumped to 1×10^{-6} amperes.

Inspection of the panel after test revealed only one pinhole current collection site, evidenced by burning at one point of an interconnection region. However, it was observed that one of the cells, near the interconnector, had shattered in a area of about 1/4-inch diameter, breaking that portion of the cell into many tiny pieces and cracking the coverslide. As a result of this, the power output capability of the panel dropped by 46 percent as determined by before-and-after measurements of the panel's illuminated current-voltage curve. A likely reason for the observed shattering is a bubble or void of entrapped gas underneath the solar cell which could not escape because of the complete encapsulation afforded by the interconnector insulation. When under vacuum, the entrapped gas exerted a net upward pressure on the cell causing it to break. Therefore, special care must be taken to avoid trapped gas if complete encapsulation of interconnectors is planned.

4.3.2.3 Solar Cell Module Encapsulated in FEP-Teflon Test Facility: SPC

A small segment of solar cells encapsulated in FEP Teflon was successfully operated for over 70 hours in a plasma (10^3 electrons/cm³) at +16 kV and -16 kV without significant plasma leakage current. At the end of 70 hours at +16 kV and -16 kV the plasma leakage current was less than 6×10^{-9} amperes.

The segment consisted of four interconnected 2 cm by 2 cm silicon solar cells laminated between sheets of FEP Teflon (two .005-inch thick sheets on the front side and two .005-inch thick sheets on the back side). The lamination was accomplished by heating the whole assembly under pressure to 600°F. Prior to lamination, the regions outside and between solar cells were filled with strips of FEP-Teflon (three strips .005 thick) to prevent thinning of the Teflon at the solar cell edges.

Samples made with only one layer of .005-inch thick FEP-Teflon on the front and back of the solar cells broke down at +5 kV in the plasma. Samples that did not have strips of FEP Teflon around and between the solar cells broke down at voltages less than 1 kV due to thinning of the Teflon at the solar cell edges.

An interesting observation was made during the +16 kV test of the successful module; the plasma leakage current decayed two orders of magnitude (from 4.5×10^{-7} amperes to 4.0×10^{-9} amperes), over the test period of 70 hours. It is suspected that the initial high current level was comprised primarily of a charging current accepted in some fashion by the encapsulated solar array segment. After the +16 kV lead was disconnected from the high voltage power supply it was noted that an arc jumped from the lead to ground, suggesting the existence of stored charge. Analysis of the charging current indicates a total stored charge of 1.6×10^{-3} coulombs. On a large area solar array the stored charge could be in the order of coulombs, which at high voltage could present a potential hazard to personnel.

4.3.2.4 Completely Insulated Solar Panel ($\sim 1 \text{ ft}^2$) Using Aluminum Dummy Cells Test Facility: LPC

A completely insulated solar panel (26 cm by 28 cm) using aluminum dummy cells mounted in a .005-inch (.0127-cm) thick Kapton sheet was tested for its ability to prevent plasma current collection. The dummy cells consisted of 14 strips of .015-cm thick aluminum 26-cm long. Bonded onto each strip were thirteen 2 cm by 2 cm microsheet glass covers .006-inch (.015-cm) thick. All the trips were electrically connected and high voltage applied to them. The 0.127-cm wide spaces between the microsheet covers were filled by "flooding" the spaces with R63-489 silicone adhesive. The resulting panel was intended to simulate a panel consisting of 182, 2 cm by 2 cm solar cells connected in series with insulated interconnectors.

The panel was situated in the LPC in the same manner as the solar panel shown in Figure 38 with the front of the panel facing the ion beam and the plasma density adjusted to 2.5×10^3 electrons/cm³. Positive voltages up to +16 kV were applied and the resulting plasma currents are shown in Figure 42, indicating that the panel was not well insulated. Post-test examination of the panel revealed (Figure 43) multiple breakdown points, all of which occurred in the R-63-489 which filled the microsheet gap between adjacent aluminum strips; the breakdowns never occurred in the microsheet gaps on the same aluminum strip. The implication of this observation is that the breakdowns were made possible by the sharp edge of the aluminum strip. Subsequent attempts to repair the panel by filling the breakdown points with R63-489 failed to completely seal out the plasma, however, only three red spots were observed in the panel at +10 kV compared with the 20 or so spots observed the first time. The panel could have probably eventually been completely sealed by continued inspection and "patching," however, it is obviously not easy to completely insulate solar panels.

4.3.3 Screen-Shielded Solar Panel ($\sim 1 \text{ ft}^2$) with Bare Interconnectors Test Facility: LPC

4.3.3.1 Positive Bias

To test the concept of electrostatically shielding a solar panel, a stainless steel screen was mounted one inch (2.54-cm) in front of the solar panel described in the preceding paragraphs. Various negative biases were applied to the screen while positive high voltages were applied to the solar panel.

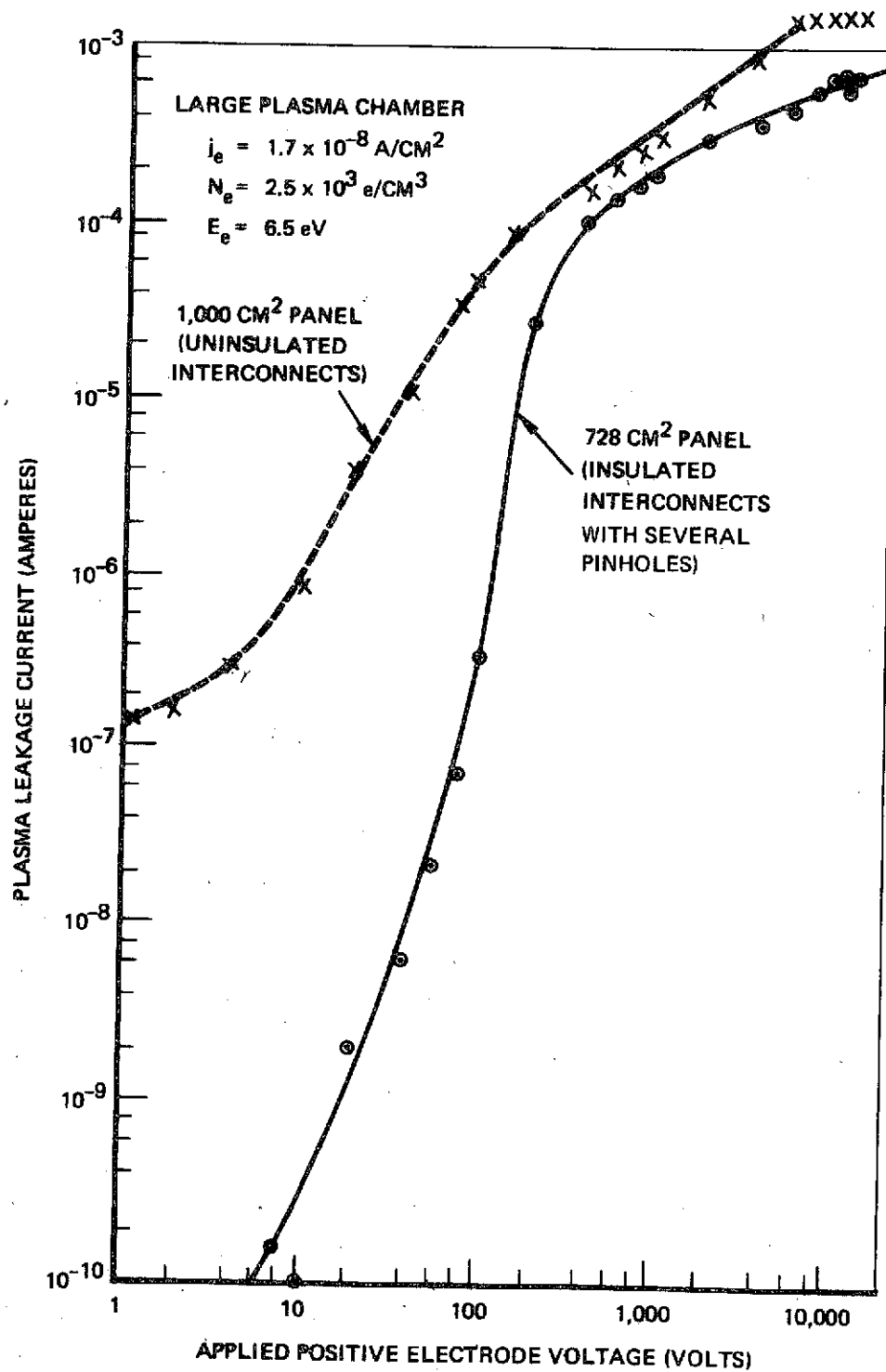


Figure 42 PLASMA LEAKAGE CURRENT COLLECTED BY A POSITIVELY BIASED, COMPLETELY INSULATED, ALUMINUM DUMMY SOLAR PANEL

This page is reproduced at the back of the report by a different reproduction method to provide better detail.

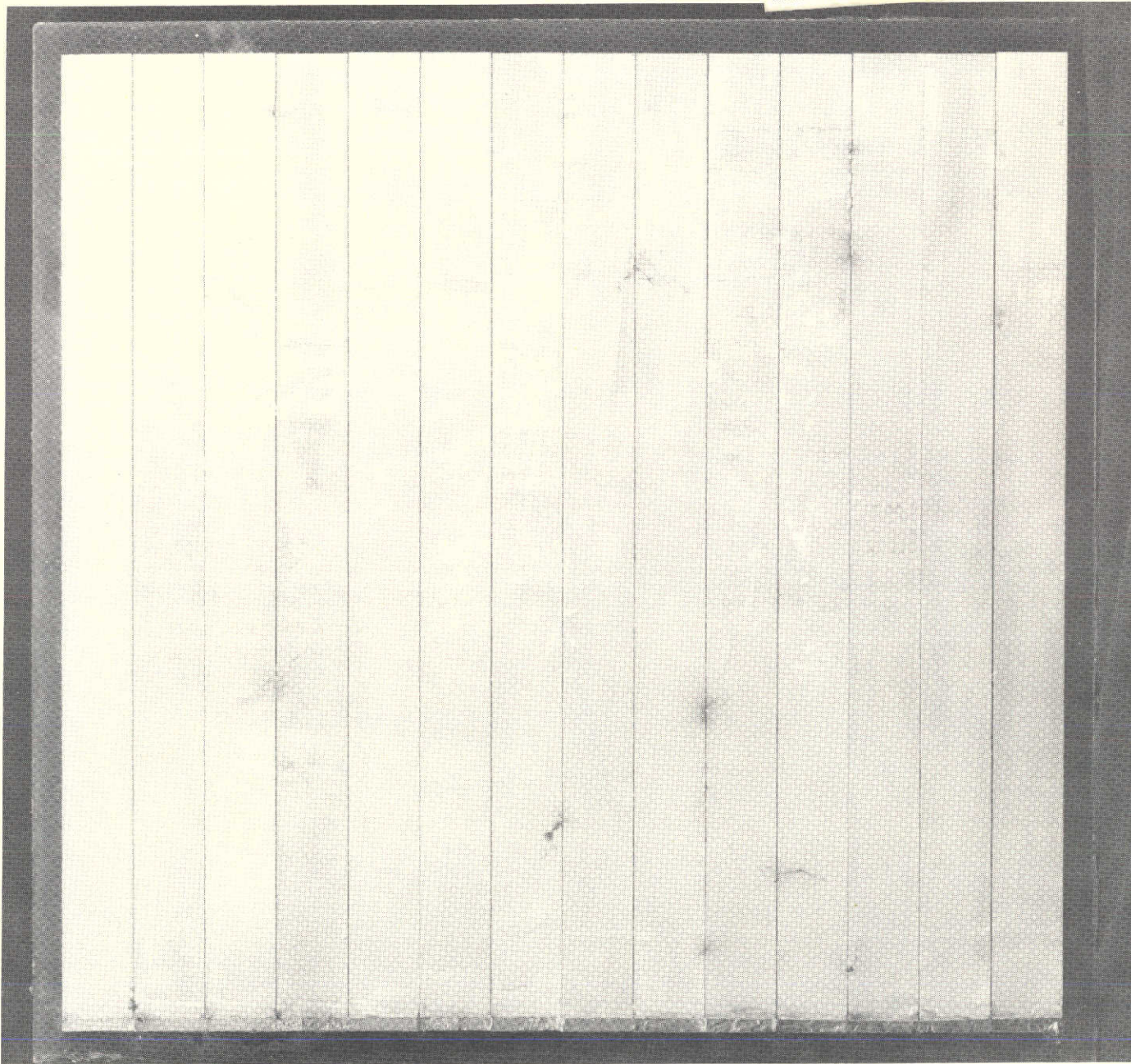


Figure 43: POST-TEST PHOTOGRAPH OF TOTALLY INSULATED ALUMINUM DUMMY SOLAR CELL PANEL

A schematic of the test setup is shown in Figure 44. The screen was comprised of 0.0635-cm diameter wire spaced on 0.254-cm centers, resulting in an optical transmission of 56-percent. Figure 45 shows that at a plasma density of 2.5×10^3 electrons/cm³ the unbiased screen reduces the panel electron current by a factor of about 5 at panel voltages between 100 and 1000 volts. With a negative screen bias of -150 volts the panel electron current is reduced by a factor of 30 or more. The ion current collected by the screen at -150 volts was nearly constant (between 6×10^{-6} and 8×10^{-6} amperes) with the solar panel biased at voltages between +100 and +10,000 volts. Similar results were obtained when the test was repeated at a lower plasma density (see Figure 46). Tables IV and V show that over the range of +100 to +10,000 volts the use of the biased screen resulted in power losses that were much less than those sustained by the unshielded panel.

No significant change in the results was observed by varying the panel-to-screen separation from 1/2-inch (1.27-cm) to 2-inches (5.08-cm).

During the test at high plasma density with the screen grounded it was observed that although the solar panel collected an electron current of 3×10^{-4} amperes at +10,000 volts, the screen collected an ion current of only 1×10^{-5} amperes, indicating that most of the electron current was indeed coming from the ambient plasma rather than from discharges in the region between panel and screen. If discharges in this region caused the 3×10^{-4} ampere panel current, then the screen current should be comparable to the panel current (ions from the discharge going to the screen, electrons going to the panel).

4.3.3.2 Negative Bias

The tests described in the preceding paragraphs (section 4.3.3.1) were repeated with negative bias applied to the solar panel. The presence of the screen reduced the solar panel leakage by a factor of 10 to 25 at negative solar panel voltages exceeding 100 volts (Figure 47). It was found that biasing the screen at voltages as much as +150 volts produced no significant change in the solar panel leakage current when the solar panel was biased at -2000 volts. As expected, the screen current resulted in prohibitive power losses when the screen was biased to +150 volts. Arcing was observed at a relatively low voltage (1,000 volts) even with the screen. The power levels at which arcing started with and without the screen were about the same ($\sim 5 \times 10^{-2}$ watts).

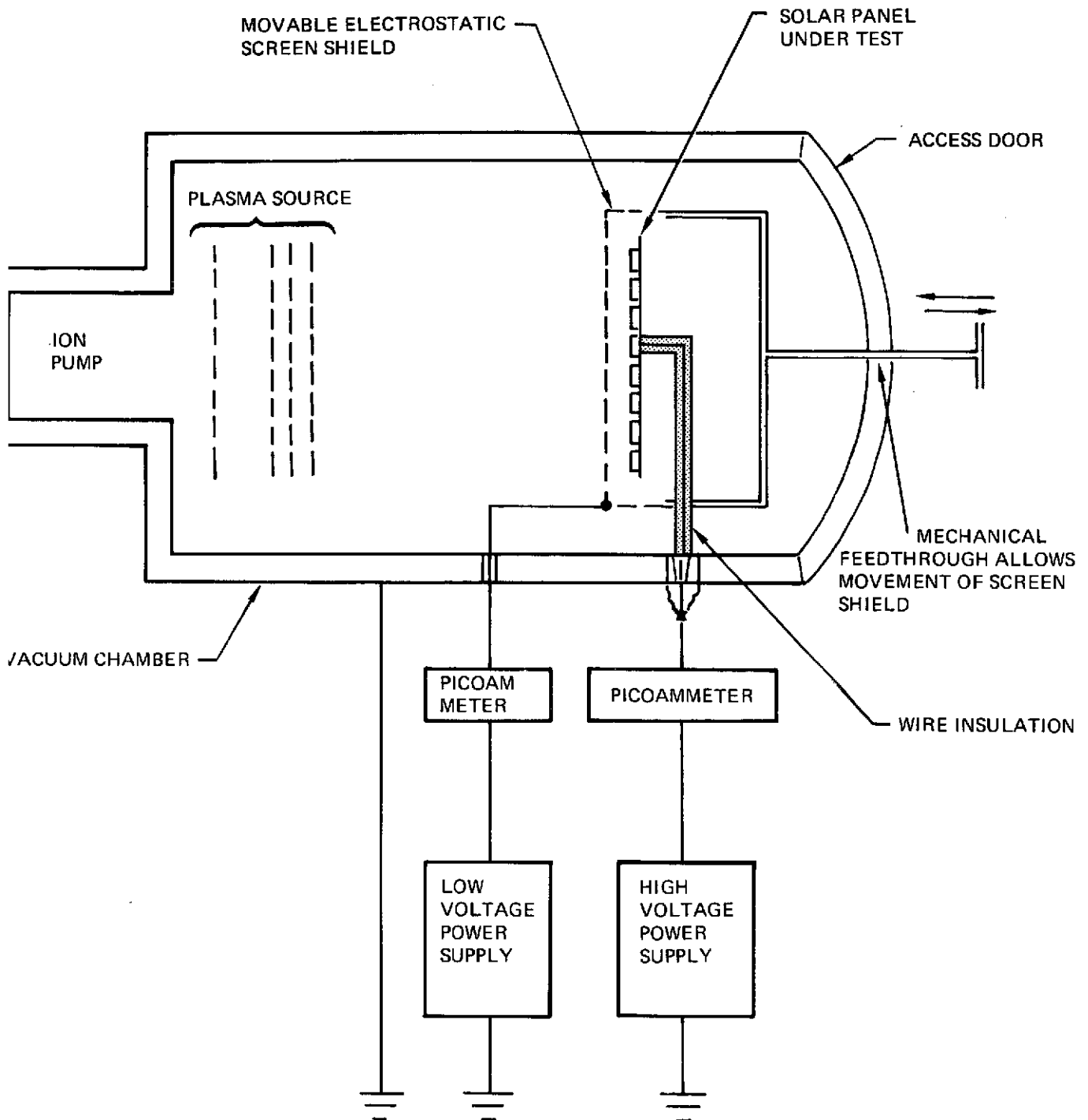


Figure 44 LEAKAGE CURRENT TESTS IN LARGE PLASMA CHAMBER

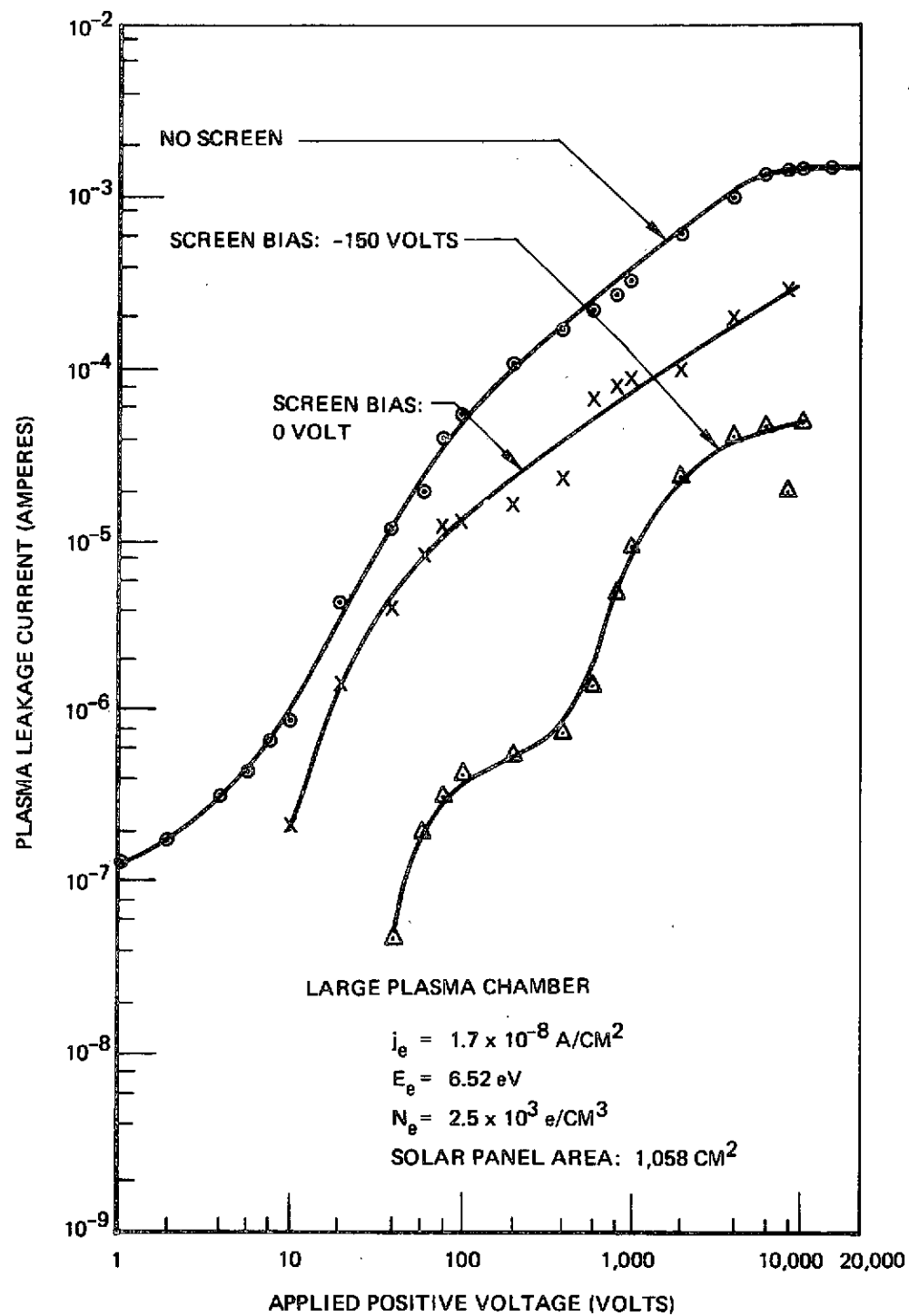
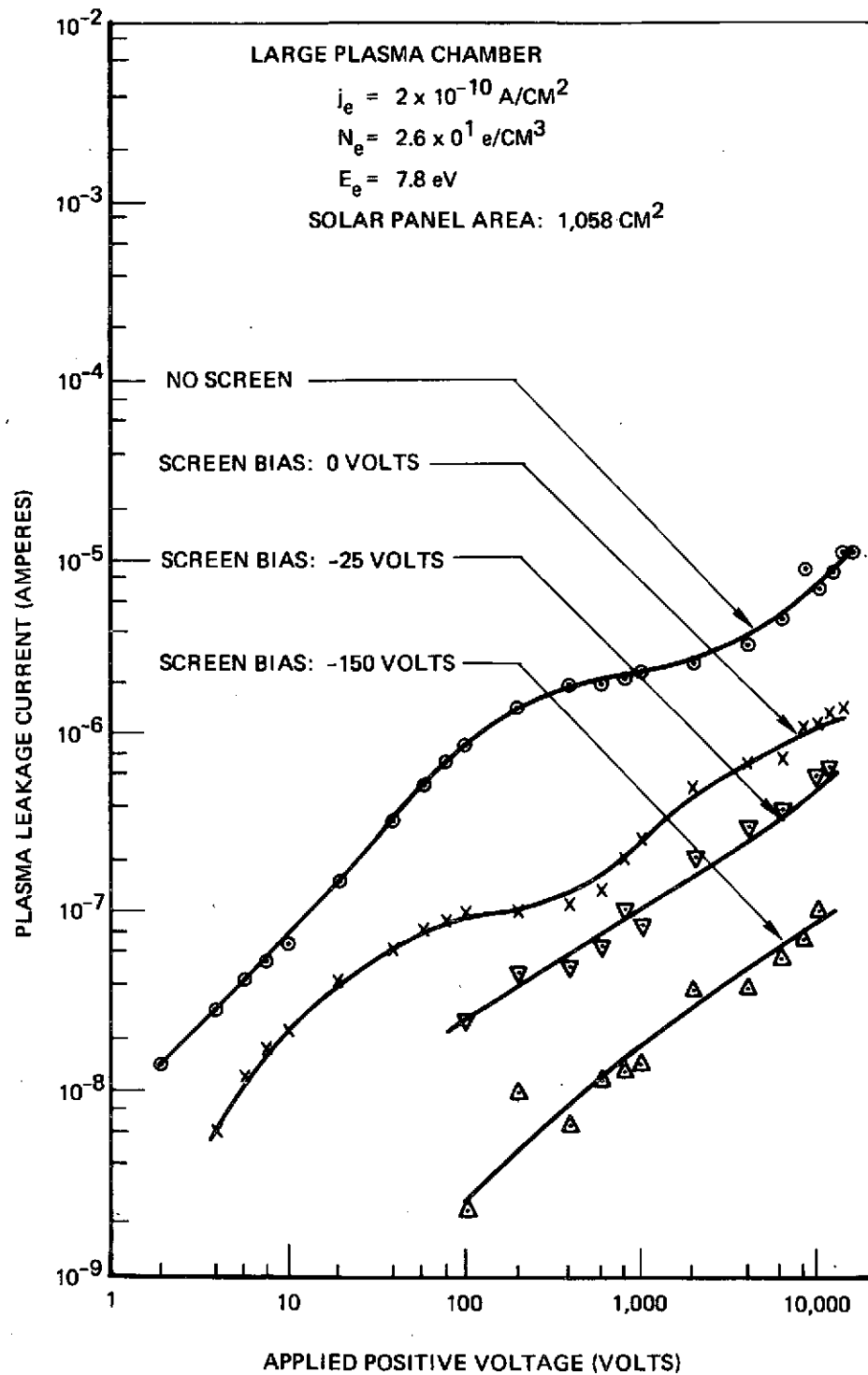


Figure 45 EFFECT OF ELECTROSTATIC SCREEN ON THE PLASMA LEAKAGE CURRENT COLLECTED BY A POSITIVELY BIASED SOLAR PANEL WITH UNINSULATED INTERCONNECTORS



C2523-48

Figure 46 EFFECT OF ELECTROSTATIC SCREEN ON THE PLASMA LEAKAGE CURRENT COLLECTED BY A POSITIVELY BIASED SOLAR PANEL WITH UNINSULATED INTERCONNECTORS

TABLE IV: PLASMA LEAKAGE POWER LOSSES IN A SHIELDED
AND UNSHIELDED SOLAR PANEL — $N_e = 2.5 \times 10^3$
ELECTRONS/CM³

WITH SCREEN AT -150 VOLTS				W/O SCREEN
V _{PANEL} (VOLTS)	P _{SCREEN} (WATTS)	P _{SOLAR PANEL} (WATTS)	P _{TOTAL} (WATTS)	P _{SOLAR PANEL} (WATTS)
+ 100	9.0×10^{-4}	4×10^{-5}	9.4×10^{-4}	5.5×10^{-3}
+ 1,000	9.9×10^{-4}	9×10^{-3}	1×10^{-2}	0.4
+10,000	1.2×10^{-3}	0.5	0.5	15

TABLE V: PLASMA LEAKAGE POWER LOSSES IN A SHIELDED
AND UNSHIELDED SOLAR PANEL — $N_e = 26$
ELECTRONS/CM³

WITH SCREEN AT -150 VOLTS				W/O SCREEN
V _{PANEL} (VOLTS)	P _{SCREEN} (WATTS)	P _{SOLAR PANEL} (WATTS)	P _{TOTAL} (WATTS)	P _{SOLAR PANEL} (WATTS)
+ 100	2.2×10^{-5}	2.7×10^{-7}	2.2×10^{-5}	9.0×10^{-5}
+ 1,000	2.4×10^{-5}	1.5×10^{-5}	3.9×10^{-5}	2.5×10^{-3}
+10,000	2.7×10^{-5}	1×10^{-3}	1×10^{-3}	7×10^{-2}

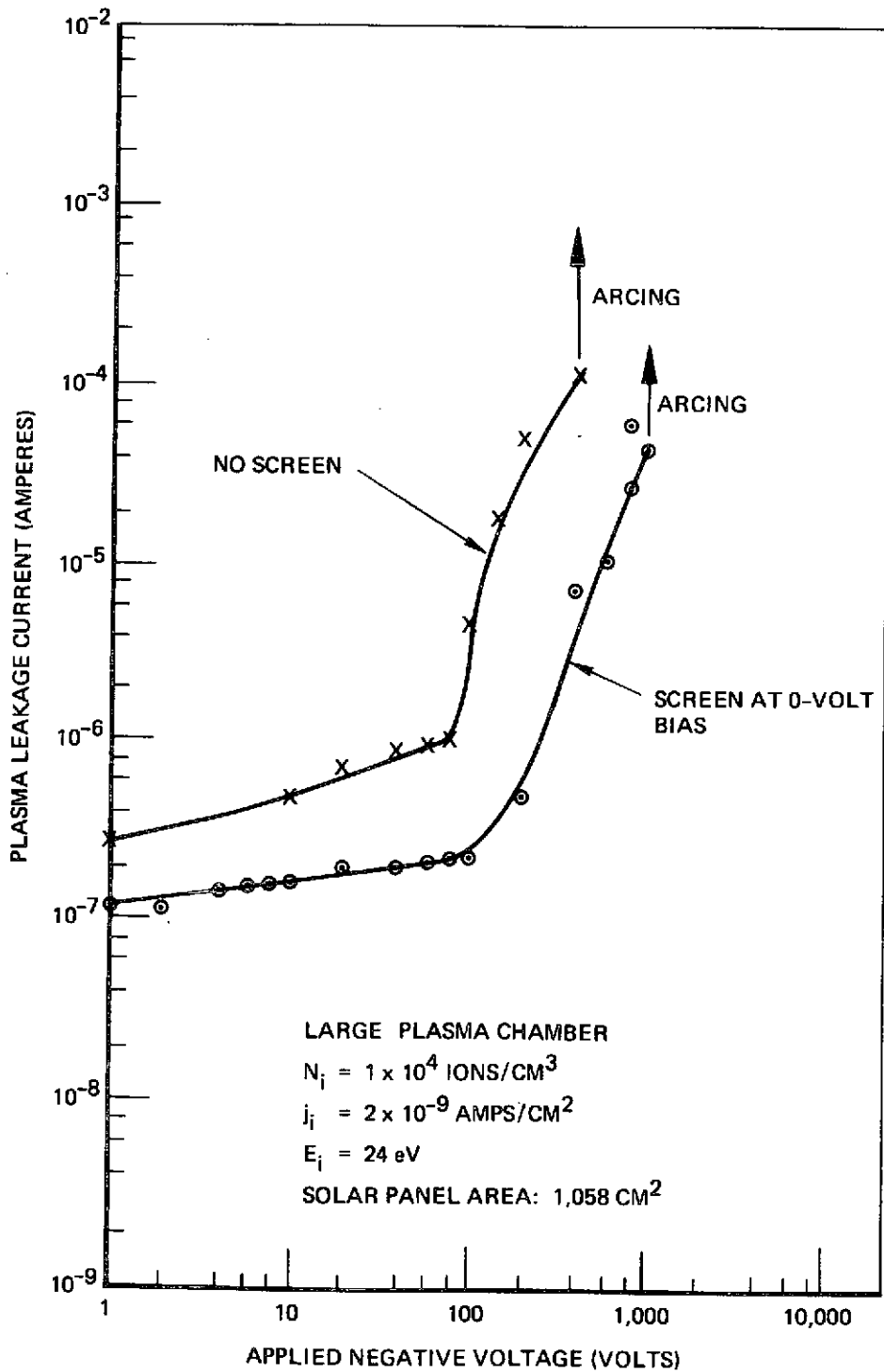


Figure 47 EFFECT OF ELECTROSTATIC SCREEN ON THE PLASMA LEAKAGE CURRENT COLLECTED BY A NEGATIVELY BIASED SOLAR PANEL WITH UNINSULATED INTERCONNECTORS

4.4 DIELECTRIC TESTS

4.4.1 Dielectric Breakdown

Table VI shows the results of testing various insulator materials in the LPC at room temperature. The tests were conducted in the same manner as the pinhole tests described earlier in section 4.2.1 except that the insulation contained no pinhole. The plasma density was maintained at 2×10^{-4} electrons/cm³. To insure that the full voltage was indeed across the test insulation, hot wire probe measurements were made within 1 cm of the insulator; no significant voltage could be detected by the probe even though +10kV was applied to the test electrode.

Table VII shows the results of similar dielectric breakdown tests conducted in the Charge Deposition Apparatus.

Although there is some variation between the results obtained in the plasma chamber and those obtained by charge deposition, they both agree that .005-inch thicknesses of Kapton and FEP Teflon, .006-inch thickness of fused silicone and R63-489 silicone are sufficient insulation to prevent breakdown in a plasma environment at voltages up to +16kV, at room temperature.

What Tables VI and VII do not show are the effects of temperature, proton and electrons radiation and time.

Tests conducted in the LPC on samples of .005-inch Kapton irradiated with 2880 hours of ultraviolet (equivalent six sun intensity) and a 7×10^{10} proton/cm² fluence of 10.5 MeV protons indicated no breakdown at voltages up to +16kV.

Also, tests performed in the LPC at voltages up to +16kV on .005-inch thicknesses of FEP Teflon and Kapton at 90°C gave no indication of breakdown.

4.4.2 Bulk Resistivity

Bulk resistivity measurements made on various dielectrics in the CDA at room temperature are shown in Table VIII. Note that in all cases the resistivity decreases with increasing voltage. Figure 48 further demonstrates this phenomenon in the case of Kapton.

It is evident from Table VIII that FEP Teflon is superior to Kapton in its insulation properties although both appear to be excellent. This difference was also observed in tests in the LPC when plasma leakage through Kapton and FEP Teflon were measured as a function of positive applied electrode voltage (Figure 49).

Effect of Ultraviolet and Proton Radiation - Figure 50 shows that the bulk leakage current of Kapton measured in the LPC is not significantly different after exposure to 2880 hours of equivalent six sun ultraviolet intensity and a 7×10^{10} proton/cm² fluence of 10.5 MeV protons.

Table VI: DIELECTRIC BREAKDOWN VOLTAGE OF SELECTED MATERIALS WITH A PLASMA ¹
ACTING AS ONE ELECTRODE

Specimen ⁶	Thickness	Positive Breakdown Voltage ²	Negative Breakdown Voltage ³
	(inches)	(kilovolts)	(kilovolts)
Kapton	0.003	> 16 ⁴	> 16
Kapton	0.005	> 16	Not Measured
FEP-Teflon	0.002	> 16	> 16
FEP-Teflon	0.005	> 16	Not Measured
Fused Silica	0.006	> 16	Not Measured
Microsheet	0.003	14	> 16
Microsheet	0.006	16	Not Measured
R63-489	0.005	> 16	> 16
RTV 560	0.001	2	6
Parylene-C	0.0015	< 1 ⁵	4
RTV 41	0.002	< 1	Not Measured
RTV 602	0.002	< 1	Not Measured

¹ Plasma Density: 2×10^4 e/cm³; Pressure $1-4 \times 10^{-6}$ Torr

² A positive potential was applied to the metal electrode in 1 kV steps.

³ A negative potential was applied to the metal electrode in 1 kV steps.

⁴ > 16 means breakdown did not occur at maximum applied voltage of 16 kV.

⁵ < 1 means breakdown occurred at a voltage less than 1 kV.

⁶ Specimen Temperature (25°C).

**TABLE VII: DIELECTRIC BREAKDOWN VOLTAGE OF
SELECTED MATERIALS WITH DEPOSITED
CHARGE ACTING AS ONE ELECTRODE**

SPECIMEN	THICKNESS (INCHES)	BREAKDOWN VOLTAGE (KILOVOLTS)	
		ELECTRONS	ARGON IONS
KAPTON	0.003	> 16 kV	19 kV
KAPTON	0.005	> 18 kV	> 24 kV
FEP TEFLON	0.002	14 kV	14 kV, 9 kV
FEP TEFLON	0.005	> 20 kV	20 kV, > 20 kV
FUSED SILICA	0.006	—	16 kV
MICROSHEET	0.003	—	9 kV
MICROSHEET	0.006	—	17 kV
R63-489	0.005	> 16 kV	—
PARYLENE C	0.0015	—	4 kV
RTV 41	0.001	9 Kv	5 kV
RTV 602	0.002	11 kV	< 1 kV

TABLE VIII: BULK RESISTIVITY OF SELECTED MATERIALS WITH CHARGE DEPOSITION APPARATUS

MATERIAL	THICKNESS, INCHES	RESISTIVITY IN OHM-CM							
		ION DEPOSITION				ELECTRON DEPOSITION			
		4 kV	8 kV	12 kV	16 kV	4 kV	8 kV	12 kV	16 kV
KAPTON	0.005	8.0×10^{15}	3.3×10^{15}	1.2×10^{15}	5.5×10^{14}	8.0×10^{15}	4.9×10^{14}	9.8×10^{14}	8.5×10^{14}
	0.003	1.4×10^{15}	1.2×10^{15}	3.7×10^{14}	1.0×10^{14}	6.8×10^{15}	1.4×10^{15}	1.4×10^{14}	1.5×10^{13}
FEP-TEFLON	0.005	6.0×10^{16}	3.1×10^{16}	1.3×10^{16}	3.1×10^{15}	2.0×10^{16}	1.3×10^{16}	6.1×10^{15}	7.0×10^{15}
	0.002	3.1×10^{16}	8.1×10^{15}	2.7×10^{15}		1.5×10^{15}	6.4×10^{15}	1.8×10^{15}	S
FUSED SILICA		4.8×10^{15}	3.2×10^{15}	1.9×10^{15}	1.1×10^{15}	7.0×10^{14}	4.1×10^{14}	1.6×10^{13}	S
MICROSHEET	0.006	3.2×10^{15}	4.7×10^{14}	1.3×10^{14}	1.3×10^{13}	2.4×10^{14}	7.9×10^{13}	2.9×10^{13}	1.1×10^{13}
	0.003	1.2×10^{15}	1.3×10^{14}			2.4×10^{14}	1.7×10^{13}	1.1×10^{13}	S
PARYLENE-C	0.0015	4.0×10^{14}	S	S	S	8.5×10^{14}	S	S	S
RTV-41	0.001	1.7×10^{15}		S	S	4.1×10^{15}	2.4×10^{14}	S	S
RTV-560	0.001	3.7×10^{13}	S	S	S	1.0×10^{14}	S	S	S
RTV-602	0.002			S	S	6.0×10^{15}	1.5×10^{15}		
XR-63-489	0.005	4.9×10^{13}		S	S	1.3×10^{14}	1.5×10^{14}	9.4×10^{13}	8.0×10^{12}
	0.002	6.0×10^{13}		S	S	S	S		

S - SATURATION BEAM CURRENT

* 15 kV VALUE, BREAKDOWN AT 16 kV

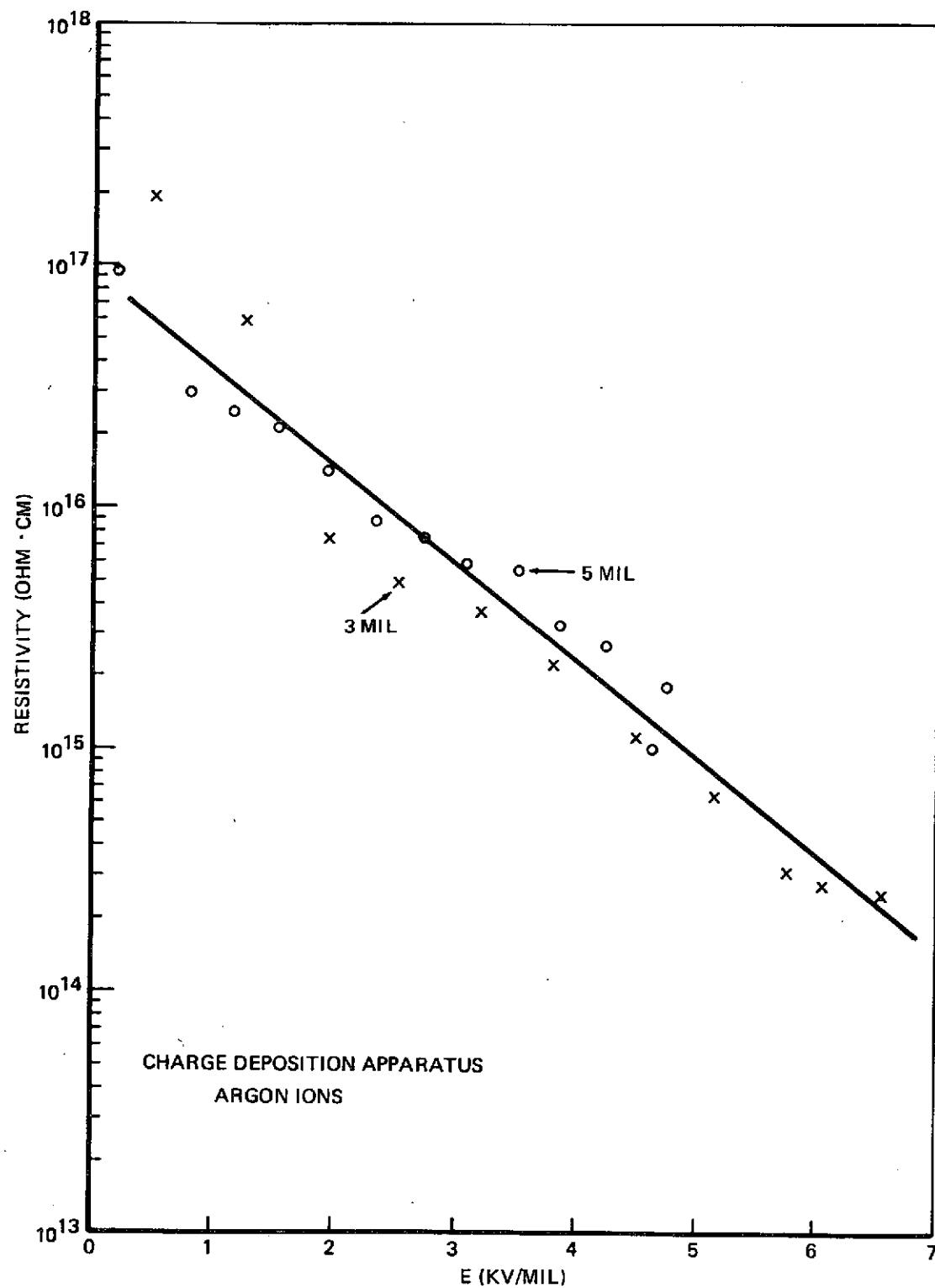


Figure 48 KAPTON - RESISTIVITY VS ELECTRIC FIELD

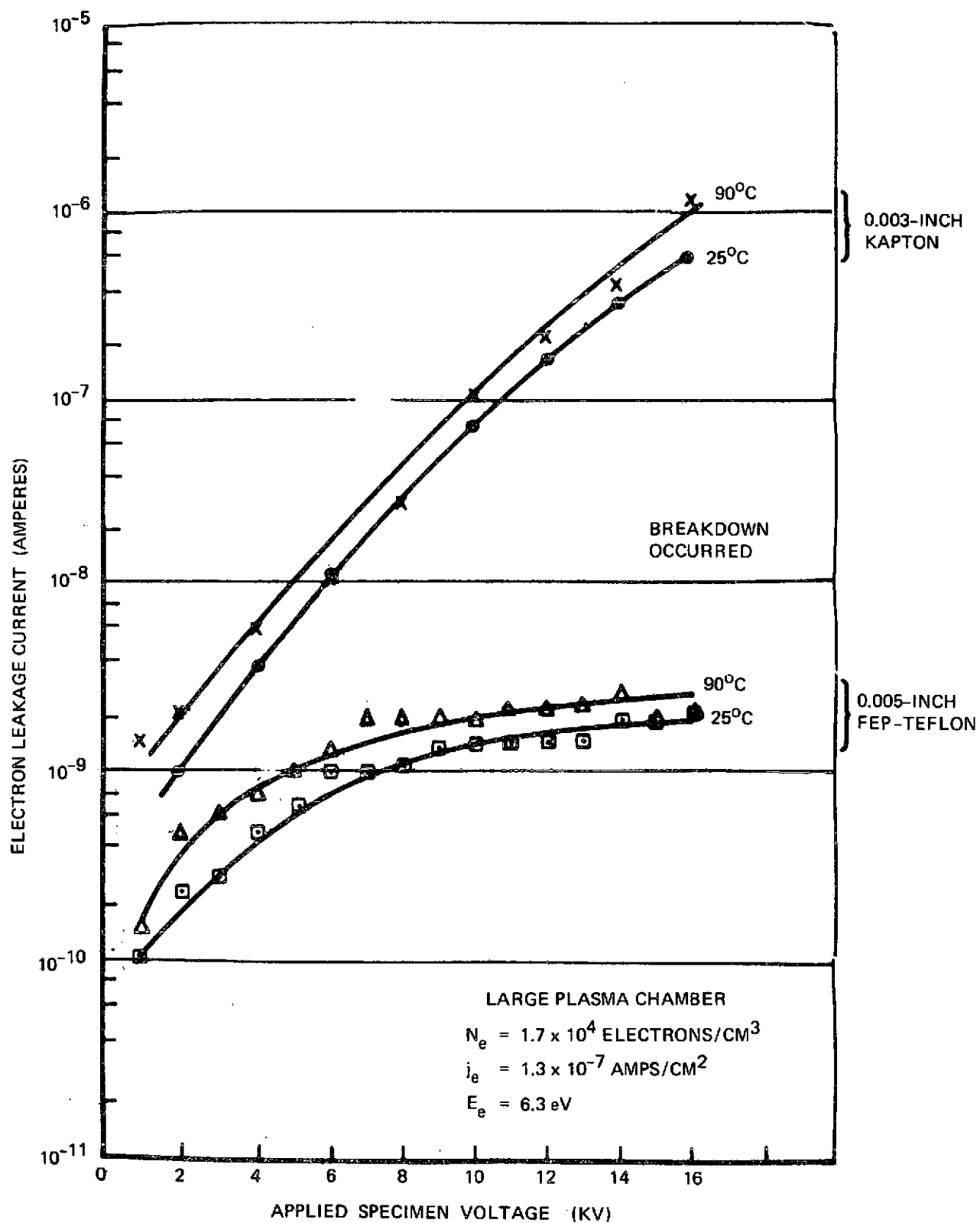


Figure 49 LEAKAGE CURRENT IN FEP TEFLON & KAPTON –
NO DEFECT IN TEST SPECIMEN – POSITIVE ELECTRODE POTENTIAL

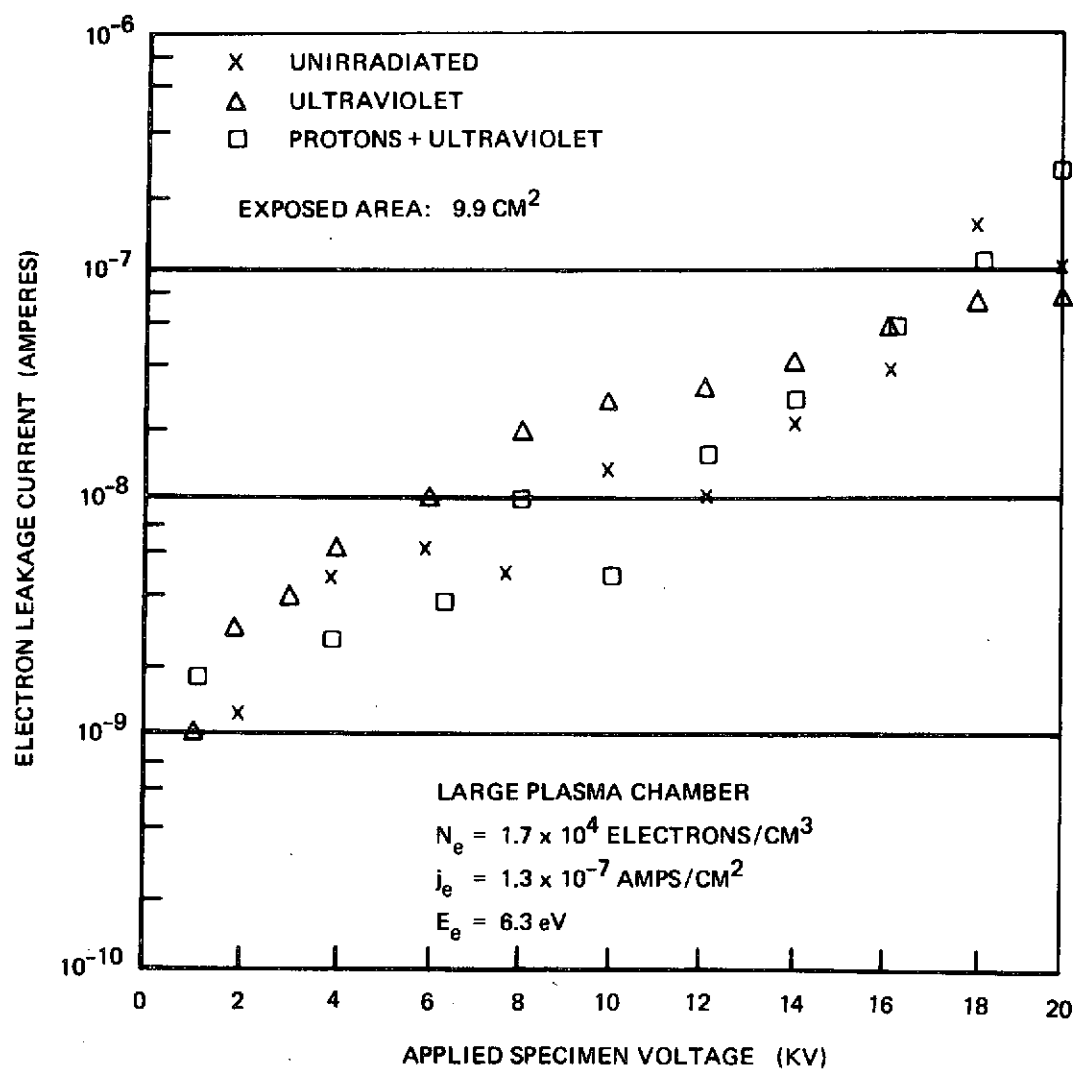


Figure 50 EFFECT OF PROTON AND ULTRAVIOLET RADIATION ON KAPTON
 HIGH VOLTAGE LEAKAGE CURRENT

Effect of Temperature - Conflicting results have been obtained in different tests. Some tests have indicated that there is little or no effect of temperature on the resistivity of FEP Teflon and Kapton up to 90°C (Figure 49) whereas other tests have indicated a dramatic difference (factor of 100 lower values at 28°C compared to 90°C). No conclusions can yet be made regarding temperature.

Effect of Light - In ref. 8, Kofoed reports that the bulk resistivity decreases by about one order of magnitude when the Kapton surface is exposed to ultraviolet light. His tests were conducted in the Charge Deposition Apparatus (CDA) with voltages applied up to 20kV. In the present program, Kofoed repeated the tests in the CDA using FEP-Teflon of the same thickness (.002-inches) and no such photoconductivity was found; the bulk resistance did not change when FEP-Teflon was exposed to the same ultraviolet intensities.

4.4.3 Surface Resistance Tests

4.4.3.1 Small Plasma Chamber (SPC)

The surface resistivity of Kapton surrounding a (0.38-cm diameter) pinhole was measured before and after a 69-hour exposure to plasma during which the pinhole collected 1×10^{-4} amperes of plasma current at +10kV. The test specimen was identical to that shown in Figure 30 except that the clamp ring was metal and was grounded via an electrometer. Surface leakage current was measured (with plasma off) by biasing the pinhole electrode and measuring the current collected by the metal ring. The results, shown in Figure 51, indicate that the surface resistance at +16kV measured immediately after the plasma exposure was about 3,000 times less than the pre-exposure value. After the plasma had been off for 4 hours, the surface resistivity (at 16kV) "healed" partially so that it was only 30 times less than the pre-exposure value. This suggests that the presence of charge on the surface may decrease the effective surface resistance of the Kapton. Perhaps this phenomenon has something to do with the pinhole "area effect" described in section 4.2.4 (i.e., perhaps plasma particles can move easily along the insulation surface surrounding a pinhole and therefore enhance pinhole current collection). The surface resistivity measurements did not vary significantly when the pressure was decreased from 1×10^{-6} Torr to 1×10^{-8} Torr (See Figure 52).

4.4.3.2 Charge Deposition Apparatus (CDA)

In order to measure Kapton surface resistivity a 2-cm diameter metal disc was placed in the center of a 7-cm diameter disc of Kapton which was bordered by a metal ring. Measurements (in vacuum) were made in two different ways: (1) the center disc was biased at voltages up to +20kV with a commercial power supply, while measuring current collected by the ring; (2) the CDA was used to deposit electrons (or ions) directly on the disc until it became charged up to voltages as high as +20kV while measuring current collected by the ring. The surface resistances obtained by charge deposition were lower than those obtained by direct bias by a factor of 30 to 100, suggesting that the presence of free charge somehow reduces surface resistance (see Figure 53).

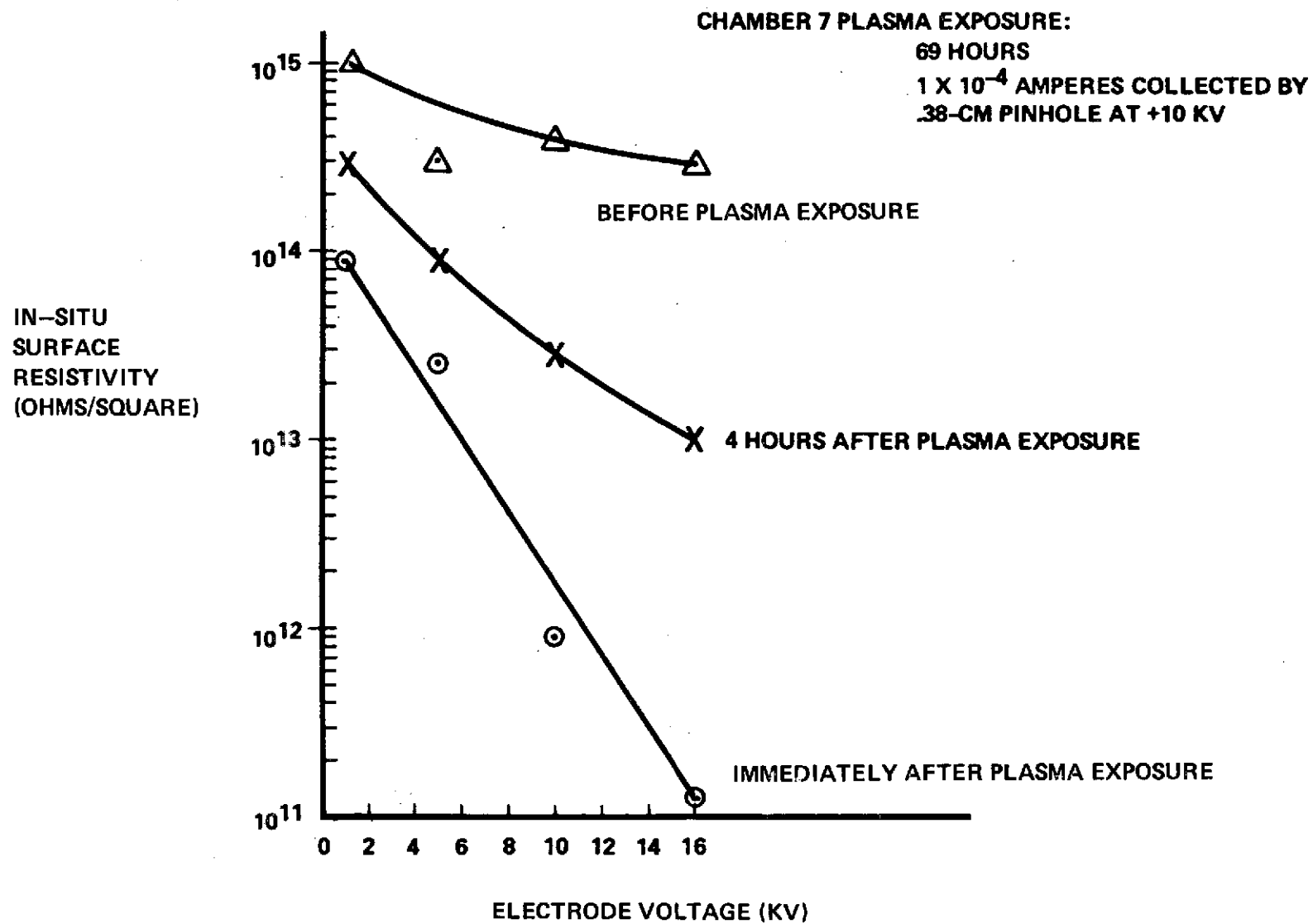


Figure 51 EFFECT OF PLASMA CURRENT COLLECTION ON KAPTON SURFACE RESISTIVITY

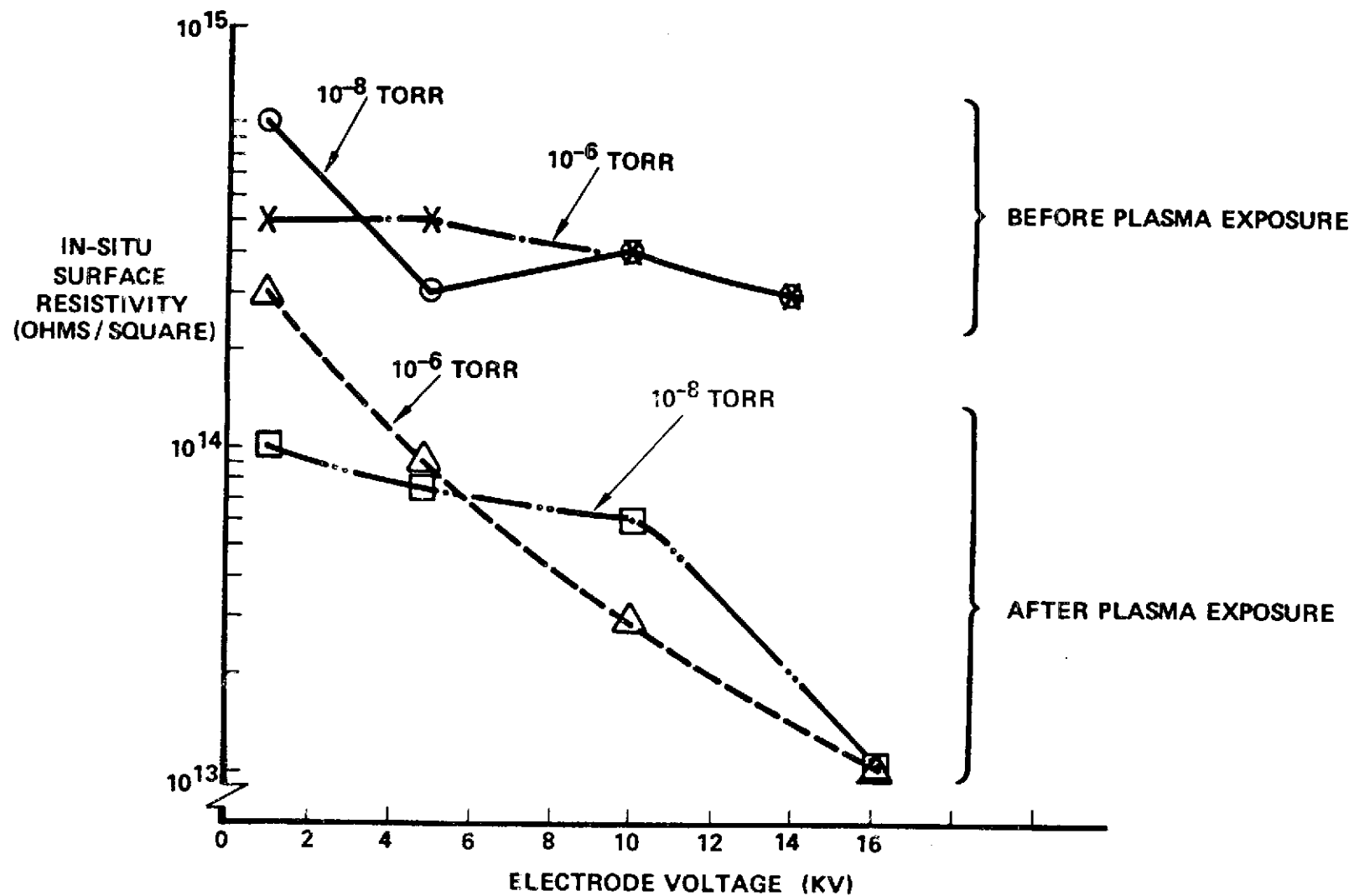


Figure 52 EFFECT OF BACKGROUND PRESSURE ON KAPTON SURFACE RESISTIVITY

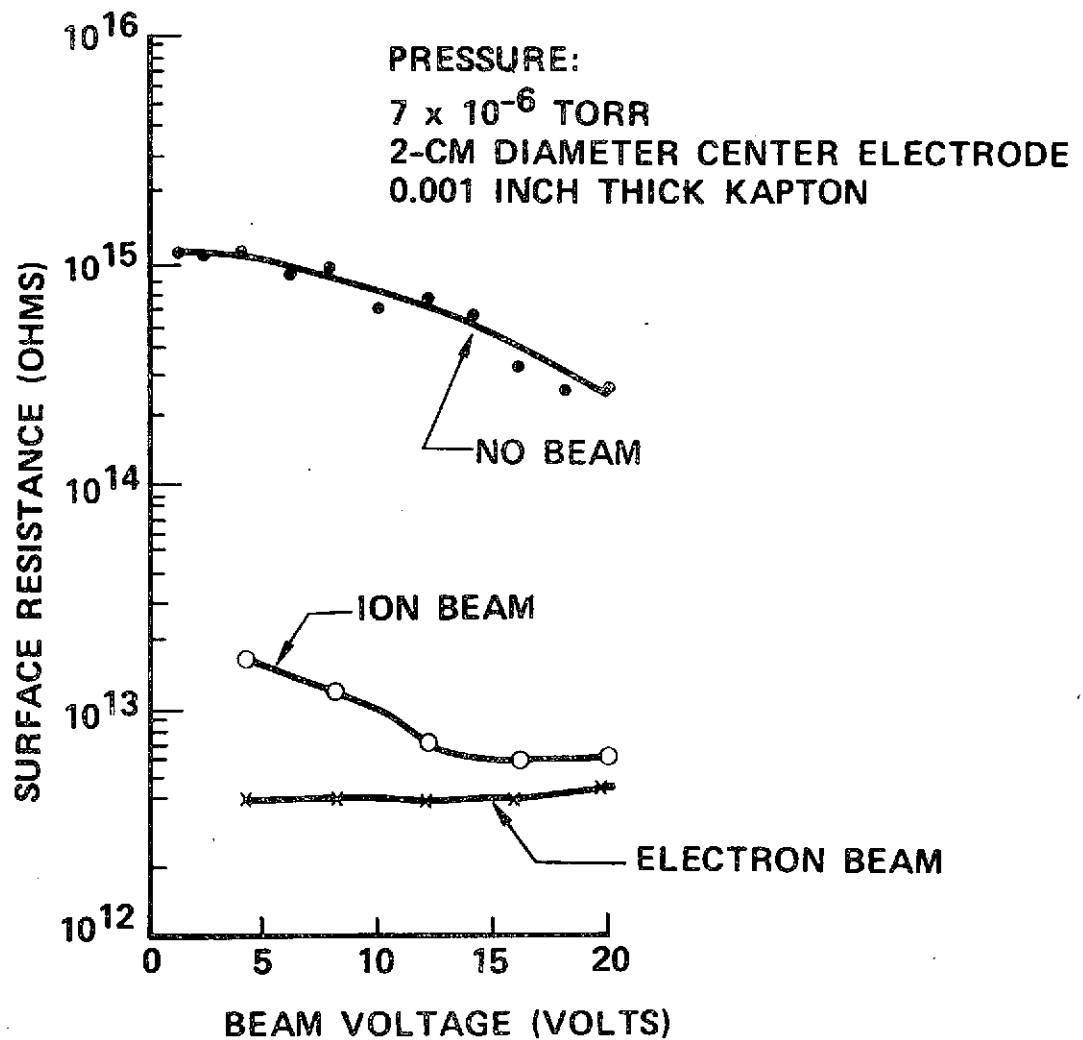


FIGURE 53 EFFECT OF FREE CHARGE ON
SURFACE RESISTANCE OF KAPTON

5.0 DISCUSSION OF RESULTS

A large quantity of data was obtained in this program, especially in measuring plasma currents collected by pinholes and solar panel segments based at high voltage. If this data is to be useful, its validity must be established. Validation was accomplished by biasing small metal spheres at high voltage in the plasma and comparing the resulting measured currents with calculated values. The excellent agreement observed over the entire range of plasma densities (Figure 10) for spheres suggests that the plasma currents measured for small test samples such as pinholes are valid. For longer test samples such as the 1 ft.² solar panel, the validity of the space plasma simulation can rightly be questioned since the limited size of the test chamber could influence the level of current collection. Damage levels could be determined with confidence for both large and small test samples since both voltage and plasma current could be controlled independently by the experimenter. With these thoughts in mind we proceed to a discussion of the results, organized in three separate subsections:

- 5.1 PINHOLES
- 5.2 SOLAR PANELS
- 5.3 DIELECTRICS

5.1 PINHOLES

It is a near certainty that even completely insulated solar arrays will eventually develop pinholes due to micrometeoroids, dielectric breakdown, insulation voids and other phenomenon. The resulting plasma currents, if sufficiently high, may cause intolerable power losses or insulation damage. Therefore, heavy emphasis was placed on the determination of pinhole current levels.

Large Pinhole Currents - The biggest surprise in the pinhole tests was the high level of pinhole currents. At voltages above 1kV, the pinholes collected much more current than that predicted on the basis of existing mathematical models. Figure 14 shows that above 1kV the measured pinhole current exceeded by several orders of magnitude that predicted for a sphere the same size of the pinhole or that predicted by the pinhole model of Parker (ref. 9). That these high currents are not a peculiarity of the test facility has been well established by the fact that metal spheres collect current in a predictable manner according to well-documented spherical probe theory.

"Area Effect" of Insulation - There is strong evidence that the insulation surrounding the pinhole is responsible for the large observed pinhole currents; when the insulation surface area was increased, the pinhole currents increased also. For example, Figure 21 shows that as the insulation area was enlarged by a factor of 100 (from 10 cm² to 1000 cm²) the pinhole current at 10kV increased by a factor of 70. This "area effect" is a repeatable phenomenon and has been observed by others. Its implications are particularly important for a large-area HVSA. Size of pinhole, type of insulation, or type of adhesive appear to be relatively unimportant in determining pinhole current levels.

One explanation for the "area effect" is that the pinholes collect current primarily by conduction of charges along the insulation surface, thereby increasing the effective surface area (ref. 6). An alternate explanation is that the pinholes collect current primarily by the capture of electrons that have been reflected from the surrounding insulation. If either of these explanations are correct, there is a line of reasoning that predicts that as the insulation surface area is increased the pinhole current will increase until it becomes limited by space charge effects. This line of reasoning is as follows. Suppose a tiny sphere is biased at high voltage and placed in a dilute plasma (10^3 electrons/cm³) in the absence of nearby insulation. The resulting current will be "orbit-limited" according to well-established spherical probe theory. This means that most of the electrons attracted towards the sphere at high voltage will orbit around the sphere and continue back into the plasma instead of being collected. If this tiny sphere were then placed on the surface of a sheet of insulation (to simulate a pinhole) the electrons that formerly orbited the sphere would instead be intercepted by the insulation and many of them subsequently collected by the pinhole. Thus the collected current would exceed that of the isolated sphere. If the insulation area were increased further, more and more electrons would be intercepted until the current became space-charge limited. Further increases in area would make no difference.

Electrode Size - It is also possible that the electrode size influences pinhole current collection. In the pinhole test referred to earlier, the insulation and electrode areas were roughly the same and it is therefore impossible to distinguish which one was primarily responsible for the observed increase in current. Testing by others (ref. 10) has suggested that electrode size may be unimportant and insulation area alone dictates pinhole currents. However, until more testing is done the possibility that electrode size is significant should not be overlooked. The following line of reasoning gives credibility to this possibility.

Without a pinhole in the insulation the field lines from the electrode terminate on the outside surface of the insulation due to bound charges which were attracted from the plasma when the voltage was first applied. However, when a pinhole is created, the pinhole may sweep some of these bound charges away and allow the field lines from the surrounding electrode area to extend into the plasma and contribute to the pinhole current-collecting capability. Since the bound charges closest to the pinhole would be swept away the easiest, the portions of the electrode closest to the pinhole would make the most significant contribution. Thus, this line of reasoning predicts that increases in electrode area would become less significant once the electrode area becomes large.

Conceptual Models May Lead to Mathematical Models - The above attempts at explaining the observed pinhole currents are merely qualitative and have not been completely validated experimentally. However, the concepts they represent may be helpful in formulating a mathematical model which could be used in a quantitative manner to predict pinhole currents for a large-area HVSA.

Pinhole Current "Jump" and Saturation - Another interesting phenomenon of pinhole current collection is the "jump" in current that occurs between 100 and 1,000 volts (see Figure 13). In this region the current may rise as much as five orders of magnitude. After this "jump" the current tends to saturate (as in Figure 13) or rise at a much slower rate ($\propto V$) (Figure 20). That these features are indeed characteristic of pinhole current collection rather than anomalies of the test setup has been verified by the fact that the current collected by spheres neither "jumps" nor saturates. One possible explanation for the observed current "jump" is as follows.

The insulation surrounding the pinhole is covered by a space charge sheath of electrons which maintains a negative potential of a few volts. When a small positive bias (e.g., 10 volts) is applied to the pinhole, this layer of surrounding negative charge reduces the effective potential of the pinhole and the pinhole current does not increase substantially. However, as the pinhole bias is raised further (e.g., to 100 volts) some of the surrounding negative charge gets swept away and the effective potential of the pinhole increases, becoming equal to that of a tiny isolated sphere. The resulting current increases dramatically as the pinhole (tiny sphere) seeks its space-charge limit and produces the observed current "jump". If the insulation surface is large enough, the current should reach its space-charge limit and thereafter should increase much more slowly with voltage (space-charge limited current for a sphere is proportional to $V^{6/7}$). This qualitatively explains the pinhole current versus voltage curve shown in Figure 20 for a large test sample. If the insulation surface is not very large (small test

sample) the current will not reach its space charge limit because some of the electrons can orbit around the test sample and return to the plasma. At the higher voltages, most of the electrons entering the space charge sheath of the pinhole will orbit the test sample and not be collected. Thus increases in voltage will not produce significant changes in pinhole current. Thus the "saturation" phenomenon shown in Figure 13 for small test samples.

Negatively-Biased Pinholes - The above discussion has been directed primarily towards the collection of electrons by a positively-biased pinhole. Negative biased pinholes were not so well characterized because of arcing problems that frequently damaged test equipment. However, limited testing has shown that the negative-bias pinholes exhibit completely different current-voltage curves. Figure 16 shows that the current is approximately proportional to the $3/2$ power of voltage over the entire voltage range (10 volts to 20,000 volts) and does not exhibit a current "jump" or saturation as in the positive polarity case. One possible interpretation of the phenomenon is that the leakage current represents space-charge limited flow between the exit screen of the plasma source and the pinhole (hence the well-known $V^{3/2}$ dependence for electrodes of fixed separation).

Damage Effects of Pinhole Currents - Pinhole currents were found to cause surface darkening and tracking in Kapton, a candidate substrate material for HVSA's. Table III shows that damage starts at power levels between 0.5 and 5 watts per pinhole. This darkening and surface tracking seems to be particularly bad in Kapton, which is otherwise a good insulator. Similar tests of FEP-Teflon sheet did not produce either of these effects.

5.2 SOLAR PANELS

Because of the large plasma currents collected by pinholes it would seem natural to eliminate such currents in a high voltage solar array by completely insulating it from the plasma. To evaluate this concept numerous small ($\leq 1/10 \text{ ft}^2$) completely-insulated solar panels were tested.

Total Insulation is Possible, But Costly and Unreliable - Tests demonstrated that small solar panels, biased at high positive and negative voltages can be completely sealed from the simulated space plasma, at least for several days. The most successful panels were comprised of solar cells having wrap-around contacts and interconnects insulated with Dow Corning 93-500 silicone adhesive. One such panel was biased at +4kV and another was biased at -10kV in two separate plasma tests which each ran over 90 hours without the occurrence of breakdown or pinholes. Also, a small four-cell module of solar cells encapsulated in FEP-Teflon was made to withstand over 70 hours in a plasma at $\pm 16\text{kV}$ without plasma leakage.

Although the above tests demonstrated the feasibility of completely insulating solar panels, they also revealed that the process of doing so is likely to be costly, unreliable, and excessively time-consuming. Because of the necessity for repeated applications of encapsulant, repeated microscopic examination, and repeated plasma seal tests when encapsulating interconnectors in the above-described test panels, it is estimated that the overall cost of a space-qualified, completely insulated array will be as much as 15% more than a conventional array just because of the added insulation. (This number is based upon the assumption that a conventional array costs \$3,000/ft.² and the technician who insulated the panels described above could learn to do the job twice as fast). If wrap-around cells are required (as the above tests indicate) the overall array cost may easily be increased by another 15%. Also, completely insulated arrays will probably weigh between 6 and 10 percent more than their conventional counterparts because of the extra adhesive required between and underneath solar cells.

Pinholes Negate Advantage of Complete Insulation - There is no assurance that insulated panels will not eventually develop pinholes due to thermal cycling, micrometeoroids, ultraviolet radiation, etc. Calculations based on the micrometeoroid model described in ref. 2 indicate that there is only a 5-percent probability that a one square foot section of a .005-inch thick Kapton substrate would be able to last one year in space without a micrometeoroid puncture. Thus it must be assumed that even a completely insulated array will develop some pinholes.

Tests conducted in this program indicate that once a completely insulated panel acquires pinholes it can draw nearly as much current at high voltage as a solar panel with bare solar cell interconnectors (see Figure 42). This is due basically to the pinhole "area effect" referred to in section 5.1 for positively biased panels. These results suggest that for positive voltages perhaps the bare interconnector approach is best.

Solar Panel Current Collection with Bare Interconnectors - Measured plasma currents collected by a 1 ft.² solar panel having bare interconnectors were found to be in fair agreement with calculated values based upon a partially

insulated spherical probe model. Agreement is best (factor of 3) for positive voltages (Figure 39). Negative voltages did not agree so well (Figure 40). When this model is used to predict currents collected by a 15kW solar array in space, plasma power losses become significant only at high positive voltages ($>2\text{kV}$) and at altitudes below about 500 miles. This model, described in Appendix C, assumes that the array is a metal sphere, partially covered with insulation, which collects current as if its effective voltage were reduced by the ratio of exposed metal area to overall surface area. The good agreement noted above is somewhat surprising since the chamber size limits the natural plasma sheath expansion of the biased panel. Nevertheless, the fact that agreement is so good over the entire range of voltages and plasma densities suggests that the proposed model is not an unreasonable one. What has not yet been accomplished is verification of this model for very large solar panels (e.g., 1500 ft.^2). In such panels the plasma current is limited by space charge effects rather than the particle-orbiting which dictates small panel (e.g., 1 ft.^2) current collection. Verification could be accomplished either by conducting tests on very large solar panels under space plasma conditions or on small panels exposed to higher density plasmas where current collection is limited by space charge.

The ability to predict plasma current levels is clearly important in providing assurance that a solar panel will not lose too much of its output power to the plasma. Equally important is a knowledge of what damage might occur as the result of exposing a HVSA to a plasma. Problem areas observed were: hot spots, negative polarity arcing, and darkening of solar cell covers.

Hot Spots - Tests conducted on a 1 ft.^2 solar panel (section 4.3.1.1) indicate that if interconnectors on a HVSA are to be left "bare", care should be taken to insure that no adhesive gets spilled in the interconnectors, otherwise plasma currents can cause damage-producing "hot spots" at the spill locations. Observations made during these tests revealed red and white spots in the interconnector regions at voltages above $+5,000$ volts and plasma currents above 1×10^{-3} amperes. Post-test inspection of the panel further revealed that these hot spots occurred at places on the interconnectors where small amounts of silicone adhesive had spilled. As a result of only 5 minutes or so of operation at these high voltages, these hot spots had completely destroyed the interconnector beneath (it was gone). When a similar test was conducted on a smaller solar panel (see section 4.3.1.2.2) where the bare interconnectors were "clean", no such hot spots were observed. These results are pertinent primarily to positively-biased panels. In the case of negatively-biased panels, arcing appears to be more significant than "hot spots" and some evidence indicates that negative arcing can be eliminated by insulating interconnectors.

Arcing Problems - Negatively-biased solar panels, when exposed to a plasma, result in arcing that occurs more frequently, is more severe, and starts at much lower voltages than that produced by positive voltages. (The concern is that such arcing could produce electrical transients that damage circuit components and, if continued indefinitely, could damage materials at the arcing spot.) Tests on a 1 ft.^2 solar panel with bare interconnectors indicate that when negative voltages were applied, heavy discharges started at voltages as low as 400 volts (Figure 40). When positive voltage was used, such discharging did not start until voltages exceeded 5,000 volts.

Similar results were obtained in tests conducted on smaller panels having bare interconnectors; a panel biased at -10kV and collecting 1×10^{-7} amperes exhibit severe arcing whereas another panel biased at +10kV and drawing much more current (5×10^{-4} amperes) exhibited no arcing. In an attempt to reduce the negative bias arcing, the interconnectors on one panel were insulated with silicone adhesive. The panel was run at -10kV in a low density plasma for about 100 hours. No arcing was observed. (A repeat of this test using a similar panel with bare interconnectors resulted in considerable arcing and observable burned spots on the Kapton substrate.) Thus interconnector insulation may be of some value for negatively-biased solar panels.

Darkening of Solar Cell Covers - An unexplained darkening of solar cell covers and interconnectors occurred when a small solar panel having bare interconnectors was exposed to the laboratory plasma for several days (114 hours) at +10kV. The darkened covers caused a 7 percent loss in output power. (A 7 percent loss in output power output in 114 hours extrapolates to a 50 percent loss in 34 days, clearly an intolerable degradation.) No such darkening or loss of power was observed in a similar panel with insulated interconnectors biased at +10kV in the plasma for the same time period. (The undarkened panel had not been collecting any measurable plasma current during this time period, whereas the darkened panel had been collecting 1×10^{-5} amperes.) The observed darkening is of concern only if it is due to contaminants produced by the solar panel, not the plasma chamber. The cause is not yet known, but appears to be due to attraction of a negative ion towards the front surface of the panel which forms a deposit upon impact.

Screen-Shielded Solar Panel - Tests indicate that a biased screen shield suspended close to the front surface of a HVSA can significantly reduce plasma power losses. Figure 45 shows that when a metal screen biased at -150 volts was placed one inch in front of a conventional solar panel (bare interconnectors) biased at +10,000 volts, the plasma current collected by the panel was reduced by a factor of 30. Similar results were found with a negatively biased panel except that it was not necessary or beneficial to bias the screen.

The screen used in these tests, although demonstrating feasibility, was much too heavy and was not transparent enough for practical space applications. Furthermore, a practical scheme for mounting the screen has yet to be developed.

The practicality of the screen shield approach will ultimately depend upon the weight and cost of a reliable space-flight design.

5.3 DIELECTRICS

Both bulk and surface dielectric properties were investigated.

Bulk Properties - Bulk dielectric properties are important because insulating materials such as solar cell covers, solar array substrate, and interconnector insulation must have a good dielectric strength to minimize the probability of pinholes. Also, the bulk resistance of these materials must be sufficiently high that current flow through them does not cause damage or significant power loss. Therefore, dielectric strength and bulk resistivity tests were performed with a plasma or deposited charge acting as one electrode and a metal disc as another electrode. The results, summarized in Tables VI and VII indicate that the bulk dielectric properties of .005-inch thicknesses of Kapton (substrate) and FEP-Teflon (cover) and .006-inch thicknesses of microsheet glass (cover), fused silica (cover) and silicone interconnector encapsulants (Dow-Corning 93-500 or R63-489) are sufficient to prevent breakdown or excessive leakage in a plasma environment up to +16kV. Since these tests were conducted at room temperature, with smooth electrodes, were of relatively short duration (few minutes), and in most cases did not account for radiation effects, the results must be used with care in designing space hardware.

A few special tests were conducted to determine the effect of ultraviolet light, protein radiation, and temperature on the bulk resistivity of Kapton and FEP-Teflon sheet. FEP-Teflon was found to be insensitive to the presence of ultraviolet light whereas Kapton bulk resistivity decreases about one order of magnitude due to photoconductivity. However, no permanent damage was found in Kapton after a prolonged exposure to high energy protons and ultraviolet radiation; its bulk resistivity remained virtually unchanged after 2880 hours of equivalent six run ultraviolet intensity and a 7×10^{10} proton/cm² fluence of 10.5 MeV protons. Conflicting results regarding the effects of temperature on Kapton were obtained; some tests indicated a dramatic decrease (factor of 100) in resistivity when the temperature rises from 28°C to 90°C whereas other tests indicated no difference. The temperature problem still remains to be resolved.

Surface Properties - The surface resistance of Kapton appears to decrease by a factor of 30 to 3000 when exposed to a dilute plasma (Figure 51) or when one electrode is charged directly by the deposition of electrons (Figure 53). Because the initial resistivity of Kapton is so high $>10^{15}$ ohms/square, this decrease in resistivity does not, in itself, lead to large surface leakage currents. However, it may be related to the "area effect" described in section 5.1 whereby pinhole current collection is enhanced by the presence of surrounding insulation. Furthermore, it may contribute to the ease with which surface darkening and tracking occurs on Kapton surfaces surrounding a pinhole.

6.0 CONCLUSIONS

Several potential problems were identified which must be better understood before a reliable HVSA can be designed. Most significant is that dangerously large plasma currents may be collected by a pinhole (e.g., micrometeoroid puncture) in a large area HVSA. Also, when a solar panel attains a negative potential relative to the plasma, arcing occurs at unexpectedly low voltage and current levels (e.g., 400 volts at 10^{-4} amperes/ft.²). Solar panels attaining a positive bias with respect to the plasma are relatively immune to arcing but are susceptible to damage-producing hot spots when the interconnectors are coated with insulation. Generally, it appears best to leave interconnectors bare and restrict the voltage and altitude of operation to levels where the plasma power losses are acceptable. One analytic model, which is consistent with the experimental data in this report, predicts that plasma power losses for a 2-16kV HVSA with bare interconnectors will not be important at altitudes above about 500 nautical miles.

A list of the most significant findings resulting from this investigation is presented below:

Space Plasma Simulation

- o The space plasma simulation used in this investigation is valid. Validation was accomplished by measuring the plasma currents collected by small metal spheres biased up to 20kV in the space plasma and finding that they agreed with calculated values based on well-established spherical probe theory.
- o One exception to the validity of the space plasma simulation is that the chamber size may have restricted the current collecting capability of the largest (1 ft.²) solar panel that was tested.

Pinholes

- o Pinholes in insulation covering high voltage (2 to 16kV) electrodes in the simulated space plasma collect much more current than that predicted by spherical probe or disc probe mathematical models. The pinhole currents are often high enough to cause significant damage to the insulation.
- o Pinhole currents are enhanced by the presence of surrounding insulation. As the surface area is increased, the pinhole current increases also. This has been termed the "area effect" and has important implications for a large-area HVSA in space. Size of pinhole, type of insulation, and type of adhesive appear to be relatively unimportant.
- o Pinhole currents rise very rapidly at voltages between 100 and 1000 volts. At higher voltages the current either saturates or rises much more slowly.

- o Pinhole currents in Kapton start causing damage (e.g., charring, surface tracking) at power levels between 0.5 and 5 watts per pinhole.

Solar Panels

- o The process of completely insulating solar panels appears to be costly, unreliable and excessively time-consuming. The extra cost may be 30 percent over that of a low voltage solar array. In addition, there is no assurance that insulated panels will not eventually develop pinholes due to thermal cycling, micrometeoroids, ultraviolet radiation, etc.
- o Tests have shown, however, that small solar panels, biased at positive and negative high voltages, can be completely sealed from the simulated space plasma, at least for several days.
- o Once a positively-biased, completely insulated solar panel acquires pinholes it will draw nearly as much plasma current as a solar panel with bare interconnectors. Thus the bare interconnector approach appears best for positive biases.
- o Plasma currents collected by a 1 ft² solar panel with bare interconnects were found to be in fair agreement with calculated values based on a partially-insulated spherical probe model. Agreement is best (factor of 3) for positive voltages. When this model is used to predict currents collected by a 15kW solar array in space, plasma power losses become significant only at high positive voltages (> 2kV) at altitudes below about 500 nautical miles. Future testing is needed to verify this model before it can be used with confidence.
- o If interconnectors on a high voltage solar panel are to be left "bare", care should be taken to insure that no adhesive gets spilled on the interconnectors. Otherwise plasma currents can cause damage-producing "hot spots" at the spill locations.
- o Negative bias voltages in plasma cause arcing that occurs more frequently, is more severe, and starts at much lower voltages than that produced by positive voltages. In one test solar panel arcing started at -400 volts, but not at +4,000 volts. Insulating the interconnectors appears to substantially reduce negative bias arcing.
- o An unexplained darkening of coverslides on a solar panel with bare interconnectors occurs after several days of exposure at 10kV in the laboratory plasma. Future testing is required to determine if the panel, not the chamber, is responsible.
- o A biased screen shield surrounding a high voltage solar array can significantly reduce plasma power losses. However, the practicality of this approach depends primarily upon the weight and cost of a reliable, lightweight, space-flight design.

Dielectrics

- o Bulk dielectric properties of .005-inch thicknesses of Kapton and FEP-Teflon and .006-inch thicknesses of microsheet glass, fused silica, and silicone encapsulants (Dow Corning 93-500 or R63-489) are sufficient to prevent breakdown or excessive leakage in a plasma environment at voltages up to ±16kV.
- o The surface resistivity of Kapton decreases in the presence of free charge (e.g., plasma) by as much as a factor of 3000.

7.0 LIMITATIONS

The findings of this investigation are incomplete or limited in the following respects:

- o The pinhole tests were not conducted on large enough electrodes to determine if pinhole currents increase indefinitely with the size of the surrounding surface area. Present electrode sizes were limited to $\sim 1 \text{ ft}^2$.
- o Plasma sheaths surrounding the 1 ft^2 uninsulated solar panel were comparable to or larger than chamber dimensions. Thus the measured currents are questionable and the partially-insulated spherical probe model needs corroboration of other experimental data before it can be used with confidence.
- o Life tests on solar panels in the simulated space plasma were limited to several days duration and did not include effects of ultraviolet and particulate radiation.
- o The question of whether or not it is worthwhile to insulate interconnectors cannot be answered until the pinhole "area effect" is better understood.
- o Most testing was conducted with positive biases. Negative bias tests were less reproducible, less well behaved, subject to much arcing, and promoted premature failures in test equipment.

Data obtained from the SPHINX (Space Plasma High Voltage Interaction Experiments) satellite (to be launched in January 1974) should fill in many of the information gaps left by these limitations, particularly long-term effects, radiation effects, and current-collecting behavior when sheath growth is unrestricted (see ref. 11).

REFERENCES

1. Knauer, W., Bayless, J. R., Todd, G. T., and Ward, J. W., "High Voltage Solar Array Study," NASA CR-72675, Hughes Research Laboratories, Malibu, California (May 1970).
2. Springgate, W. F., "High Voltage Solar Array Study," NASA CR-72674, The Boeing Company, Seattle, Washington (May 1970).
3. Cole, R. K., Ogawa, H. S., and Sellen, J. M., Jr., "Operation of Solar Cell Arrays in Dilute Streaming Plasmas," AIAA 7th Electric Propulsion Conference, Williamsburg, Virginia, Paper 69-262 (March 1969).
4. McKinzie, D. J. and Grier, N. T., "Dielectric Breakdown in a Dilute Plasma - A 20 Kilovolt Limited Study," NASA Technical Memorandum TMX-2444 (January 1972).
5. Grier, N. T. and McKinzie, D. J., "Current Drainage to a High Voltage Probe in a Dilute Plasma," AIAA 10th Aerospace Sciences Meeting, San Diego, California, Paper No. 72-105 (January 1972).
6. Bayless, J. R., Herron, B. G., and Worden, J. D., "High Voltage Solar Array Technology," AIAA 9th Electric Propulsion Conference, Bethesda, Md., Paper No. 72-443 (April 1972).
7. Burrowbridge, D. R., "A Technique for Simulating the Ionospheric Plasma", NASA-Goddard Space Flight Center Report No. X-325-68-172 (May, 1968).
8. Kofoed, M. J. and Cleva, H. V., "Photoconductivity in Electrically Stressed Dielectrics," Proceedings of National Academy of Sciences Conference on Electrical Insulation and Dielectric Phenomenon," Buck Hills Falls, Pennsylvania (October 1972)
9. Parker, L.W., and Whipple, E.C., "Theory of a Satellite Electrostatic Probe", Annals of Physics 44, pp. 126-167 (1967).
10. Private communication with Stan Domitz, NASA-LeRC (1973).
11. Stevens, J.N., "Solar Array Experiments on the SPHINX Satellite", NASA Technical Memorandum TMX-71458 (November 1973).
12. Chen, F. F., "Electric Probes," Plasma Diagnostic Techniques, Huddleston, R. H. and Leonard, S. L., editors, Academic Press, New York, pp. 113-119 (1965).
13. Langmuir, I., "Currents Limited by Space Charge Between Concentric Spheres," Phys. Rev. 23, p. 49 (1924).

APPENDIX A - PLASMA DIAGNOSTICS

Electron Parameters - A Langmuir probe consisting of a 1.27-cm diameter stainless steel sphere was used to determine electron parameters in the Large Plasma Chamber: j_{eo} , electron thermal current density; \bar{E}_e , average electron energy; and N_e , electron number density. Two different methods were used, namely, the "saturation current" method and the "positive slope" method. The former was used as the primary method and the latter used occasionally as a check.

The "saturation method" required biasing the probe between -35 and +35 volts while measuring the probe current. Figure A-1 shows typical data and outlines the method of determining the electron parameters:

$$j_{eo} = I_{sat}/A_p \quad (\text{amps/cm}^2) \quad (A-1)$$

$$\bar{E}_e = \frac{\Delta V_p}{\Delta (\ln I_e)} \quad (\text{electron volts}) \quad (A-2)$$

$$N_e = 3.70 \times 10^{18} \frac{j_{eo}}{\sqrt{\bar{E}_e}} \quad (\text{electrons/cm}^3) \quad (A-3)$$

where

I_{sat} = saturation current (amperes)

A_p = probe surface area (cm^2)

V_p = probe voltage (volts)

I_e = electron current collected by probe (amperes)

The electron current, I_e , is obtained at any voltages by subtracting the ion saturation current from the probe current. To determine I_{sat} one must first find V_0 , the plasma potential. V_0 is taken as the intersection of two straight lines drawn through the retarding and attracting portions of the curve of I_e vs V_p . V_0 normally varied between -12 to +12 volts, depending upon plasma conditions. I_{sat} is taken as the current corresponding to V_0 . \bar{E}_e is the slope of the portion of the I_e vs V_p curve at voltages $V_p < V_0$. Equation A-3 above is derived from the basic equation

$$j_{eo} = 1/4 N_e e \bar{V}_e \quad (A-4)$$

where

e = electronic charge

\bar{V}_e = average electron velocity assuming a Maxwellian distribution

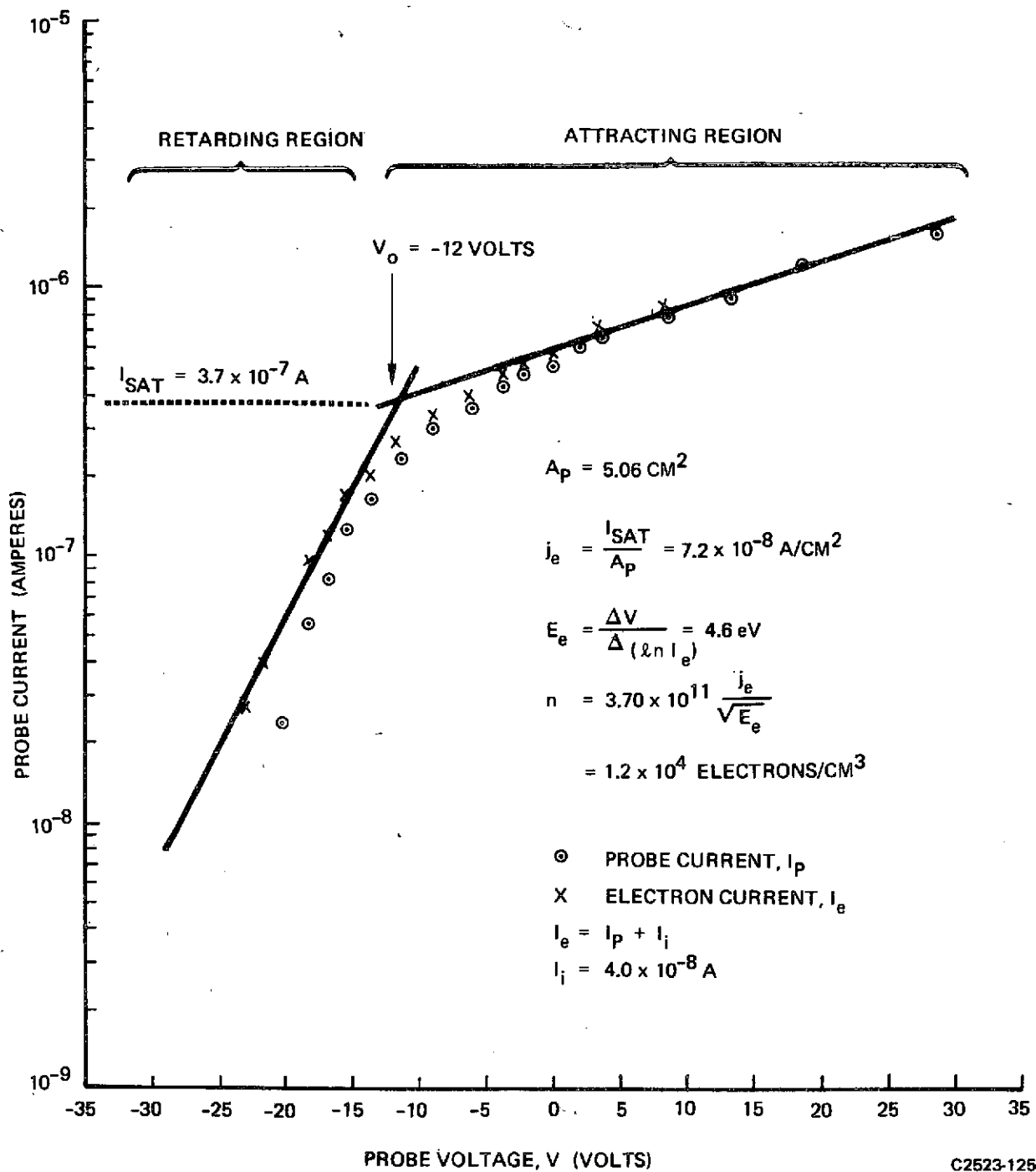


Figure A-1: DETERMINATION OF PLASMA NUMBER DENSITY BY "SATURATION CURRENT" METHOD

The "positive slope" method required biasing the probe between +20 and +100 volts while measuring the probe current. Figure A-2 shows typical data and outlines the method of determining the electron parameters:

$$N_e = 3.70 \times 10^{11} \left(\frac{dI_p}{dV_p} \frac{\sqrt{E_e}}{A_p} \right) \text{ (electrons/cm}^3\text{)} \quad (\text{A-5})$$

To use this method, one must use the value of E_e obtained from the retarding portion of the curve in Figure A-1. Equation A-5 assumes that the sphere current is orbit-limited and is given by (ref. 12)

$$I_p = A_p j_{eo} \left(1 + \frac{V_p}{E_e} \right) \quad (\text{A-6})$$

Differentiating A-6 with respect to V_p , replacing j_{eo} with an expression obtained from A-3, and rearranging, one is able to derive equation A-5.

The electron number density, N_e , determined by the two methods normally agreed within a factor of 2 (compare values of N_e on Figures A-1 and A-2). When the positive slope method was tried at even higher voltages (up to +16kV) the results were the same (see Figure A-3 and A-4).

Ion Parameters - A three-grid disc probe, described earlier in Section 3.1.2, was used to determine ion parameters in the Large Plasma Chamber: j_{i0} , ion beam current density; \bar{E}_i , average ion energy, and N_i , ion number density. Figure A-5 shows a typical plot of ion current density on the collector plate as a function of ion retarding voltages on one of the screens. The value at zero retarding voltage is taken as j_{i0} after being corrected for transmission of the screens:

$$j_{i0} = \frac{I_{co}}{A_c} \left(\frac{1}{T} \right) \quad (\text{A-7})$$

where

I_{co} = collector current at zero retarding voltage

A_c = area of collector plate

T = net transmission of screens

Figure A-6 shows the result of differentiating the data in Figure A-5 with respect to retarding voltage, indicating an ion energy spectrum which peaks at about 25 eV and has a half-width, half-maximum bandwidth of 7.5 eV. The average ion energy is determined by using the values of dj_i/dE_i from Figure A-6 in the following equation:

$$E_e = 4.6 \text{ eV (FROM FIGURE A-1)}$$

$$A_p = 5.06 \text{ CM}^2$$

$$n = 3.70 \times 10^{11} \left(\frac{dI}{dV} \right) \frac{\sqrt{E_e}}{A_p}$$

$$= 6.4 \times 10^3 \text{ ELECTRONS/CM}^3$$

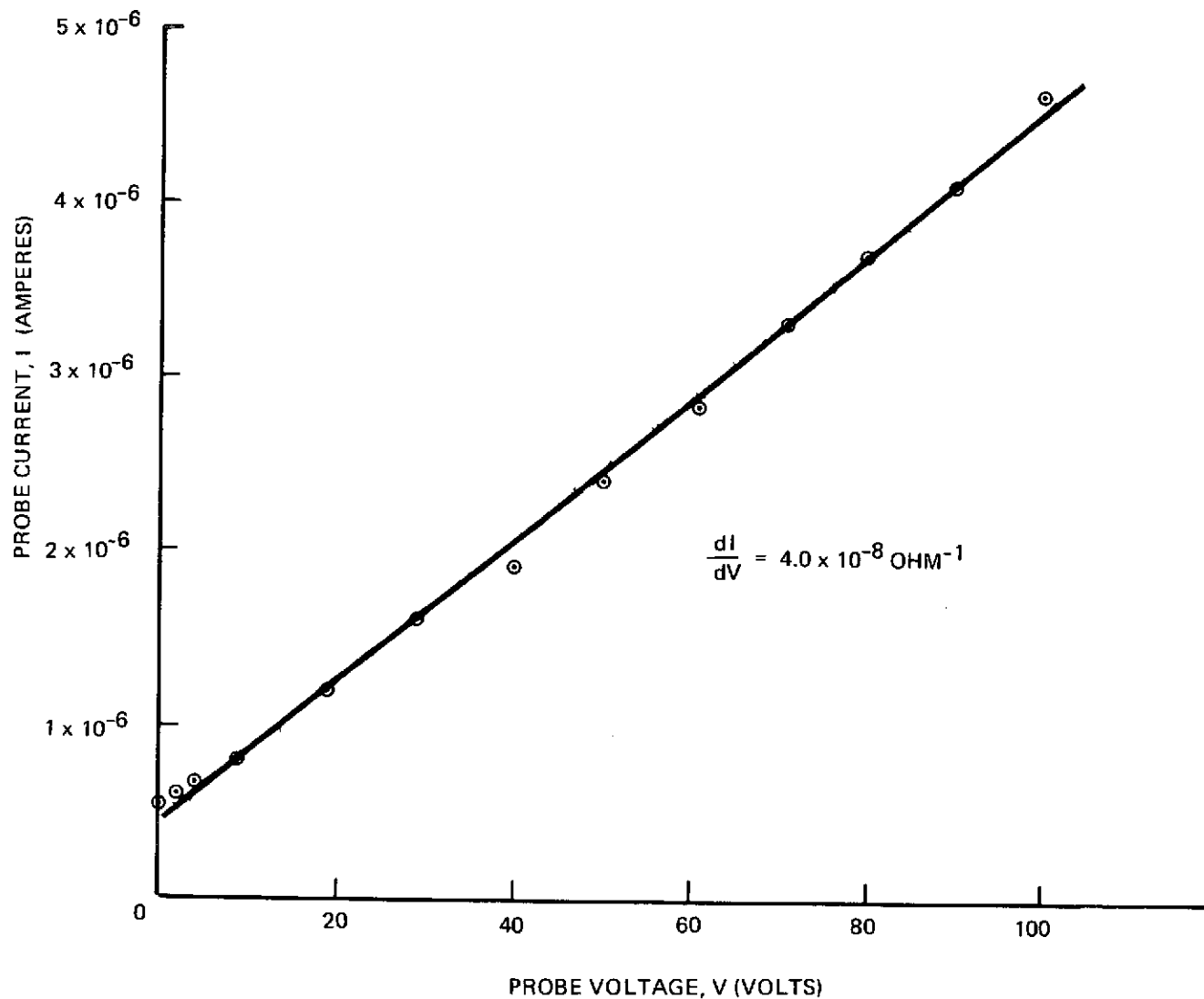


Figure A-2: DETERMINATION OF PLASMA NUMBER DENSITY BY "POSITIVE SLOPE" METHOD AT LOW VOLTAGES

$$E_e = 4.6 \text{ eV (FROM FIGURE A-1)}$$

$$A_p = 5.06 \text{ CM}^2$$

$$n = 3.7 \times 10^{11} \left(\frac{dI}{dV} \right) \frac{\sqrt{E_e}}{A_p}$$

$$= 6.8 \times 10^3 \text{ ELECTRONS/CM}^3$$

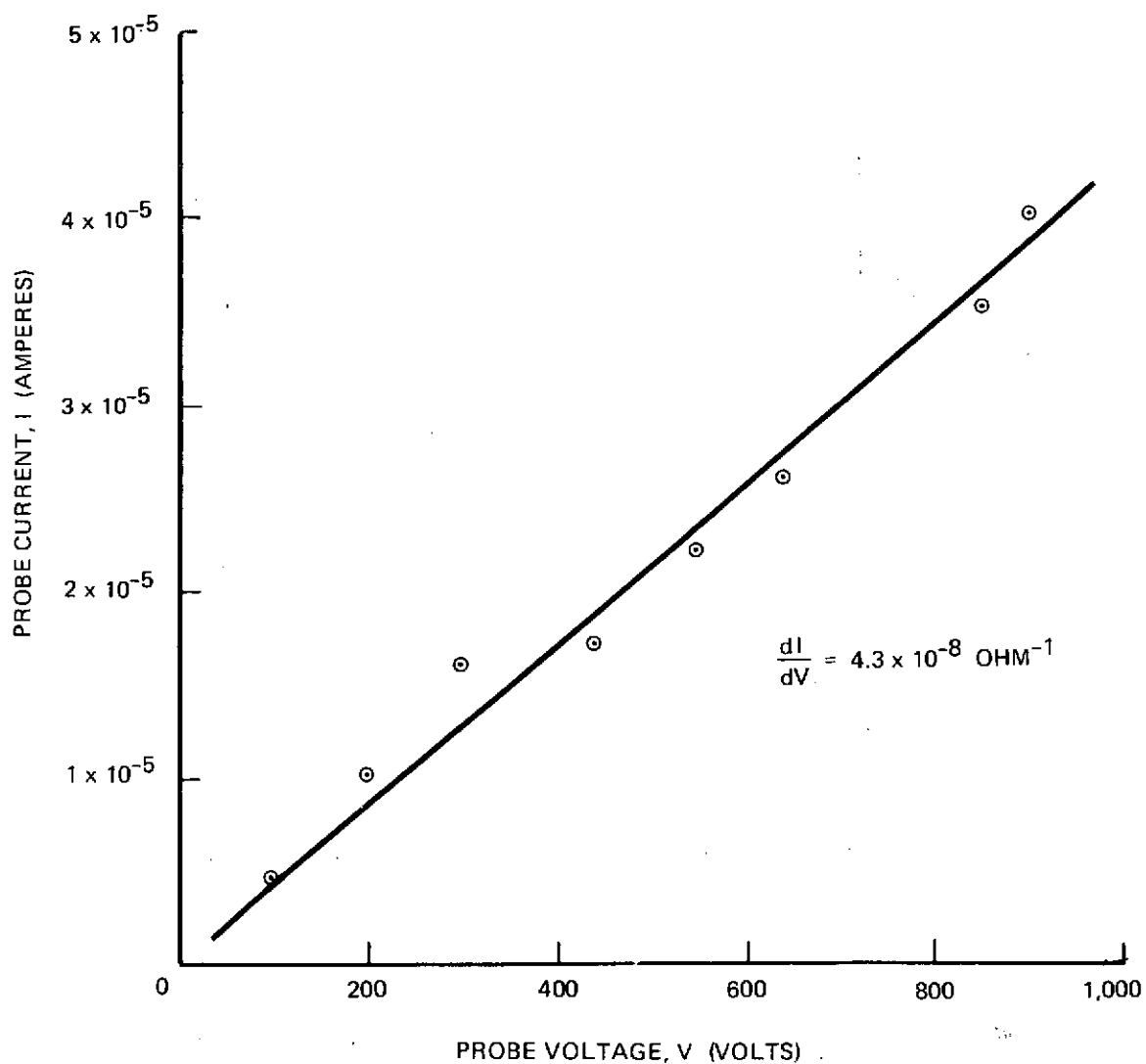


Figure A-3: DETERMINATION OF PLASMA NUMBER DENSITY BY "POSITIVE SLOPE" METHOD AT MEDIUM VOLTAGES

$$E_e = 4.6 \text{ eV (FROM FIGURE A-1)}$$

$$A_p = 5.06 \text{ CM}^2$$

$$n = 3.7 \times 10^{11} \left(\frac{dI}{dV} \right) \frac{\sqrt{E_e}}{A_p}$$

$$= 8.0 \times 10^3 \text{ ELECTRONS/CM}^3$$

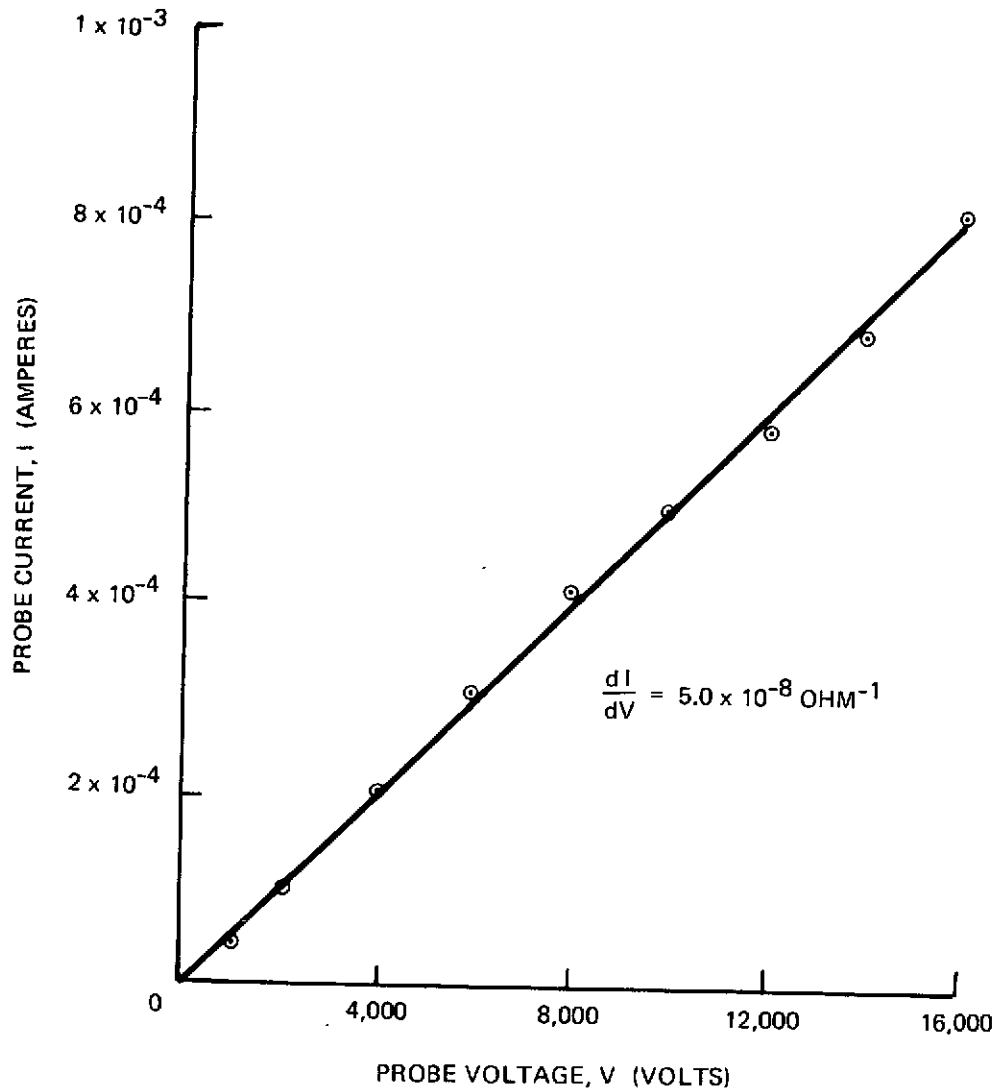


Figure A-4: DETERMINATION OF PLASMA NUMBER DENSITY BY "POSITIVE-VOLTAGE SLOPE" METHOD AT HIGH VOLTAGES

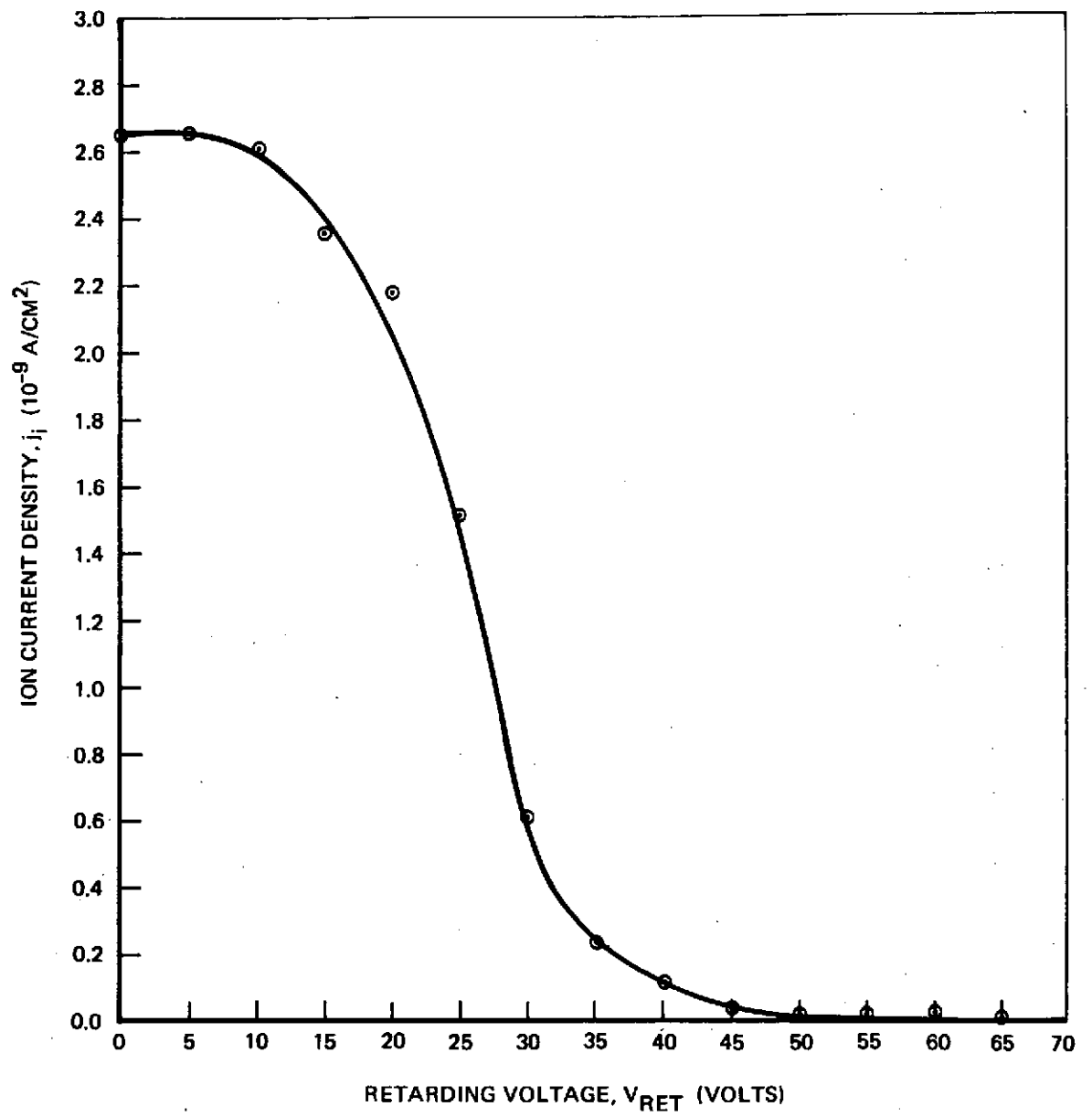


Figure A-5: ION CURRENT DENSITY VERSUS ION RETARDING VOLTAGE

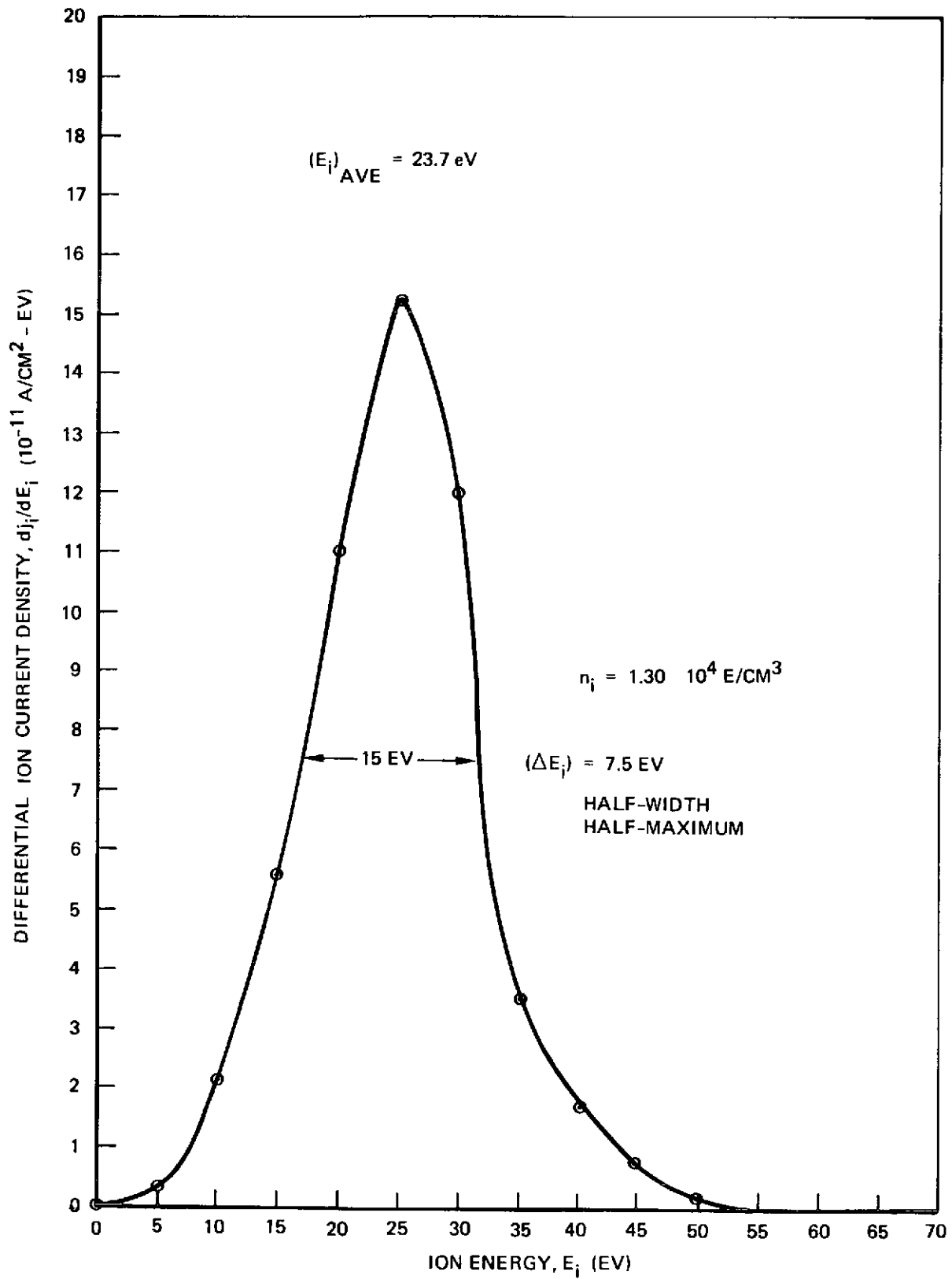


Figure A-6: DIFFERENTIAL ION CURRENT DENSITY VERSUS ION ENERGY

$$\overline{E_i} = \left[\frac{j_i}{\int_0^{E_{\max}} E_i^{-1/2} \frac{dj_i}{dE_i} dE_i} \right]^2 \quad (\text{A-8})$$

where

j_i = ion current density (A/cm^2)

$\overline{E_i}$ = average ion energy (eV)

E_i = individual ion energy (eV)

E_{\max} = maximum ion energy (eV)

$\frac{dj_i}{dE_i}$ = differential ion current density ($\text{A}/\text{cm}^2\text{-eV}$)

Ion number density, N_i , is obtained from the equation

$$N_i = 2.39 \times 10^{13} \frac{j_i}{\sqrt{E_i}} \quad (\text{A-9})$$

Equations (A-8) and (A-9) are derived from the simple expression

$$j_i = N_i q_i V_i$$

where

q_i = charge of ion

V_i = ion velocity

and the ion is taken as a single-ionized nitrogen molecule.

APPENDIX B

CURRENT COLLECTION BY A SPHERICAL PROBE

The electron or ion current collected by a spherical probe in an isotropic plasma is given by

$$I = \begin{cases} 4\pi r_o^2 j_r ; & r_o \leq p \text{ (Space Charge Limited Current)} & (B-1) \\ 4\pi p^2 j_r ; & p \leq r_o \text{ (Orbit-Limited Current)} & (B-2) \end{cases}$$

where

r_o = space charge sheath thickness (cm)

p = impact parameter (cm)

j_r = ion or electron random thermal current density (amperes/cm²)

I = ion or electron current collected by sphere (amperes)

The space-charge sheath radius, r_o , can be determined by solving the following equation from Langmuir (ref. 13).

$$I = 4\pi r_o^2 \left(\frac{D}{r_o^2 \alpha^2} \right) \quad (B-3)$$

where

$$D = \frac{\sqrt{2}}{9\pi} \sqrt{\frac{e}{M}} v^{3/2} \\ = 2.336 \times 10^{-6} v^{3/2} \text{ (electrons)} \quad (B-4)$$

$$= 5/455 \times 10^{-8} v^{3/2} / \sqrt{M} \text{ (ions)} \quad (B-5)$$

where M is the molecular weight on the ion and α^2 is a complicated function of a and r_o which has been tabulated in Ref. 13, Table II. To determine r_o , one must substitute equation B-1 into B-3 and solve by iteration. Specifically, one must solve the following equation:

$$r_o = \sqrt{\frac{D}{j_r \alpha^2}} \quad (B-6)$$

This is a simple matter if one uses the tables of α^2 prepared by Langmuir (ref. 13, Table II).

When the space charge sheath radius is large ($r_0 \gg a$) the above process can be simplified. Specifically, α^2 can be approximated by the following expression when $r_0 \gg a$:

$$\alpha^2 = 1.16 (r_0/a)^{3/2} \quad (\text{B-7})$$

Note: Equation B-7 is an approximation of the expression

$$\alpha^2 = 1.11 (r_0/a - 1.64)^{3/2} \quad (\text{B-12})$$

which calculates α^2 accurately for $r_0/a \gg 1$.

Although Langmuir (ref. 13) states:

$$1/2 \alpha^2 = (1.11 r_0/a - 1.64)^{3/2}$$

a review of his paper reveals that equation B-12 is the correct expression and can be further approximated by equation B-7.

Substituting B-1 and B-7 into B-3, one gets

$$r_0 = \begin{cases} 2.36 \times 10^{-2} \frac{(aV)^{3/7}}{j_r^{2/7}} ; & (\text{electrons}) \end{cases} \quad (\text{B-8})$$

$$\begin{cases} 8.06 \times 10^{-3} \frac{(aV)^{3/7}}{M^{1/7} j_r^{2/7}} & (\text{ions}) \end{cases} \quad (\text{B-9})$$

where

M = molecular weight of ion (AMU)

V = probe voltage relative to plasma potential (volts)

j_r = random current density of plasma electrons or ions (amperes/cm²)

a = probe radius (cm)

r_0 = space charge sheath radius (cm)

Equations B-8 and B-9 approximate r_0 within ten percent for $r_0/a > 10$.

The impact parameter, p , is given by

$$p = a \sqrt{1 + \frac{V}{E}} \quad (\text{B-8})$$

where

V = probe voltage relative to plasma potential (volts)

E = average energy of electrons or ions (eV)

a = probe radius (cm)

Figure B-1 shows calculated values of p and r_o for a 1.27-cm diameter sphere in the Large Plasma Chamber (LPC) indicating that $p < r_o$ and therefore orbit limited theory (equation B-2) applies.

The following equations represent probe current collected by a sphere in the LPC when orbit-limited theory applies:

$$I = j_{eo} A (1 + V/E_e); V \geq 0 \quad (B-10)$$

$$I = -j_{eo} A \exp(-V/E_e) + j_{io} A (1 + V/E_i); V < 0 \quad (B-11)$$

where

$$A = 4\pi a^2$$

Equation B-10 was used to obtain the calculated values in Figure 10, Section 4.1, and both equations B-10 and B-11 were used to obtain the calculated values in Figure 12, Section 4.1.

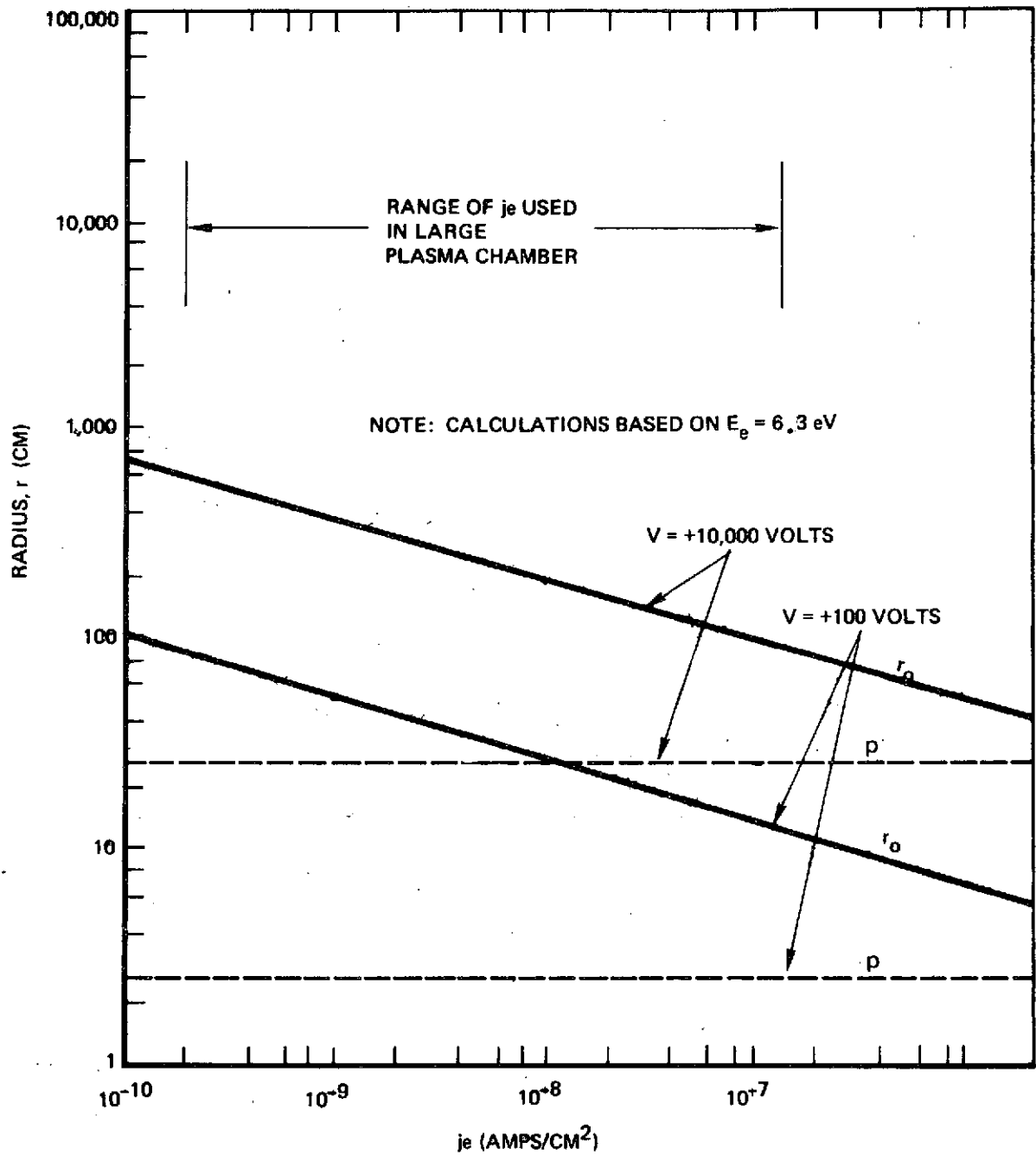


Figure B-1: COMPARISON OF IMPACT PARAMETER AND SPACE CHARGE SHEATH RADIUS FOR 1.27-CM SPHERE IN LARGE PLASMA CHAMBER

APPENDIX C

PARTIALLY-INSULATED SPHERICAL PROBE MODEL

The analysis in this section concerns the current-collecting characteristics of a metal sphere of radius a , whose surface is partially insulated with 2 cm by 2 cm coverslides in the fashion of a solar panel. This model assumes that the exposed metal represents a fraction β of the overall surface area. It is not unreasonable to hypothesize that the plasma current collected by such a sphere in space would be very close to that collected by a flat panel having the same surface area.

The ion or electron current collected by this model should behave similar to the bare spherical probe discussed in Appendix B except that the average surface potential, \bar{V}_p , will be less than the applied potential V_p . According to Ref. 1, p 17, 18 the average surface potential is simply β times the applied potential: $\bar{V}_p = \beta V_p$. Particles more than 2 cm away from the surface will behave exactly as if the surface were bare with an applied potential of \bar{V}_p . Thus the current-collecting characteristics of our model can be obtained by substituting $\bar{V}_p = \beta V_p$ into the bare sphere equations of Appendix B:

$$I = \begin{cases} 4\pi r_o^2 j_r; & r_o \leq p \text{ (Space-Charge Limited Current)} \\ 4\pi p^2 j_r; & p \leq r_o \text{ (Orbit-Limited Current)} \end{cases} \quad \begin{matrix} (C-1) \\ (C-2) \end{matrix}$$

$$r_o = \sqrt{\frac{D}{j_r \alpha^2}} = \text{Space-Charge Sheath Radius (cm)} \quad (C-3)$$

$$D = \begin{cases} 2.336 \times 10^{-6} (\beta V_p)^{3/2}; & \text{(electrons)} \end{cases} \quad (C-4)$$

$$D = \begin{cases} 5.455 \times 10^{-8} \frac{(\beta V_p)^{3/2}}{M}; & \text{(ions)} \end{cases} \quad (C-5)$$

α^2 = a function of r_o/a which is tabulated in Ref. 13

j_r = random current density of plasma electrons or ions (amps/cm²)

$$p = a \sqrt{1 + \frac{\beta V_p}{E}} = \text{impact parameter (cm)} \quad (C-6)$$

a = radius of sphere (cm)

β = fraction of sphere surface area uncovered

V_p = potential applied to sphere (volts)

E = average energy of electrons or ions (eV)

M = molecular weight of ion (AMU)

I = electron or ion current collected by the sphere (amperes)

The above equations are valid providing $(r_0 - a) \gtrsim 2$ cm and $V/E_e \gg 1$.

When $r_0 \gg a$, equation C-3 reduces to the following:

$$r_0 = \begin{cases} 2.36 \times 10^{-2} \frac{(a\beta V_p)^{3/7}}{j_r^{2/7}} & \text{; (electrons)} \end{cases} \quad (C-7)$$

$$r_0 = \begin{cases} 8.06 \times 10^{-3} \frac{(a\beta V_p)^{3/7}}{M^{1/7} j_r^{2/7}} & \text{; (ions)} \end{cases} \quad (C-8)$$

Equations C-7 and C-8 approximate r_0 within 10 percent for $r_0/a > 10$.

Comparison with Laboratory Test Data

Section 4.3.1 describes tests conducted on a small (1058cm²) solar panel having 10- percent of its front surface represented by bare interconnectors; the rest of the front surface is covered with glass coverslides and the back-side is completely insulated. The corresponding sphere model has a radius of $a = 9.2$ cm. If one calculates the space charge sheath radius, r_0 , and the modified impact parameter, p , for the plasma conditions in the large Plasma Chamber, it becomes evident that $p < r_0$ for any voltage. Thus orbit-limited theory applies (equations C-2, C-6):

$$I = j_r A_p \left(1 + \frac{\beta V_p}{E}\right); \quad V_p/E_e \gg 1 \quad (C-9)$$

Equation C-9 applies only for large voltages, however the following analysis shows how it can be modified to apply over the entire range.

As $V_p \rightarrow 0$, we expect only the exposed regions between coverslides to intercept the random thermal flux of electrons or ions. Thus

$$I = j_r \beta A_p; \quad V \rightarrow 0 \quad (C-10)$$

For $V_p/E \gg 1$, Equation C-9 can be written

$$I = j_r A_p (\beta V_p/E); \quad V/E_e \gg 1 \quad (C-11)$$

Equations C-10 and C-11 can be combined into a single equation which satisfies the high and low voltage limits as well as providing a smooth transition between these limits at intermediate voltages:

$$I = j_r \beta A_p \left(1 + \frac{V_p}{E}\right) \quad (C-12)$$

Equation C-12 was used as the basis for making calculations of plasma current to compare with measured data.

Total current (electron + ion) collected by the solar panel is therefore given by:

$$I = j_{eo} \beta A_p \left(1 + \frac{V_p}{E_e}\right); \quad V > 0 \quad (C-13)$$

$$I = j_{io} \beta A_p \left(1 + \frac{V_p}{E_i}\right) - j_{eo} \beta A_p \exp(-V/E_e); \quad V \leq 0 \quad (C-14)$$

Figure 39, Section 4.3.1.1.1 shows a comparison between measured panel current at positive biases and calculated values based on equation C-13. Figure 40, Section 4.3.1.1.2, shows a comparison between measured panel current at negative biases and calculated values based on equation C-14. Note that the agreement is fairly good for positive biases but not so good for negative biases.

Predicting Solar Panel Plasma Current in Space

Equations C-1 through C-8 can be used to predict the plasma current collected by a solar panel with bare interconnectors in space. When the calculations are performed, it is found that for solar panels larger than ~ 15 ft² the plasma currents collected are space-charge limited rather than orbit-limited (i.e., $r_0 < p$) and therefore equations C-1 and C-3 are the applicable ones. Figures C-1 and C-2 show how the plasma power loss ($I \times V$) per square foot decreases with increasing solar panel size for positive biases at low and high altitude. Similar behavior is found for negative biases. Figure C-3 shows the calculated plasma power loss for a positively and negatively biased 15 kw solar panel as a function of altitude, indicating that power loss only becomes a problem for positive biases, and only then at very low altitudes. It should be remembered that these calculations are for a large (1500 ft²) solar panel whose current collection is space-charge limited whereas laboratory plasma tests were conducted with a small (1 ft²) solar panel whose current collection was orbit-limited and perhaps influenced by the plasma chamber walls. Thus the calculated plasma losses in Figure C-3 remain questionable until further plasma tests can validate the partially-insulated spherical probe model under space-charge limited conditions where the plasma sheath is not restricted. Such a test will be performed on the solar array segments to be flown on the SPHINX earth-orbiting satellite to be launched in January 1974 (ref. 11).

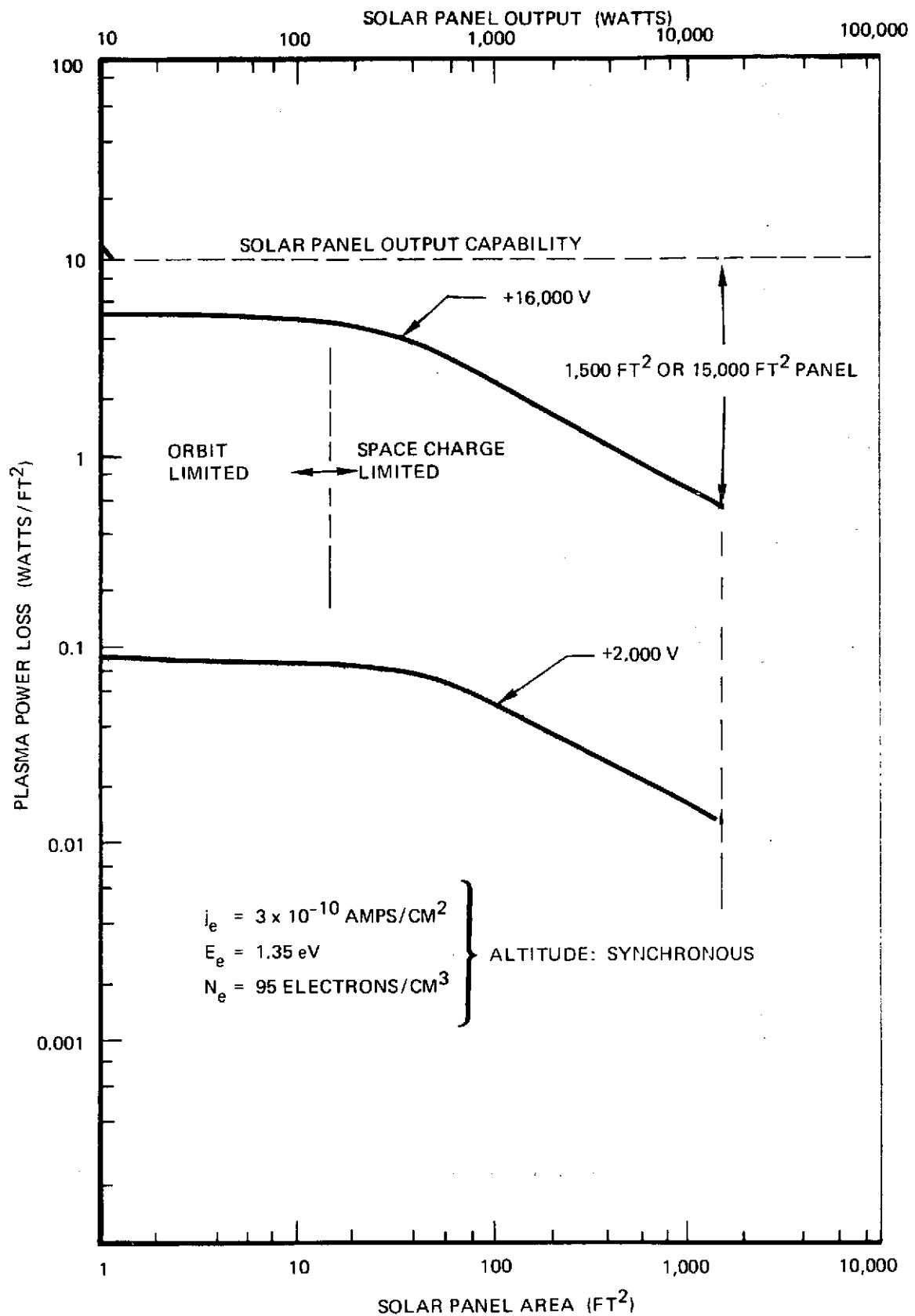


Figure C-1: EFFECT OF SOLAR PANEL AREA IN PLASMA POWER LOSS
AT HIGH ALTITUDE - POSITIVE BIAS

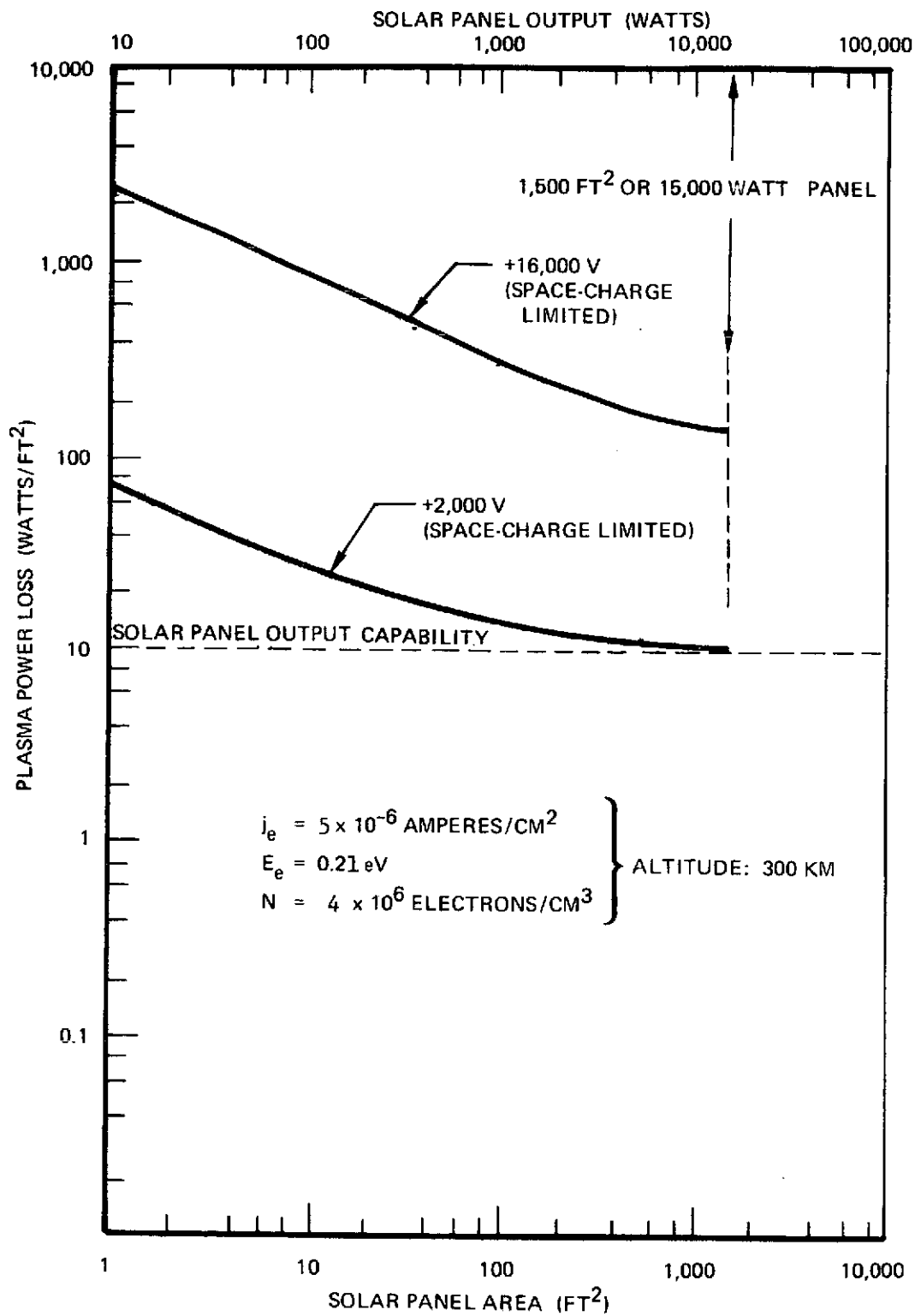


Figure C-2: EFFECT OF SOLAR PANEL AREA ON PLASMA POWER LOSS AT LOW ALTITUDE – POSITIVE BIAS

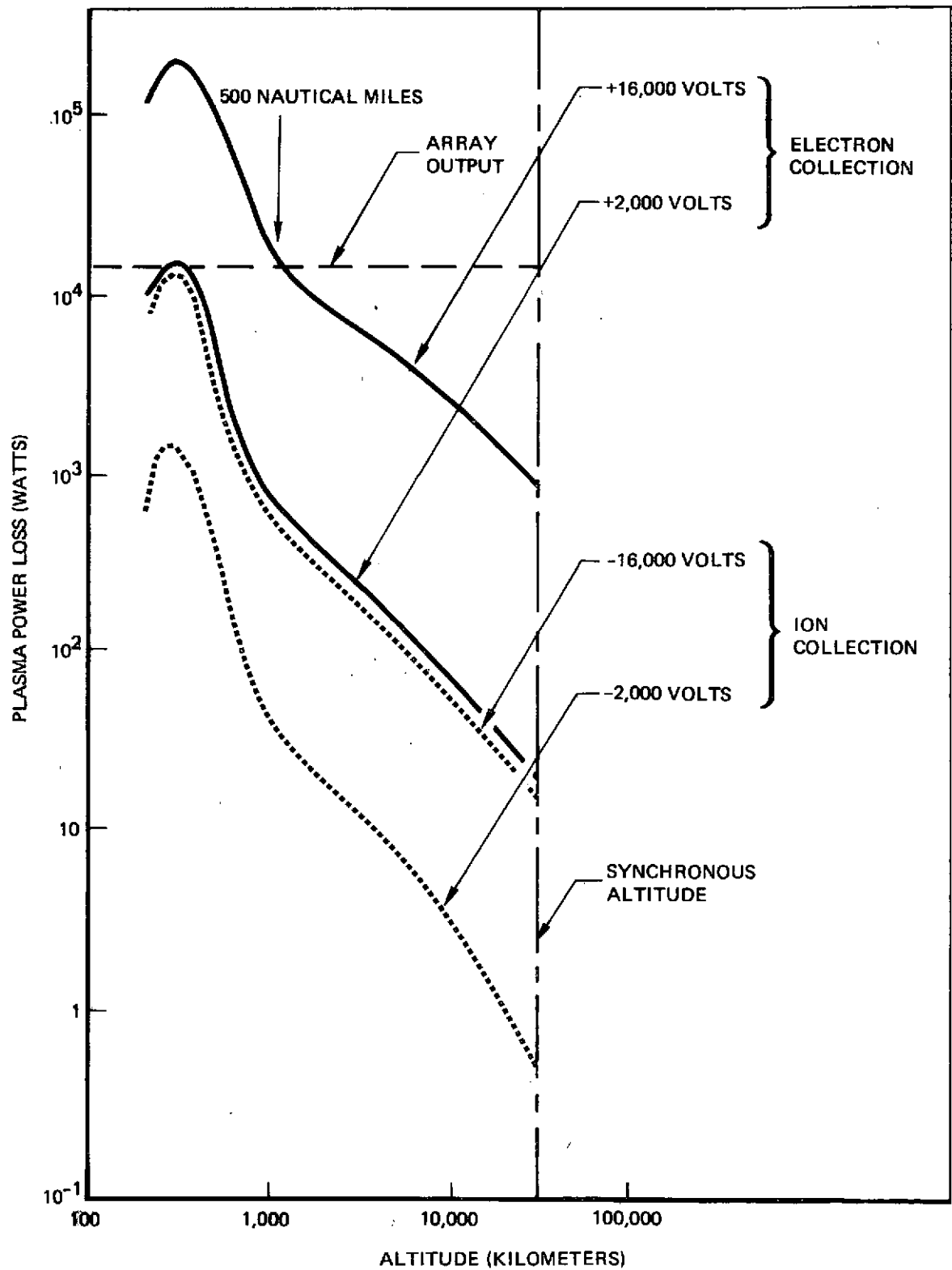


Figure C3: PLASMA POWER LOSSES OF A BIASED 15kW SOLAR ARRAY WITH 90% INSULATING SURFACE